Vortex dynamics in superconductors in the presence of anisotropic pinning

Dissertation

zur Erlangung des Grades

Doktor der Naturwissenschaften (Dr. rer. nat.)

am Fachbereich Physik

der Johannes Gutenberg-Universität Mainz

von

Oleksiy K. Soroka

geb. in Kremenec' (Ukraine)

Mainz, 2004

Tag der Einreichung: 08.11.2004

Tag der mündlichen Prüfung: 15.03.2005

Vortex dynamics in superconductors in the presence of anisotropic pinning

Ph. D. thesis

by

Oleksiy K. Soroka

Mainz, 2004

Contents

List of Figures

List of Tables

Chapter 1

Basic concepts of superconductivity

Perfect conductivity, i.e. the complete disappearance of the electrical resistance of a material below a critical temperature T_c, which is characteristic of the material, was first observed in 1911 by H. Kamerlingh Onnes when measuring the resistivity of a Hg sample at low temperatures [1].

Another fundamental characteristic of a superconductor is perfect diamagnetism in weak magnetic fields. Experimentally it was first found in 1933 by W. Meissner and R. Ochsenfeld [2]. The magnetic field is not only excluded from the interior of a superconductor cooled below T_c and then brought in magnetic field, which can be explained by perfect conductivity alone. The field is also actively expelled as the superconductive sample with $T > T_c$ is cooled below T_c in magnetic field; a perfect conductor would tend to trap the magnetic field in the sample in this case. This effect is called the Meissner-Ochsenfeld effect.

The superconductive state is destroyed at high temperature and magnetic field, however. The thermodynamic critical magnetic field $H_c \equiv B_c/\mu_0$ is determined by the free-energy density difference between the normal and the superconductive states in zero field, the so called condensation energy of the supercon-

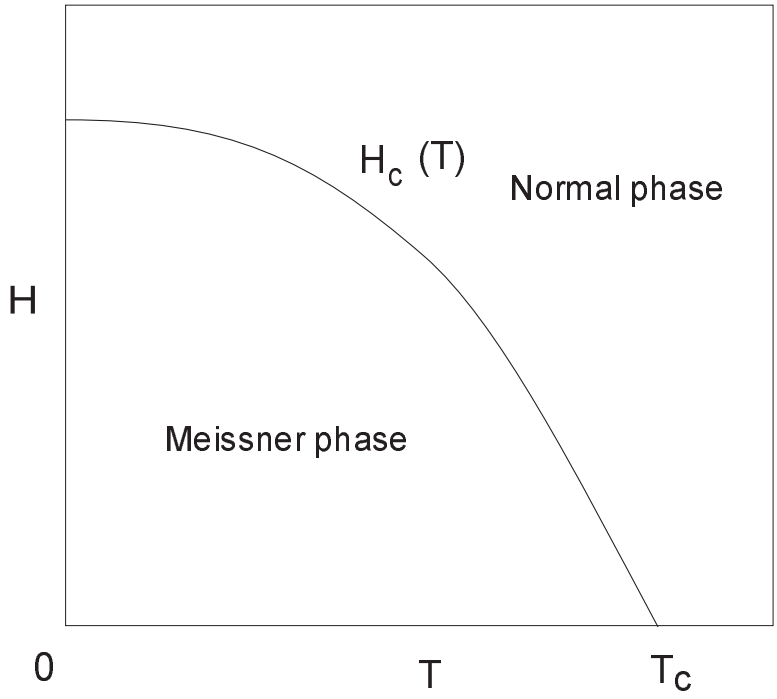

Figure 1.1: *H-T phase diagram of a superconductor.*

ductor:

$$\frac{B_c^2(T)}{2\mu_0} = f_n(T) - f_s(T)$$

The curve $H_c(T)$ (see Fig. 1) separates the superconducting and normal states of the superconductor.

The electrodynamic properties of superconductors were described at first in 1935 by the brothers F. and H. London [3].

$$\mathbf{E} = \frac{\partial}{\partial t}(\Lambda \mathbf{J}_s) \tag{1.1}$$

$$\mathbf{B} = -\nabla \times \Lambda \mathbf{J}_s \tag{1.2}$$

where $\mathbf{E}$ is an electrical field vector, $\mathbf{J}_s$ is a superconducting current, $\Lambda = \mu_0 \lambda^2 = \frac{m_s}{n_s q_s^2}$, where m_s, n_s and q_s denote the mass, number density and charge of the superconducting charge carriers, respectively. Using the equations 1.1 in conjunction with Maxwell's equations one can obtain a solution for the magnetic field $B \propto \exp(-x/\lambda)$. This corresponds to the existence of a screening supercurrent

within a characteristic penetration depth λ near the surface of the superconductor.

V. L. Ginzburg and L. D. Landau in 1950 proposed a new theoretical approach to the problem [4]. They introduced a complex pseudo-wave function ψ as an order parameter on the basis of Landau's general theory of second-order phase transitions. Function ψ describes the local density of the superconducting electrons: $|\psi(x)|^2 = n_s$. Using a series expansion of the free energy in powers of ψ and $\nabla\psi$ they derived the following differential equation for ψ

$$\frac{1}{2m^*}(\frac{\hbar}{i}\nabla - e^*A)^2\psi + \beta|\psi|^2\psi = -\alpha(T)\psi$$

where α and β are the expansion coefficients. This theory introduces a new important quantity which is a characteristic length, usually called the Ginzburg-Landau coherence length, over which $\psi(x)$ can vary without undue energy increase

$$\xi(T) = \frac{\hbar}{|2m^*\alpha(T)|^{1/2}}.$$

A further characteristic quantity of a superconductor is the Ginzburg-Landau parameter

$$k = \frac{\lambda}{\xi}.$$

Because both ξ and λ diverge as $(T_c - T)^{-1/2}$ near T_c this dimensionless ratio is approximately independent of temperature. The Ginzburg-Landau parameter k is related to the surface energy associated with a domain wall between normal and superconducting regions of the material. For typical classical superconductors $k \ll 1$.

1.1 Type II superconductors, vortices

A. A. Abrikosov showed in 1957 that the energy associated with a domain wall between normal and superconducting regions in a homogeneus material will turn negative for $k > \sqrt{1/2}$ [5]. In this case a system will favor an arrangement with

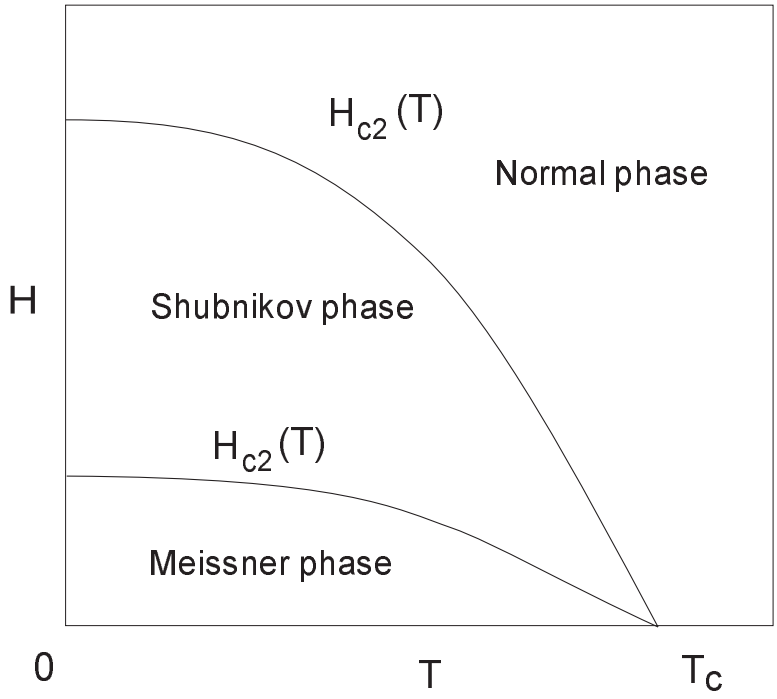

Figure 1.2: *H-T phase diagram of the type II superconductor.*

many separate superconductive and normal domains maximizing the area of the phase boundary. Such behaviour is radically different from the classical superconductors. Abrikosov called superconductors with $k > \sqrt{1/2}$ type II superconductors, whereas the ones with $k < \sqrt{1/2}$ are of type I. For type II superconductors there is no discontinuous breakdown of the superconductivity in a phase transition at H_c. Instead, the magnetic flux penetrates the material, starting at a lower critical field $H_{c1}(T)$ and reaching $B = \mu_0 H$ at an upper critical field $H_{c2}(T)$.

Between these two fields, H_{c1} and H_{c2}, a type II superconductor is in the so called mixed state or Shubnikov phase (see phase diagram in the Fig. 1.2). Abrikosov showed that in this state the magnetic flux penetrates the material not in the form of laminar domains but as a regular array of flux tubes, each carrying an elementary quantum of flux, given by

$$\Phi_0 = \frac{h}{2e} \approx 2.07 \cdot 10^{-15}\mathrm{Vs} \tag{1.3}$$

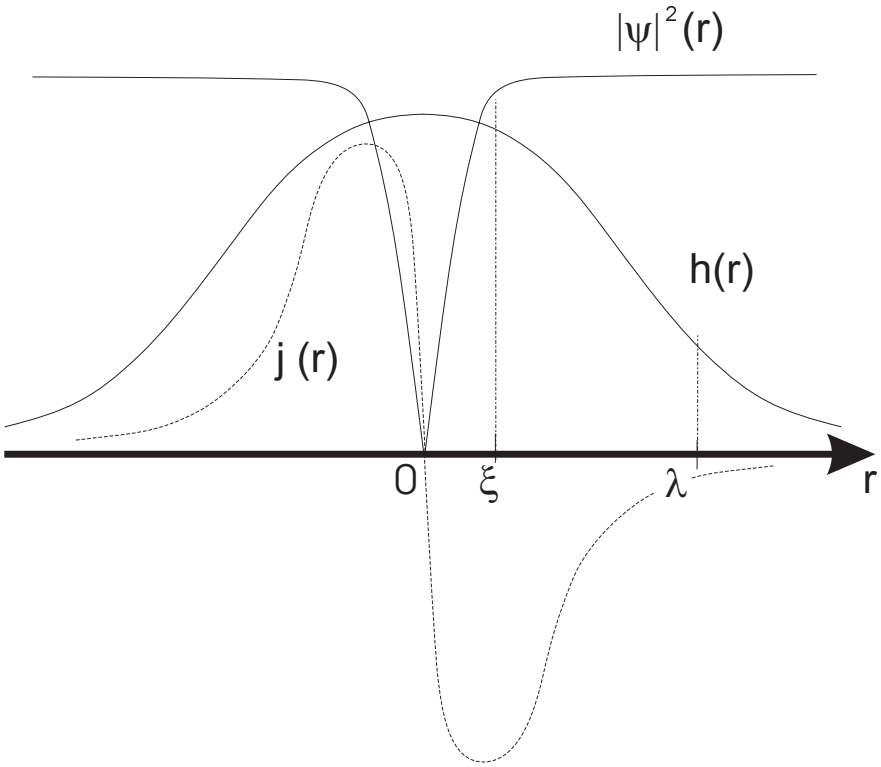

Figure 1.3: *Spatial distribution of the local magnetic field h, squared absolute value of the order parameter ψ and superconducting current density j across the magnetic flux tube.*

Each flux tube is surrounded by a circular supercurrent which shields the superconducting domain outside from the normal core inside the flux line as schematically shown in Fig. 1.3. Therefore the term vortex is usually used to refer to the whole arrangement associated with a flux line. According to Abrikosov vortices will form a triangular vortex lattice in a type II superconductor.

In the presence of a superimposed transport current with current density j vortices experience a Lorentz force

$$\mathbf{F}_L = \mathbf{j} \times \mathbf{\Phi_0} \tag{1.4}$$

per unit length. The Lorentz force induces a movement of the vortices perpen-

dicular to the transport current and this movement produces an electric field

$$\mathbf{E} = \mathbf{B} \times \mathbf{v}. \tag{1.5}$$

J. Bardeen and M. J. Stephen [6] showed that in an ideal homogeneous material such a vortex motion is damped only by a viscous (drag) force $\mathbf{F} = -\eta\mathbf{v}$ where $\mathbf{v}$ is the steady state velocity of the vortex system, η is a friction coefficient, $\eta \approx \mu_0^2 H H_{c2}/\rho_n$, here ρ_n is the normal-state resistivity. Since $\mathbf{j}$ and $\mathbf{E}$ are parallel to each other, a longitudinal resistive voltage $\mathbf{E}$ results in power dissipation and type II superconductors should show a resistance reduced only by a factor $\sim H/H_{c2}$ as compared with the normal state resistivity.

1.2 Flux pinning and creep

In real materials in some T-H regions a mechanism exists that prevents vortex motion and thus allows to obtain a dissipation free transport current flow in a type II superconductor. The vortices can be pinned by secondary phases inclusions or spatial inhomogeneities of the crystal lattice, such a quenched disorder as, for example, cavities, impurities, secondary phases inclusions, grain boundaries [7, 8], dislocations [9, 10, 11], and twin planes [12, 13, 14]. All of these defects usually suppress the order parameter ψ in their vicinity [15]. This means they present energetically favored locations for a vortex, because on these defects less condensation energy is required for the reduction of the order parameter in the vortex core. The driving Lorentz force $\mathbf{F}_L$ is now counteracted by the pinning force $\mathbf{F}_p$ and the vortex velocity $\mathbf{v}$ stays equal to zero as long as the transport current density does not exceed the critical depinning current density $j_{dp} = F_p/\Phi_0$ (assuming $\mathbf{j} \perp \mathbf{B}$). If j_c is the critical current density which destroys the superconductivity, the dimensionless parameter j_{dp}/j_c is a measure of the pinning strength in the superconductor [15].

The dynamics of the vortex system in type-II superconductors is strongly de-

pendent on the kind of disorder. Disorder affects the properties of the vortex state, it destroys the triangular vortex lattice and thus changes the H-T phase diagram of the vortex matter. One can distinguish between, randomly distributed defects, such as structural point defects, oxygen vacancies in high temperature superconductors, grain boundaries, and defects with a correlated spatial distribution, for example, parallel pinning planes or artificially formed defects caused by heavy ions radiation. Another kind of disorder is introduced into the vortex system by thermal fluctuations. The vortex lines can perform thermally activated motion which leads to the creep phenomenon in type II superconductors. Creep is a small directed motion of the vortex lines which entails dissipation in the system. Very similar to thermal fluctuations are quantum fluctuations. They affect the superconductivity via fluctuations of the order parameter and induce a quantum motion of vortices (quantum creep) [15].

The classical creep theory developed in 1960-1962 by Anderson and Kim [16, 17] suggests that the thermal fluctuations induce jumps of vortex bundles and vortex segments between pinning sites. If there exists a current density in the system the whole vortex system moves with a finite average creep velocity. At small current densities $j \to 0$ this velocity is proportional to the current density and the system shows an Ohmic behavior with a resistance $\rho \propto \rho_n \exp(-U_0/k_BT)$, where k_B is Boltzmann constant, U_0 is the height of the pinning barrier, ρ_n is the normal-state resistivity. If the pinning barrier becomes small as compared to the temperature $U_0 \ll k_BT$, the vortex motion is essentially unaffected by the pinning and the external driving force can lead to the free flow of the vortices producing the so called flux flow (FF) regime. The resistivity in this case is given by the flux flow resistivity

$$\rho_f \approx \rho_n \frac{H}{H_{c2}} \tag{1.6}$$

In the case of large pinning barriers $U_0 \gg k_BT$ the resistivity becomes exponen-

tially small,

$$\rho(T) \approx \frac{\rho_f}{A} \exp(\frac{-U_0}{k_B T}), \quad A \ll 1$$

and shows an activated behavior. This regime is called the thermally-assisted flux flow (TAFF) regime [18].

1.3 High-temperature superconductors

The discovery of high-temperature superconductivity in 1986 by G. Bendorz and K.A. Müller [19] opened a new chapter in the field of superconductor physics. High-temperature superconductors (HTSC) are layered materials dominated by copper oxide planes. Because of their layered structure they are very anisotropic. The anisotropy parameter is defined as $\varepsilon = (m_{ab}/m_c)^{1/2} \ll 1$, where m_{ab} and m_c are the effective electron masses in the *ab*-plane and along the **c** axis, respectively. The critical temperatures for high-temperature superconductors are about 100 K. HTSCs have a small coherence length, $\xi_{ab}(T = 0) \sim 15$ Å, $\xi_c(T = 0) \sim 1.5$ Å and a large penetration depth $\lambda_{ab}(T = 0) \sim 1400$ Å, $\lambda_c(T = 0) \sim 7000$ Å [20]. Critical fields for these materials are of the order of $H_{c1}(T = 0) \sim 0.01$ T, and $H_{c2}(T = 0) \sim 100$ T. Any operation at comparatively high temperatures makes the influence of thermal fluctuations on the vortex system essential. These fluctuations strongly affect the static and dynamic properties of the vortex system. The interplay between the vortex interaction energy, the vortex thermal energy and pinning energy give rise to many different phases of the vortex matter which posses different static and dynamic properties. The phase diagram of such a superconductor is much more complicated. In Fig. 1.4a the phenomenological phase diagram for the anisotropic HTSCs is schematically shown. Due to thermal fluctuations the vortex lattice phase is melted over a substantial part of the phase diagram. The reentrant behavior of the melting line $H_m(T)$ can be explained with the melting of the vortex phase with decreasing field because of the exponentially vanishing shear modulus with a decreasing of the intervortex distances and the

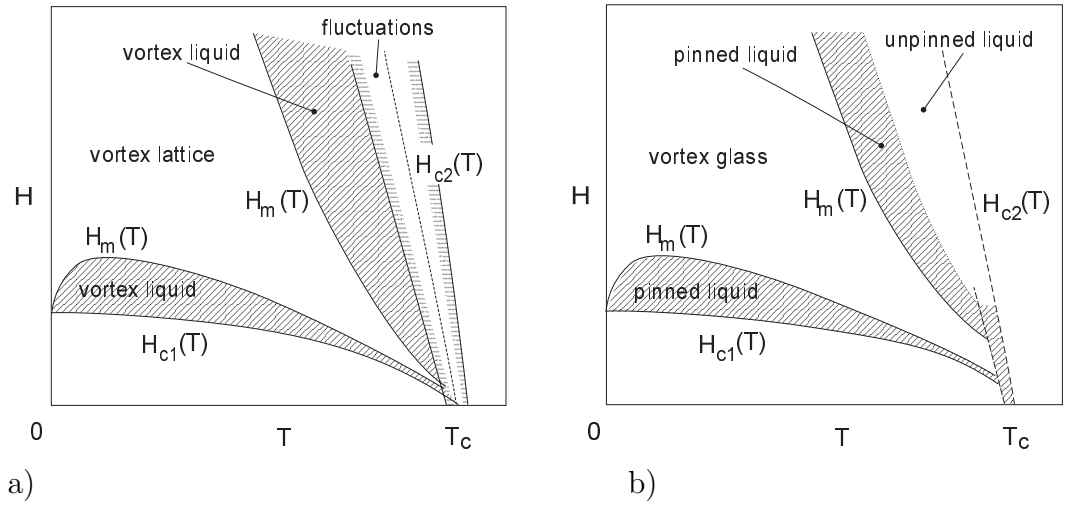

Figure 1.4: *Phenomenological phase diagram (after [15]) for the anisotropic HTSC, including the effects of thermal fluctuations (a), thermal fluctuations and pinning (b).*

melting with increasing temperature because of thermal fluctuations.

If the interaction between thermal fluctuations and pinning is taken into account, the phase diagram changes as schematically shown in Fig. 1.4b. Disorder is relevant for the vortex lattice with its finite shear modulus, it turns the lattice into a vortex glass phase. The vortex liquid is insensitive to the disorder and it remains a liquid. The unpinned liquid corresponds to the FF regime where the barriers do not affect the motion. For larger pinning barriers in the regions of a pinned liquid a TAFF regime is established.

Chapter 2

Guided vortex motion, theoretical description

2.1 Introduction

As it was shown in the previous chapter the mixed state properties of superconductors are largely dominated by the dynamics of the flux-line array. The influence of pinning on the vortex dynamics becomes even more relevant in the presence of anisotropic pinning. In the presence of parallel planar defects the pinning force in a superconductor is anisotropic: it is much stronger in the transverse direction with respect to the pinning plane than in the parallel direction. The most specific manifestation of such a pinning anisotropy are effects associated with the directed motion of vortices along the planar pinning defects, the so-called guided vortex motion or guiding, when the vortices tend to move along the pinning planes even if the external force acting on them is not aligned parallel to this planes. Another important feature of pinning anisotropy is that the longitudinal and transverse magnetoresistivity of the sample depend substantially on the angle α with which the vector $\mathbf{j}$ intersects the pinning planes.

The first experimental observation of the guided vortex motion in the flux-

flow regime was made by A. K. Niessen and C. H. Weijsenfeld in 1969 [21]. They studied guided motion by measuring transverse voltages of cold-rolled sheets of a Nb-Ta alloy for various magnetic fields, transport currents, temperatures, and different angles α between the rolling and current direction. Field and temperature dependences of the cotangent of the angle β between the average vortex velocity and the transport current direction[1] were presented. For the discussion, a simple phenomenological model was suggested, based on the assumption that pinning and guiding can be described in terms of an isotropic pinning force plus a pinning force with a fixed direction, for example, perpendicular to the rolling direction. This theoretical model could not describe the nonlinear temperature and current dependencies of the sample's magnetoresistivities. Nevertherless the experimentally observed dependence of the transverse and longitudinal voltages on the magnetic field in the FF regime as function of the rolling direction was in agreement with this model.

Following the discovery of the high temperature superconductors the interest for the influence of anisotropic pinning on the vortex dynamics was renewed. This is connected with two circumstances. First, in many of the currently known high temperature superconductors during crystal growth crystalographic twins are formed with twin planes oriented parallel to the c axis. It was proven that a twin boundary forms an anisotropic pinning site for the vortices. The strength of this pinning was shown to be significantly larger for the vortices moving perpendicular to the twin direction than for the vortices moving parallel to the twin boundaries [13, 14]. Second, in layered anisotropic high temperature superconductors the system of parallel ab planes itself can be considered as a set of unidirectional planar defects, which are a source of the so-called intrinsic pinning for the vortices located parallel to the ab planes when subjected to the Lorentz force directed along the **c** axis [15].

The first observation of an odd – with respect to the magnetic field reversal

[1]This angle is caled the guiding angle.

– component of the longitudinal magnetoresistivity $\rho_{\parallel}^{-}$, which is one characteristic feature of the pinning anisotropy was made by A. A. Prodan et al [22] and V. V. Chabanenko et al. [23] on a $YBa_2Cu_3O_{7-\delta}$ single crystal. The dependencies $\rho_{\parallel}^{-}(H)$ and $\cot\beta(H)$ were measured for $\mathbf{H}||\mathbf{c}$ with the angle between the twins direction and the transport current fixed at 45°. These dependencies were explained based on a phenomenologic model of anisotropic pinning [24, 25].

Another experimental setup was used by H. Pastoriza et al. [26] and V. Berseth et al. [27, 28]. They measured the anisotropy of the longitudinal magnetoresistivity with regard to the transport current and studied the guided vortex motion and the influence of the planar pinning on the Hall effect in twinned $YBa_2Cu_3O_{7-\delta}$ single crystal using a "orientable-current-source" setup for their measurements. The sample was patterned in such a way as to allow the simultaneous application of two transport currents in mutually perpendicular planar directions simultaneously. As a consequence, the direction of the resulting current could be easily controlled. Four voltage contacts situated in the middle of the sample were used to measure an electric field induced by the vortex motion. Such experiments give the angular dependence of the sample resistivity in the most simple way.

Some theoretical studies to describe the magneto-resistive response of a system of vortices in the presence of anisotropic pinning were published within the last years. In Sonin's phenomenological model [29, 30] Ohm's law was assumed to be applicable for an anisotropic conductor with current flowing in the xy plane and in a magnetic field $\mathbf{H}\|z$. This model predicts a resistive response of the sample at an arbitrary angle α between the transport current $\mathbf{j}$ and the pinning plane direction using the components of the magnetoresistivity tensor with components ρ_l, ρ_{Hl}, ρ_t, ρ_{Ht}. The components ρ_l, ρ_{Hl} are the longitudinal and transversal (with regard to the transport current direction) magnetoresistivities of the sample in the case of $\alpha = 90°$. The components ρ_t, ρ_{Ht} are the analogous magnetoresistivities in the case of $\alpha = 0°$.

A generalization of this phemomenological model for the nonlinear case which

leads to the deduction of interrelationships between the phenomenological magnetoresistivity components and linear electronic and nonlinear vortex-velocity-dependent pinning viscosities was made later by V. A. Shklovskij in [24, 25]. It was shown, still based on a phenomenological description [24, 25, 30], that for $\alpha \neq 0°, 90°$ there are additional magnetoresistivity components induced solely by the pinning anisotropy. These are the longitudinal odd component $\rho_{\parallel}^{-}$ and the transversal even component $\rho_{\perp}^{+}$ (even and odd again with respect to the magnetic field sign reversal). The origin of the component $\rho_{\perp}^{+}$ is due to the anisotropy of the pinning viscosity, i.e. the difference in ρ_l and ρ_t, and is connected with the guiding of the vortices. The appearance of $\rho_{\parallel}^{-}$ is explained within this model by the influence of pinning planes on the Hall resistivity and the resulting anisopropy $\rho_{Hl} \neq \rho_{Ht}$.

Another theoretical approach is based on a two-dimensional stochastic model for the vortex dynamics introduced by Y. Mawatari [31, 32]. This model is based on the Fokker-Plank equation for the probability density of the vortex position and probability flux density of the vortex position. In general form Fokker-Plank equation describes a Brownian motion; it is a partial differential equation for the probability density function of a position of a particle [33, 34]. This approach takes into account stochastic properties of thermal fluctuations in vortex position and allows the deduction of the temperature dependence of the magnetoresistive response of the system in the whole temperature range $0 < T < T_c$. This stochastic model was developed further by V. A. Shklovskij et.al in [35, 36, 37, 38].

Vortex dynamics in the presence of anisotropic pinning forces was also studied using numerical simulations [39, 40, 41]. Two of these studies made by G. W. Crabtree et. al [39] and J. Groth et. al [40] examined the interaction of moving vortices with an isolated twin boundary and investigated a number of interesting dynamical peculiarities of this interaction. However, in actual transport experiments the self averaged dynamics of vortices is studied, which is a

consequence of the interaction of the vortices with many twin boundaries. This self-averaging apparently smears out some of the fine features of the interaction of the vortices with an isolated twin boundary.

A different model was investigated by B. U. Zhu et. al [41]. In this work, the equation of motion of a vortex was derived that takes into account the interaction of the vortices with each other, and also with point defects and planar defects in the presence of thermal fluctuations. However, the large number of independent physical parameters in the investigated problem greatly hinders a proper choice of their values, whose variation leads to nontrivial physical results.

In the following emphasis is laid on the stochastic model for the vortex dynamics [35, 36, 37, 38].

2.2 The Fokker-Planck method in the anisotropic pinning model

Let us assume that a flat sample with a set of parallel pinning planes is in a magnetic field directed parallel to the pinning planes as shown in Fig. 2.1. Transport current of the density J flows directed at the angle α to the pinning planes. Longitudinal and transverse resistivities with regard to the current direction are measured for two oppositely directed magnetic fields.

For the theoretical description the model described in [31, 35, 36] is considered here. The Langevin equation for a vortex moving with velocity $\mathbf{v}$ in a magnetic field $\mathbf{B} = \mathbf{n}B$ ($B \equiv |\mathbf{B}|$, $\mathbf{n} = n\mathbf{z}$, $\mathbf{z}$ is the unit vector in the z direction, and $n = \pm 1$) has the form

$$\hat{\eta}\mathbf{v} + n\alpha_H[\mathbf{v} \times \mathbf{z}] = \mathbf{F}_L + \mathbf{F}_p + \mathbf{F}_{th} \tag{2.1}$$

where $\mathbf{F}_L = n\Phi_0\mathbf{J} \times \mathbf{z}$ is the Lorentz force per unit length of the vortex, Φ_0 is the magnetic flux quantum, c is the speed of light, and $\mathbf{J}$ is the current density. $\mathbf{F}_p = -\nabla U_p$ is the pinning force (U_p is the pinning potential created by the

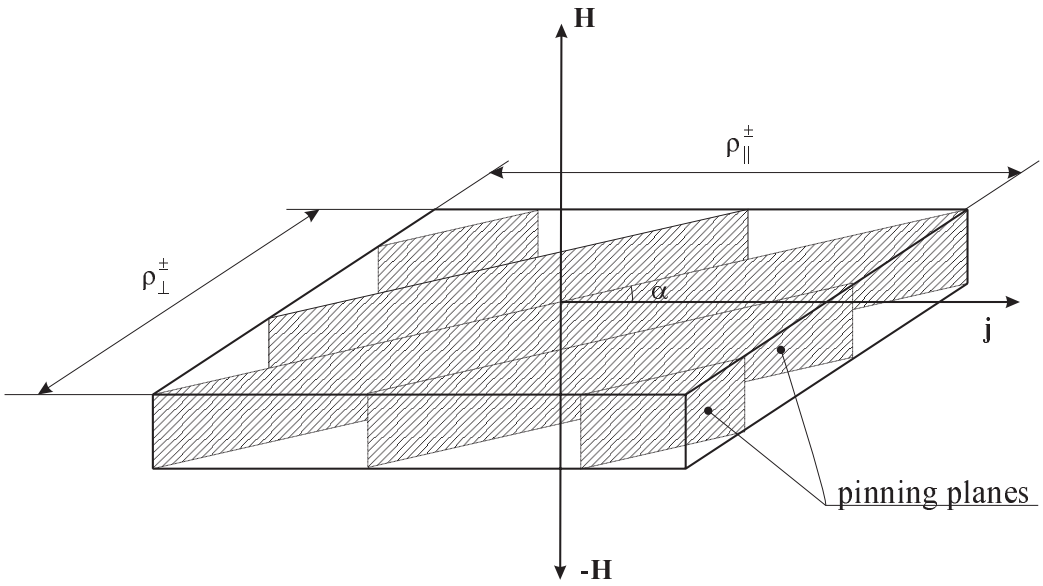

Figure 2.1: *Sample with unidirected pinning planes in magnetic field* **H**.

pinning planes), $\mathbf{F}_{th}$ is the thermal fluctuation force, $\hat{\eta}$ is the electronic viscosity tensor, and α_H is the effective Hall coefficient. If x and y are the coordinates parallel and transverse to the anisotropy axis (see Fig. 2.2), then the tensor $\hat{\eta}$ is diagonal in the xy representation, and it is convenient to define η_0 and γ by means of the formulas

$$\begin{aligned} \eta_0 = \sqrt{\eta_{xx}\eta_{yy}}, \quad \gamma = \sqrt{\eta_{xx}/\eta_{yy}}, \\ \eta_{xx} = \gamma\eta_0, \qquad \eta_{yy} = \eta_0/\gamma. \end{aligned} \tag{2.2}$$

Here γ is the anisotropy parameter and η_0 is the averaged viscous friction coefficient. The fluctuational force $\mathbf{F}_{th}(t)$ is represented by Gaussian white noise, whose stochastic properties are defined by the relations

$$< F_{th,i}(t) >= 0, \quad < F_{th,i}(t)F_{th,j}(t') >= 2k_BT\eta_{ij}\delta(t-t') \tag{2.3}$$

where T is the temperature. Employing relations 2.3, one can reduce Eq. 2.1 to a system of Fokker-Plank equations:

$$\frac{\partial P}{\partial t} = -\nabla \cdot \mathbf{S} \tag{2.4}$$

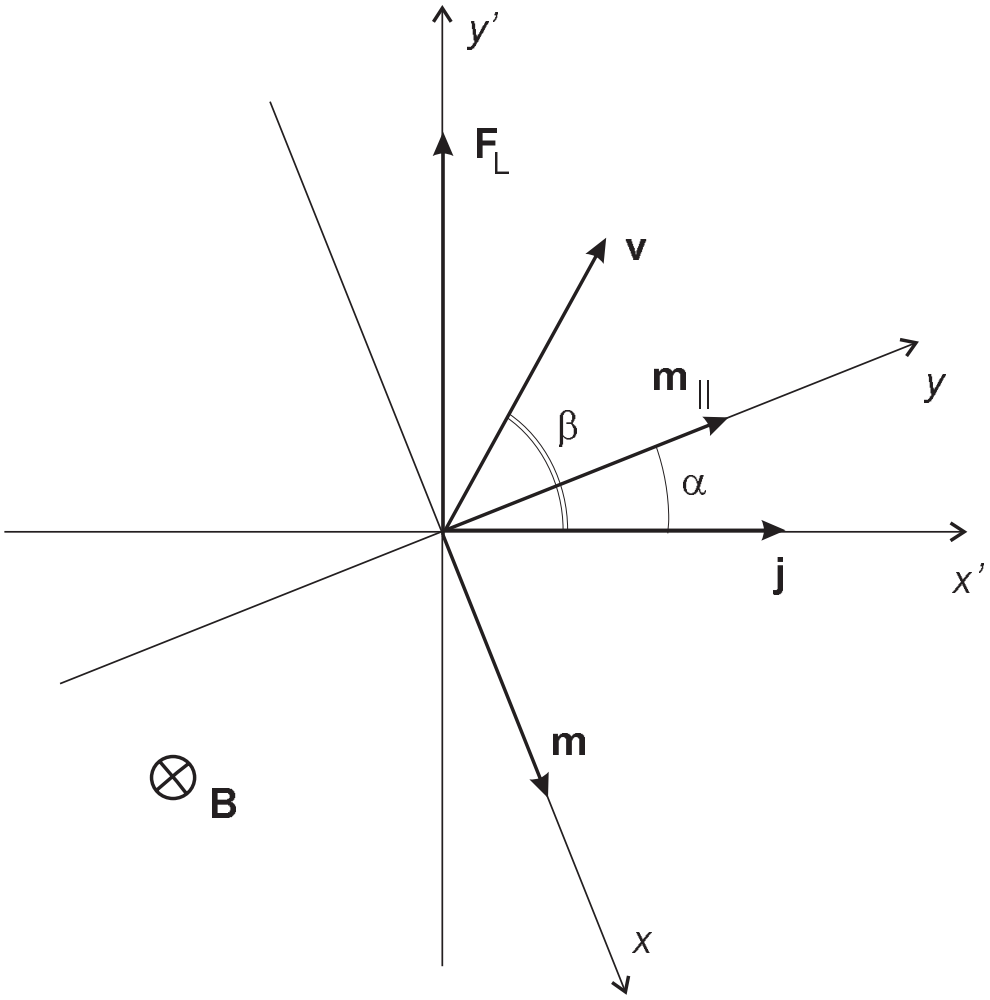

Figure 2.2: *System of coordinates xy associated with the pinning planes. The anisotropy vector* $\mathbf{m}$ *points along the x axis.* α *is the angle between the pinning plane and the dimensionless transport current density vector* $\mathbf{j}$ *(see text),* β *is the angle between the average velocity vector of the vortices* $\mathbf{v}$ *and the dimensionless current density vector* $\mathbf{j}$*;* $\mathbf{F}_L$ *is the Lorentz force.*

$$\hat{\eta}\mathbf{S} + n\alpha_H \mathbf{S} \times \mathbf{z} = (\mathbf{F}_L + \mathbf{F}_p)P - k_B T \nabla P, \tag{2.5}$$

Equation 2.4 reflects continuity of the probability density $P(\mathbf{r}, t)$ associated with finding the vortex at the point $\mathbf{r} = (x, y)$ at the time t. Equation 2.5 specifies the probability flux density of the vortex $\mathbf{S}(\mathbf{r}, t) \equiv P(\mathbf{r}, t)\mathbf{v}(\mathbf{r}, t)$. The definition of the mean vortex velocity is as following

$$< \mathbf{v} >= \frac{\int\int \mathbf{S} d^2 r}{\int\int P d^2 r} \tag{2.6}$$

Since the anisotropic pinning potential is assumed to depend only on the x coordinate and is assumed to be periodic ($U_p \equiv U_p(x) = U_p(x + a)$, where a is the period), the pinning force is always directed along the anisotropy axis x (with unit anisotropy vector $\mathbf{m}$, see Fig. 2.2) so that it has no component along the y axis ($F_{py} = -dU_p/dy = 0$). This then implies that P and $\mathbf{S}$ are only functions of x and Eq. 2.5 in the stationary case for the functions $P = P(x)$ and $\mathbf{S} = (S_x(x), S_y(x))$ reduces to the equations

$$\gamma\eta_0 S_x + n\alpha_H S_y = (F_{Lx} - \frac{dU_p}{dx})P - k_B T \frac{dP}{dx}, \tag{2.7}$$

$$-n\alpha_H S_x + \frac{\eta_0}{\gamma} S_y = F_{Ly} P. \tag{2.8}$$

Eliminating S_y from Eqs. 2.7 and 2.8, one obtains

$$k_B T \frac{dP}{dx} + (-F + \frac{dU_p}{dx})P = -\gamma\eta_0(1 + \epsilon^2) S_x. \tag{2.9}$$

where $\epsilon \equiv \alpha_H/\eta_0$ is a dimensionless Hall coefficient, and $F \equiv F_{Lx} - n\gamma\epsilon F_{Ly}$. From the mathematical point of view, Eq. 2.9 is the Fokker-Planck equation of one-dimensional vortex dynamics [43, 44]. Thus, the problem of two-dimensional vortex motion reduces to a one-dimentional problem, where a combination of x and y components of the Lorentz force enters as the external force:

$$F = n\Phi_0(J_y + n\gamma\epsilon J_x) = n\Phi_0(\cos\alpha + n\gamma\epsilon \sin\alpha)J \tag{2.10}$$

Here α is the angle between the direction of the current and the vector $\mathbf{m}_\parallel$ directed perpendicular to the anisotropy axis (Fig. 2.2). In the stationary case from

continuity equation 2.4 follows that $dS_x/dx = 0$ and thus S_x is independent on x. By direct integration the solution of Eq. 2.9 for periodic boundary conditions $P(0) = P(a)$ and pinning potential of general form is

$$P(x) = \frac{\gamma\eta_0(1+\epsilon^2)S_x}{k_BT}\frac{f(a)f(x)}{f(a)-f(0)}\int_x^{x+a}\frac{d\xi}{f(\xi)} \tag{2.11}$$

where $f(x) = \exp[(Fx - U_p(x))/k_BT]$. Hence one obtains an expression for the x component of the vortex mean velocity:

$$< v_x >= \frac{F\nu_a(F)}{\gamma\eta_0(1+\epsilon^2)}, \tag{2.12}$$

where

$$\frac{1}{\nu_a(F)} \equiv \frac{F}{k_BTa(1-exp(-Fa/k_BT))}\int_0^a dx\int_0^a dx' exp(-\frac{Fx}{k_BT})exp(\frac{U_p(x+x')-U_p(x')}{k_BT}). \tag{2.13}$$

The dimensionless function $\nu_a(F)$ in the limit $F \to 0$ coincides with the analogous quantity introduced in Ref. [31]. It has the physical meaning of the probability of the vortex sitting on the pinning plane to overcome the potential barrier, the characteristic value of which is denoted as U_0. This can be seen by considering the limiting cases of high ($k_BT \gg U_0$) and low ($k_BT \ll U_0$) temperatures. In the case of high temperatures $\nu_a \approx 1$, and expression 2.12 corresponds to the flux-flow regime. Indeed, in this case the influence of pinning can be neglected. In the case of low temperatures ν_a is a function of the current. For strong currents ($Fa \gg U_0$) the potential barrier disappears leading to $\nu_a \approx 1$, and the FF regime is realized. For small currents ($Fa \ll U_0$) function $\nu_a \sim exp(-U_0/k_BT)$, which corresponds to the regime of thermally activated flux flow (TAFF) [15]. The transition from the TAFF regime to the FF regime is associated with a lowering of the potential barrier with increase of the current.

2.3 The nonlinear conductivity and resistivity tensors

The electric field field induced by a moving vortex system is

$$\mathbf{E} = \mathbf{B}\times < \mathbf{v} >= nB(- < v_y > \mathbf{m} + < v_x > \mathbf{m}_{\|}). \tag{2.14}$$

This can be also written in form

$$\begin{aligned} E_x &= -nB < v_y >, \\ E_y &= nB < v_x > . \end{aligned} \tag{2.15}$$

Since the mean velocity of a vortex is equal to

$$< \mathbf{v} >= \frac{\int\int \mathbf{S} d^2r}{\int\int P d^2r} = \frac{\int_0^a \mathbf{S}(x)dx}{\int_0^a P(x)dx} \tag{2.16}$$

and taking into account Eq. 2.15, integration of Eq. 2.8 leads to the following simple linear relation between the electric field components E_x, E_y and the transport current density J_x:

$$(1/\gamma)E_x + n\epsilon E_y = \rho_f J_x, \tag{2.17}$$

where $\rho_f \equiv \Phi_0 B/\eta_0$ is the average (see Eq. 2.2) resistivity to flux flow. Because $J_x = \sigma_{xx}E_x + \sigma_{xy}E_y$, it follows from Eq. 2.17 that the components of the conductivity tensor are $\sigma_{xx} = (\gamma\rho_f)^{-1}$ and $\sigma_{xy} = n\epsilon/\rho_f$, and they obey linear scaling

$$\sigma_{xy}/\sigma_{xx} = \rho_{yx}/\rho_{yy} = n\gamma\epsilon.$$

Below we will see that such simple scaling does not exist for the components σ_{yy} and σ_{yx} of the conductivity tensor.

From formulas 2.12, 2.15, and 2.17 one obtains the current-voltage characteristics in the xy coordinate system:

$$e_x = \gamma j_x - \frac{\epsilon\nu_a(f)f}{1+\epsilon^2} \tag{2.18}$$

$$e_y = \frac{n\nu_a(f)f}{\gamma(1+\epsilon^2)} \tag{2.19}$$

Here the dimensionless components of the electric field are measured in units of $E_0 = \sqrt{4\pi\varepsilon_0}BU_0/(a\eta_0)$ and of the current in units of $J_0 = U_0/(\Phi_0 a)$; and $f = Fa/U_0 = nj(\cos\alpha + n\gamma\epsilon\sin\alpha) = nj_y + \gamma\epsilon j_x$. From expressions 2.18 and 2.19 on can find the conductivity tensor whose components are measured in units of $1/\rho_f$ for the nonlinear law $\mathbf{j} = \hat{\sigma}(\mathbf{E})\mathbf{E}$:

$$\hat{\sigma} = \begin{pmatrix} \sigma_{xx} & \sigma_{xy} \\ \sigma_{yx} & \sigma_{yy} \end{pmatrix} = \begin{pmatrix} 1/\gamma & n\epsilon \\ -n\epsilon & \sigma_{yy}(E_y) \end{pmatrix}, \tag{2.20}$$

where the only component depending on the electric field (or current), σ_{yy}, is given by

$$\sigma_{yy}(e_y) = \frac{n}{e_y}\tilde{\nu_a}^{-1}(n\gamma(1+\epsilon^2)e_y) - \gamma\epsilon^2, \tag{2.21}$$

$\tilde{\nu_a}^{-1}$ is the inverse function of $\tilde{\nu_a}(f) \equiv \nu_a(f)f$. From physical arguments it follows that the function $\nu_a(f)$ is monotonically increasing with f and, consequently, $\tilde{\nu_a}(f)$ is also monotonic and its inverse function $\tilde{\nu_a}(f)^{-1}$ is unique. From the definition 2.13 it can be shown that for a periodic potential possessing even parity, $U_p(-x) = U_p(x)$, the function $\nu_a(f)$ is even in f, i.e., $\nu_a(-f) = \nu_a(f)$. Correspondingly, $\tilde{\nu_a}(f)$ is odd in f. The resistivity tensor $\hat{\rho}$ whose components are measured in units of ρ_f, which is the inverse tensor to $\hat{\sigma}$, has the form

$$\hat{\rho} = \begin{pmatrix} \rho_{xx} & \rho_{xy} \\ \rho_{yx} & \rho_{yy} \end{pmatrix} = \begin{pmatrix} \gamma[1-\epsilon^2\nu_a(f)/(1+\epsilon^2)] & -n\epsilon\nu_a(f)/(1+\epsilon^2) \\ n\epsilon\nu_a(f)/(1+\epsilon^2) & \nu_a(f)/[\gamma(1+\epsilon^2)] \end{pmatrix}. \tag{2.22}$$

It is evident from Eq. 2.22 that all components of the tensor $\hat{\rho}$ (in contrast to the tensor $\hat{\sigma}$) are functions of the current density $\mathbf{j}$ and the angle α between the direction of the current and the vector $\mathbf{m}_{||}$.

One can introduce the L and T geometries in which $\mathbf{j} \,||\, \mathbf{m}$ and $\mathbf{j} \perp \mathbf{m}$, respectively. In other words, in the L geometry vortex motion is longitudinal, in the T geometry vortex motion is transversal with respect to the pinning planes. If one neglects the Hall terms in Eq. 2.22 (i.e. $\epsilon \to 0$), then in the L geometry vortex motion takes place along the pinning planes, and in the T geometry transverse to the pinning planes. In the L geometry the critical current is equal to zero since

the flux-flow regime is realized for guided vortex motion along pinning planes[1]. In the T geometry, a pronounced nonlinear regime is realized for $k_BT \ll U_0$, the onset of which corresponds to the crossover point $j = j_{cr}$, and for $T = 0$ one has $j_{cr} = j_c$, where j_c is the critical current.

The experimentally measured quantities are referenced with regard to the coordinate system associated with the current (see Fig. 2.2). The longitudinal and transverse components of the electric field relative to the direction of the current, $e_{||}$ and $e_{\perp}$, respectively, are related in a simple way to e_x and e_y:

$$e_{||} = e_x \sin\alpha + e_y \cos\alpha, \tag{2.23}$$

$$e_{\perp} = -e_x \cos\alpha + e_y \sin\alpha, \tag{2.24}$$

The field $e_{||}(j, \alpha)$ as a function of j for $\alpha = \text{const}$ is monotonically increasing and reduces to $e_{\parallel} = e_x(j)$ for $\alpha = \pi/2$ (the L geometry) and $e_{\parallel} = e_y(j)$ for $\alpha = 0$ (the T geometry). The field $e_{\perp}(j, \alpha)$ as a function of j for $\alpha = \text{const}$ exhibits a pronounced nonlinearity and has an extremum associated with the guiding effect.

2.4 Model potential and calculation of the magnetoresistivities

The nonlinear properties of the resistivity tensor $\hat{\rho}$ are completely determined by the behavior of the function $\nu_a(F, T)$ which has the physical meaning of the probability of a vortex overcoming the potential barrier created by the pinning sites. In turn, the function $\nu_a(F, T)$, according to formula 2.13, depends on the form of the pinning potential. Here this potential is specified.

Pinning planes are the regions of lowered value of the order parameter; an example is the twins in HTSC [13, 14, 15]. Therefore it is energetically favorable

[1]Isotropic pinning which is usually present in real system and leads to the existence of a nonzero critical current in this geometry is not taken into account in this model.

for vortices to localize in the vicinity of a pinning plane. The resistive properties will be analyzed here on the basis of a pinning potential of the form (Fig. 2.3)

$$U_p = \begin{cases} -F_p x, & 0 \le x \le b \\ F_p(x-2b), & b \le x \le 2b \\ 0, & 2b \le x \le a \end{cases}, \tag{2.25}$$

where $F_p = U_0/b$ is the pinning force. Wells of width $2b$ given by the potential 2.25 correspond to regions of pinning. As the parameter characterizing the defect density the parameter $q = 2b/a$ is used.

Substituting the potential 2.25 into formula 2.13 for the probability function ν_a gives the following expression:

$$\nu_a(f,t,q) = \frac{2f(f^2-1)^2}{2f(f^2-1)(f^2-1+q) - qtG} \tag{2.26}$$

with

$$G = \left[(3f^2+1)\cosh\left(\frac{f}{tq}\right) + (f^2-1)\cosh\left(\frac{f(1-2q)}{tq}\right) \right.$$
$$-2f(f-1)\cosh\left(\frac{f(1-q)}{tq} - \frac{1}{t}\right)$$
$$\left. -2f(f+1)\cosh\left(\frac{f(1-q)}{tq} + \frac{1}{t}\right) \right] \Big/ \sinh\left(\frac{f}{tq}\right)$$

In formula 2.26 the effective external force F acting on the vortices in the direction perpendicular to the pinning planes and causing them to move in this direction is characterized by the parameter f, which gives ratio of this force to the pinning force $F_p = U_0/b$ on the plane defects. The temperature is characterized by the parameter t, which gives the ratio of the energy of the thermal fluctuations of the vortices to the depth of the potential wells U_0 created by the planar defects, $t = k_B T/U_0$. The influence of the external force F acting on the vortices is that it lowers the height of the potential barrier for vortices localized on the pinning planes and, consequently, increases the probability to escape from them. Raising the temperature also increases the probability that a vortex will escape from a

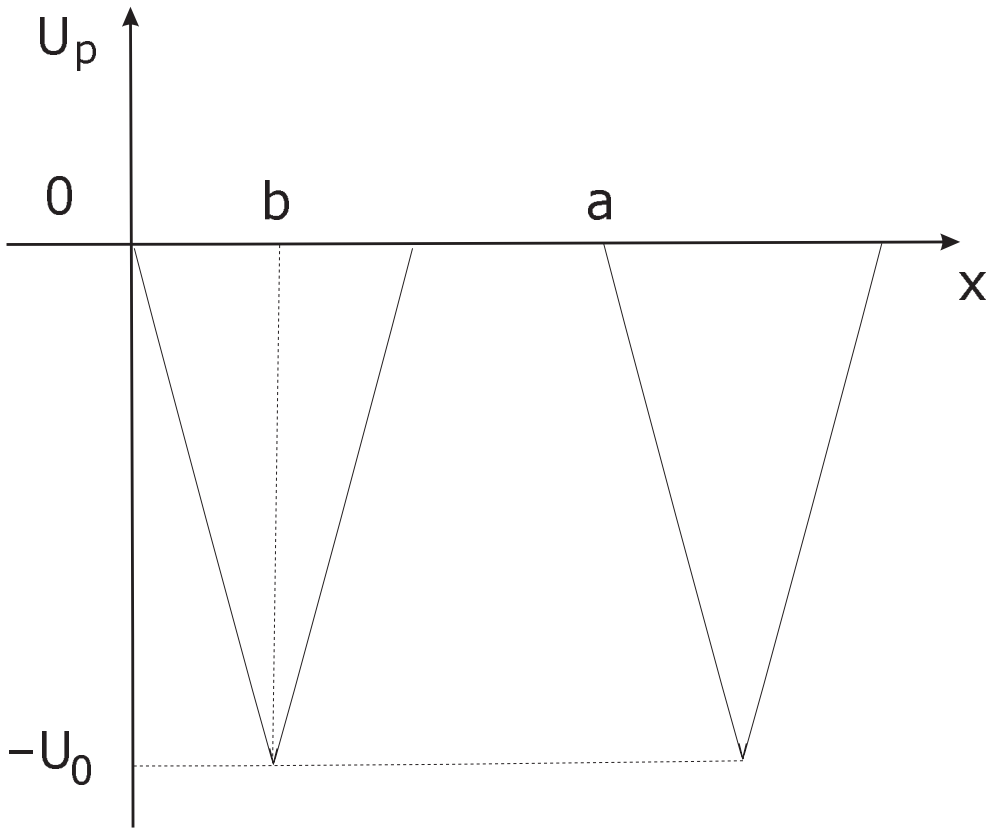

Figure 2.3: *Model pinning potential $U_p(x)$. The period of the potential is a, the width of the potential well is equal to $2b$, U_0 is the depth of the potential well, $q = 2b/a$ characterizes density of the pinning planes. In all of the following dependencies $q = 0.001$.*

pinning plane because of the increase in the energy of the thermal fluctuations of the vortices on the pinning planes. Thus, the pinning potential, tending to localize the vortices, can be suppressed both by an external force and by an increase in temperature.

The function $\nu_{a_0}(f,q)$ (see the case $t=0$ in Fig. 2.4)

$$\nu_{a_0}(f)=\begin{cases} 0, & 0\le t\le 1, \\ (f^2-1)/(f^2-1+q) & f>1, \end{cases} \tag{2.27}$$

corresponds to the zero-temperature limit. In the zero temperature limit, for $F<F_p$, the vortices are trapped in the potential wells of the planar defects and cannot move, while for $F>F_p$ the potential barrier disappears and they begin to move. The value of the current at which $F=F_p$ corresponds to the critical current at zero temperature. Let us consider in turn the dependence of the probability function $\nu_a(f,t,q)$ on each of the quantities f, t for the remaining quantities held fixed (denoted by the subscript "0").

The dependence $\nu_a(f)=\nu_a(f,t_0,q_0)$ characterizing ν_a as a function of the external force acting on a vortex at constant temperature for constant pinning plane density is monotonically increasing from the value $\nu_a(0,t_0,q_0)$ to its limiting value of 1 as $f\to\infty$ (see Fig. 2.4). For $f\gg 1$ the function $\nu_a(f)$ has an expansion $\nu_a(f)\approx 1-q_0f^{-2}$. This corresponds to the physical meaning ν_a as a probability to overcome the potential barrier, $\nu_a\to 1$ if $f\to\infty$. The qualitative form of the dependence $\nu_a(f)$ is determined by the value of the dimensionless parameter t_0 characterizing the temperature. At low temperatures $k_BT\ll U_0$ a nonlinear transition takes place from the TAFF regime of vortex motion perpendicular to the pinning planes to the FF regime when the external force is increasing. In this transition region the function $\nu_a(f)$ has a characteristic nonlinear shape (Fig. 2.4). At high temperatures ($k_BT\ge U_0$) the FF regime is realized over the entire range of variation of the external force.

The dependence $\nu_a(t)=\nu_a(f_0,t,q_0)$, characterizing ν_a as a function of temperature for the external force and pinning plane density fixed, is also a mono-

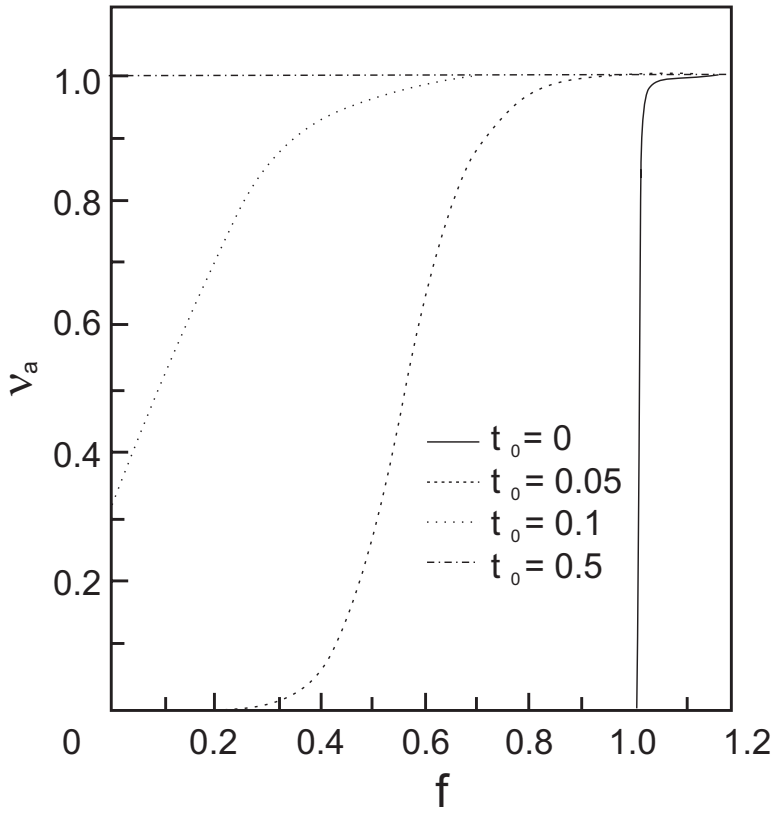

Figure 2.4: *The dependence of the probability function ν_a on the dimensionless parameter f (see text) for different values of the parameter t_0 as indicated.*

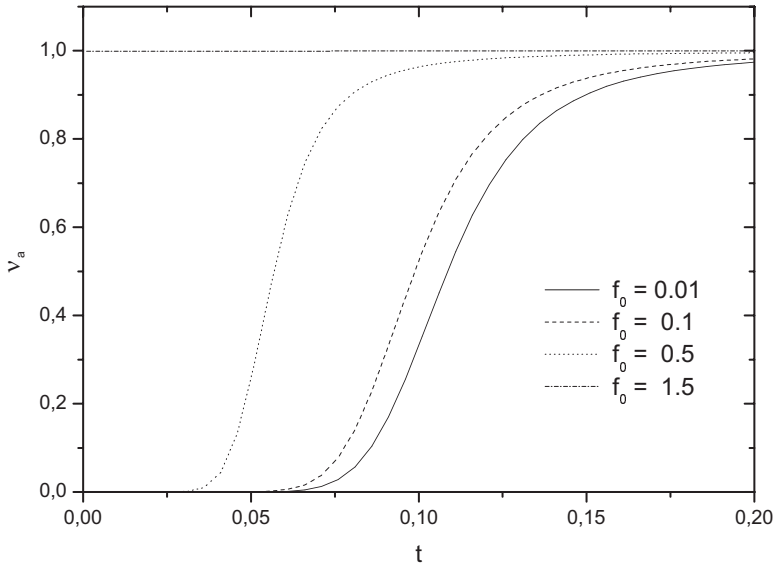

Figure 2.5: *The temperature dependence of the probability function ν_a for different values of the parameter f_0 as indicated ($t = k_BT/U_0$).*

tonically increasing function, and its qualitative form is determined by the value of the parameter f_0. For $t \geq 1$ the expansion of $\nu_a(t)$ in a power series in t has a form $\nu_a(f_0, t, q_0) \approx 1 - q_0 t^{-2}$. Thus, the temperature dependence $\nu_a(t)$ (Fig. 2.5) depicts the nonlinear transition from the TAFF regime of vortex motion perpendicular to the pinning planes to the FF regime as the temperature is raised. It also follows from the above said that the width of the transition from the TAFF to the FF regime, depending on t or f, decreases as q is reduced (see also equation 2.27).

The dynamics of a vortex system with the Hall effect taken into account depends substantially on the direction of the magnetic field. According to equation 2.10, an effective external force F perpendicular to the pinning planes is created by a uniform transport current flowing through the sample. Such a force contains two components – the Lorentz force $n\Phi_0 j_y$ and the Hall force $\phi_0\gamma\epsilon j_x$, acting on the vortex along the x axis. Depending on the direction of the magnetic field indicated by the factor $n = \pm 1$, these two components can be identically or

oppositely directed, and the resulting force will be different in these two cases. In what follows the current density is expressed in unites of $j_c = U_0/(\Phi_0 b)$ so that for the dimensionless parameter f, characterizing the external force, one obtains

$$f = nj\phi(\alpha),\ \phi(\alpha) = \cos\alpha + n\gamma\epsilon\sin\alpha.$$

Thus, the value of the external force $F = F_p$ at which the height of the potential barrier vanishes corresponds to the dimensionless current $j = 1/\phi(\alpha)$, which is equal to the critical current at $T = 0$. In the case $0 < k_B T \ll U_0$ it corresponds to the crossover current j_{cr}. In the function $\nu_a(j\phi(\alpha), t) = \nu_a(f, t, q_0)$ the even component $\nu_a^+ = (\nu_a(+n) + \nu_a(-n))/2$ and the odd component $\nu_a^- = (\nu_a(+n) - \nu_a(-n))/2$ in the magnetic field can be separated. These components determine the observed resistive characteristics - the even and odd components (with respect to magnetic field) of the longitudinal and transverse resistivity $\rho_{||,\perp}^{\pm}$. From the definition of $\nu_a^{\pm}$ it follows that their possible values for any values of j, t, α, ϵ, and q, in according with the values of the function ν_a, always lie between zero and one. It is easy to see that the component ν_a^+ is even in ϵ, i.e., $\nu_a^+(-\epsilon) = \nu_a^+(\epsilon)$, and the component ν_a^- is odd, i.e., $(\nu_a^-(-\epsilon) = -\nu_a^-(\epsilon))$. Therefore, for $\epsilon = 0$ the even component $\nu_a^+ \equiv \nu_a(j_y, t)$, and the odd component $\nu_a^- \equiv 0$. The qualitative behavior and the limits of the component $\nu_a^+(j)$ as $j \to 0$ or $j \to \infty$ coincide with the corresponding limits of $\nu_a(f)$. The component $\nu_a^-(j)$ tends to zero in the linear regimes (as $j \to 0$ or $j \to \infty$) and is nonzero in the region of nonlinearity of ν_a, forming a characteristic peak (see Fig.2.6). The limits of the components $\nu_a^+(t)$ and $\nu_a^-(t)$ as $t \to \infty$ are the same as for $j \to \infty$, and for $t \to 0$ they are equal to the corresponding components $\nu_{a0}^{\pm}$ of the function $\nu_{a0}(j\phi(\alpha))$.

One can obtain expressions from formulas 2.22, 2.23, 2.24 for the experimentally observed longitudinal $\rho_{\|} = e_{\|}/j$ and transverse $\rho_{\perp} = e_{\perp}/j$ resistivities (relative to the current direction) with the Hall effect taken into account. Their even $\rho^+ = (\rho(n) + \rho(-n))/2$ and odd $\rho^+ = (\rho(n) - \rho(-n))/2$ components relative

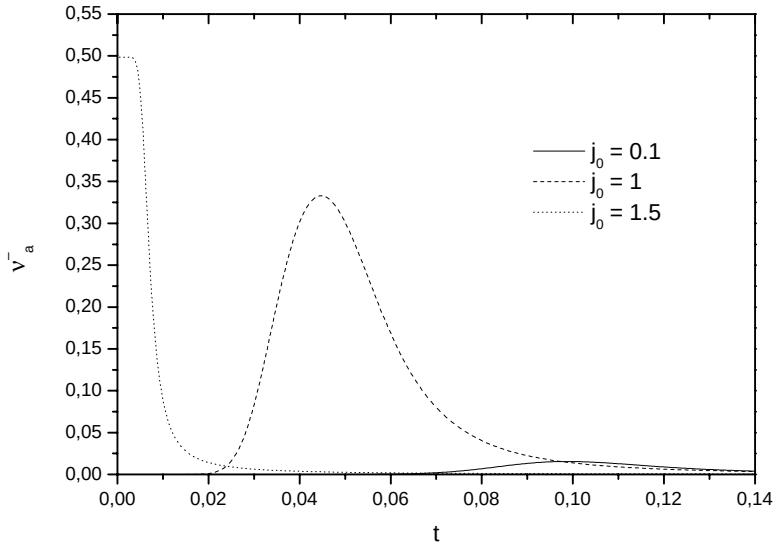

Figure 2.6: *The temperature dependence of the odd component* ν_a^- *of the probability function for the different values of parameter* j_0 *as indicated,* $\alpha = 45°$, $\gamma = 1$, $\epsilon = 0.1$

to the magnetic field inversion are as following:

$$\rho_{\parallel}^{\pm} = \frac{1}{1+\epsilon^2}\left(\frac{1}{\gamma}\cos^2\alpha - \gamma\epsilon^2\sin^2\alpha\right)\nu_a^{\pm} + \frac{\gamma}{2}(1\pm 1)\sin^2\alpha, \tag{2.28}$$

$$\rho_{\perp}^{\pm} = \frac{1}{1+\epsilon^2}\left(n\epsilon\nu_a^{\mp} + (\frac{1}{\gamma} + \gamma\epsilon^2)\nu_a^{\pm}\sin\alpha\cos\alpha\right) - \frac{\gamma}{2}(1\pm 1)\sin\alpha\cos\alpha, \tag{2.29}$$

where $\nu_a^{\pm}$ are the above-defined even and odd components, relative to the magnetic field direction, of the function $\nu_a(j\phi(\alpha), t)$. In equations 2.28 and 2.29 the nonlinear and linear (nonzero only for $\rho_{\parallel,\perp}^{\pm}$) terms separate out in a natural way. The physical reason for the appearance of linear terms is that in the model under consideration for $\alpha \neq 0$ there is always FF regime of vortex motion along the pinning planes.

2.5 Probability function and the average pinning force

The physical meaning of the introduced ν_a-function is a probability of the vortex to jump over the pinning barrier. There exists an another physical interpretation and it is shown below that ν_a-function has a close relationship to the average pinning force acting on the vortex.

Neglecting a Hall-effect, i.e. $\epsilon \ll 1$, and taking anisotropy parameter $\gamma = 1$ one can average Eq. 2.1 as follows:

$$\eta_0 < \mathbf{v} > = < \mathbf{F}_L > + < \mathbf{F}_p > \tag{2.30}$$

Because the pinning potential U is a function of only coordinate x, the pinning force $\mathbf{F}_p$ has only an x-component and

$$\begin{cases} \eta_0 < v_x > = F_{Lx} + < F_p > \\ \eta_0 < v_y > = F_{Ly}. \end{cases} \tag{2.31}$$

On the other hand for $\epsilon \ll 1$ and $\gamma = 1$

$$\begin{cases} \eta_0 < v_x > = F_{Lx}\nu_a(F_{Lx}) \\ \eta_0 < v_y > = F_{Ly}, \end{cases} \tag{2.32}$$

where the first equation follows directly from Eq. 2.12 and the second is obtained by integration of Eq. 2.8, taking into account the definition of the average velocity (Eq. 2.6).

Comparing Eqs. 2.31 and 2.32 it is evident that the average pinning force acting on the vortex is connected with ν_a-function in an easy way

$$< F_p > = -F_{Lx}(1 - \nu_a). \tag{2.33}$$

The ν_a-function is a probability function so it always fulfills the condition $0 \leq \nu_a \leq 1$. There are two limiting cases for this function. The condition $\nu_a = 1$ corresponds to the case when the probability of the vortex to jump across the

pinning barrier is equal to 1 and the pinning barriers do not affect the vortex motion any more. According to Eq. 2.33 the average pinning force is equal to zero in this case which is quite consistent with a qualitatively expected physical picture.

If $\nu_a = 0$, i.e. the probability of the vortex to jump across the pinning barrier is zero. The average pinning force acting on the vortex is maximal and equal to $-F_{Lx}$ according to Eq. 2.33.

The dependence of the guiding angle β on ν_a-function is also clear from Eq. 2.32. The magnitude of this angle is defined by the ratio v_x/v_y. It is easy to see, that with growth of ν_a-function v_x component increases and thus the guiding angle increases. If $\nu = 0$ than the guiding angle is equal to the angle α between the transport current direction and the pinning planes.

2.6 Influence of additional point-like pinning on the guided vortex motion

In the model described up to now only anisotropic pinning produced by the parallel pinning planes is taken into account. The absence of isotropic pinning leads to the absence of a critical current for all current directions with respect to the pinning planes, except for $\alpha = 0$. To remedy this obvious discrepancy with regard to the experimental observations, an isotropic pinning caused by uncorrelated point-like defects must also be considered. In this chapter a short summary of an extension of the described theoretical model on anisotropic pinning is given.

In the presence of uncorrelated point-like defects each vortex moving with velocity $\mathbf{v}$ is subject of an isotropic pinning force $\mathbf{F}_p^i$ which can be formulated as

$$\mathbf{F}_p^i = -\eta_i(v)\mathbf{v}, \tag{2.34}$$

where $\eta_i(v)$ is a velocity-dependent viscosity and $v = |\mathbf{v}|$. The Langevin equation

for vortex motion (Eq. 2.1) must be modified in this case as follows

$$\eta_0 \mathbf{v} + n\alpha_H[\mathbf{v} \times \mathbf{z}] = \mathbf{F}_L + \mathbf{F}_p^a + \mathbf{F}_p^i + \mathbf{F}_{th}. \tag{2.35}$$

For purely isotropic pinning, $\mathbf{F}_p^a = 0$, and for $\mathbf{F}_{th} = 0$ solution of Eq. 2.35 was obtained in [88]. One can show that this solution can be presented in general case in terms of the probability function of overcoming the effective current- and temperature-dependent potential barrier of isotropic pinning, $\nu_i(F_L)$, which is simply related to η_i as $\nu_i(F_L) = \eta_0/\eta_i(v)$ [45].

Using the ansatz 2.34 one can reduce Eq. 2.35 to the form

$$\eta \mathbf{v} + n\alpha_H[\mathbf{v} \times \mathbf{z}] = \mathbf{F}_L + \mathbf{F}_p^a + \mathbf{F}_{th} \tag{2.36}$$

where $\eta = \eta(v) \equiv \eta_0 + \eta_i(v)$. It was shown in [45] that using the results from the previous section the solution of Eq. 2.36 can be written in the form

$$\eta_0 < \mathbf{v} >= \nu_i(F_H)\mathbf{F}_H \tag{2.37}$$

where the vector $\mathbf{F}_H$ has the following components:

$$\begin{aligned} F_{Hx} &= (F_x \nu_a(F_x))/(1+\tilde{\epsilon}^2), \\ F_{Hy} &= F_{Ly} + (n\tilde{\epsilon} F_x \nu_a(F_x))/(1+\tilde{\epsilon}^2). \end{aligned} \tag{2.38}$$

Here $F_x \equiv F_{Lx} - n\tilde{\epsilon}F_{Ly}$. $F = \sqrt{F_{Hx}^2 + F_{Hy}^2}$, F_{Lx} and F_{Ly} are the $x-$ and $y-$ components of the Lorentz force, respectively and $\tilde{\epsilon} \equiv \epsilon\nu_i(F_H)$. The functions ν_i and ν_a have the physical meaning of the probability to overcome the isotropic and anisotropic pinning barrier, respectively. Both, ν_i and ν_a can be calculated using a simple model potential as described earlier (see Eq. 2.25 and Fig. 2.3) with different potential depths U_0, period a, and the characteristic dimension of the potential well b for isotropic and anisotropic pinning.

In the limit of a small Hall constant, $\tilde{\epsilon}$ is simplified to $\epsilon \ll 1, \quad \tilde{\epsilon} = \epsilon\nu_i(F_{H0})$, where $F_{H0} \equiv F_H(\epsilon = 0)$ and the right-hand part of Eq. 2.37 becomes v-independent. All the subsequent results will be discussed in this limit.

Analogous to the previous section the even and odd components of the longitudinal and transverse magnetoresistivities, defined by the relations $\rho^{\pm} = (\rho(n) \pm \rho(-n))/2$, were calculated in [45, 46]:

$$\begin{aligned} \rho_{\parallel}^{+} &= (\sin^2\alpha + \nu_a(F_{Lx})\cos^2\alpha)\nu_i(F_{H0}), \\ \rho_{\parallel}^{-} &= (\sin^2\alpha + \nu_a(F_{Lx})\cos^2\alpha)\nu_i^{-}(F_H) + \nu_i(F_{H0})\nu_a^{-}(F_x)\cos^2\alpha. \end{aligned} \tag{2.39}$$

$$\begin{aligned} \rho_{\perp}^{+} &= -\nu_i(F_{H0})(1-\nu_a(F_{Lx}))\sin\alpha\cos\alpha, \\ \rho_{\perp}^{-} &= n\epsilon\nu_a(F_{Lx})\nu_i^2(F_{H0}) + \Big(\nu_a^{-}(F_x)\nu_i(F_{H0}) - \nu_i^{-}(F_H)(1-\nu_a(F_{Lx}))\Big)\sin\alpha\cos\alpha. \end{aligned} \tag{2.40}$$

Here ν_i^{-} and ν_a^{-} are the odd components of the probability functions $\nu_i(F_H)$ and $\nu_a(F_x)$, respectively. The dependence of function ν_i^{-} on the parameters j and t are analogous to those of the function ν_a^{-} as described in the previous section.

In the isotropic case $\nu_a = 1$ and from Eqs. 2.39, 2.40 follows that

$$\rho_{\parallel}^{+} = \rho_{\parallel i} = \nu_i(F_i), \qquad \rho_{\perp}^{-} = \rho_{\perp i} = n\epsilon\nu_i^2(F_i), \tag{2.41}$$

where $F_i = F_{H0}(\nu_a = 1) = |\mathbf{F}|$. The well-known scaling relation $\rho_{\parallel i} \propto \rho_{\perp i}^2$, derived in [88], follows from Eqs. 2.41. Note also that in the isotropic case $\rho_{\parallel i}^{-} = \rho_{\perp i}^{+} = 0$.

For convenience equations 2.39, 2.40 can be represented in the form

$$\rho_{\parallel}^{+} = \tilde{\rho}_{\parallel i} \cdot \rho_{\parallel a}^{+}, \quad \rho_{\perp}^{+} = \tilde{\rho}_{\parallel i} \cdot \rho_{\perp a}^{+}, \tag{2.42}$$

$$\rho_{\parallel}^{-} = \nu_i^{-}\rho_{\parallel a}^{+} + {\tilde{\rho}_{\parallel i}}^2 \cdot \rho_{\parallel a}^{-}, \quad \rho_{\perp}^{-} = \tilde{\nu}_{\parallel i}^2 \cdot \rho_{\perp a}^{-} - \frac{1}{2}\nu_i^{-}(1-\nu_a)\sin 2\alpha. \tag{2.43}$$

Here $\tilde{\rho}_{\parallel i} \equiv \nu_i(F_{H0})$ is the probability function ν_i of the anisotropic argument $F_{H0} = \sqrt{F_{Lx}^2\nu_a^2(F_{Lx}) + F_{Ly}^2}$. The magnetoresistivities $\rho_{\parallel a}^{\pm}$, $\rho_{\perp a}^{\pm}$ and the $\nu_a \equiv \nu_a(F_{Lx})$ function are the same as $\rho_{\parallel}^{\pm}$, $\rho_{\perp}^{\pm}$ and ν_a presented in section 2.4, respectively. Furthermore, $\nu_i^{-} = \nu_i^{-}(F_H(n))$ and $F_H(n) = [F_{Ly}^2 + F_{Lx}^2\nu_a^2(F_x) + 2n\epsilon\nu_i(F_{H0})F_{Lx}F_{Ly}\nu_a(1-\nu_a)]^{1/2}$.

It is clear from Eqs. 2.42 and 2.43 that the current and temperature dependencies of the magnetoresistance components $\rho_{\parallel,\perp}^{\pm}$ is governed only by the dependencies on the current and temperature of the odd and even components of the

probability functions ν_i and ν_a. It can also be shown that for the case of a small Hall effect, $\epsilon \ll 1$, terms proportional to ϵ are absent in the even components of the longitudinal and transversal resistivity and only contributions describing the competition between isotropic pinning and nonlinear guiding at the pinning planes in terms of the $\nu_i^{\pm}$ and $\nu_a^{\pm}$ functions are present [45, 46].

In order to describe the guided vortex motion along the pinning planes, the angle β between the transport current direction and vortex velocity can be used (see Fig. 2.2). It can be shown that $\cot\beta = -\rho_{\perp}^{+}/\rho_{\parallel}^{+}$ [35]. On the other hand, in the case of a small Hall effect ($\epsilon \ll 1$) and for a small normal-state anisotropy ($\gamma = 1$) from Eqs. 2.42 and 2.28, 2.29 it follows that

$$\cot\beta = -\frac{\rho_{\perp}^{+}}{\rho_{\parallel}^{+}} = \frac{1-\nu_a}{\tan\alpha + \nu_a \cot\alpha} \tag{2.44}$$

From this relation it is easy to see that the guiding angle β is not influenced by the isotropic disorder because it does not depend on ν_i. Isotropic pinning therefore influences only the magnitude of the vortex velocity but not the direction of it [46].

2.7 Conclusions

As was briefly shown, it is possible to describe analytically the vortex dynamics in a superconductor with correlated pinning planes and uncorrelated point like defects using a simple potential form (Eq. 2.25 and Fig. 2.3) based on a model of pinnig developed in [24, 31, 35, 37, 38, 45, 46]. This model gives relations between the experimentally observed nonlinear resistivities $\rho_{\parallel,\perp}^{\pm}$ in external magnetic field and the functions ν_a and ν_i which are the probabilities of a vortex to overcome the anisotropic and isotropic pinning barrier, respectively. The nonlinear dependence of these probability functions on current and temperature leads to nonlinearities in the magnetoresistive response of the superconductor in the mixed state. The appearence of two new resistivity components, namely $\rho_{\parallel}^{-}$ and $\rho_{\perp}^{+}$ due only to

the pinning anisotropy, is predicted. The anisotropy in this theoretical model is produced solely by planar defects, the randomly distributed point like pinning centers have an effect only on the absolute value of the vortex velocity but they do not affect its direction. The additional isotropic point-like pinning results furthermore in an appearance of a critical current j_c for all transport current orientations, whereas in the previous model, with only anisotropic pinning taken into account (see section 2.2), a critical current exists only for the current oriented at an angle $\alpha = 0$ with regard to the planar defects.

Chapter 3

Guided vortex motion in unidirectionally twinned $YBa_2Cu_3O_{7-\delta}$ films

3.1 Twin formation in $YBa_2Cu_3O_{7-\delta}$

The crystal structure of $YBa_2Cu_3O_{7-\delta}$ depends on the value of the parameter δ. $YBa_2Cu_3O_6$ has a tetragonal symmetry (space group P4/mmm), corresponding to a unit cell as is schematically shown in Fig. 3.1(a). The (001) plane of $YBa_2Cu_3O_6$ (the base plane of the cell shown in the picture) contains only Cu atoms. The cell parameters are $a = b = a_t = 0.3865$ nm, $c = 1.1825$ nm (see Table 3.1). With increasing δ a transition into orthorhombic symmetry (space group Pmmm) occurs. Additional oxygen atom occupy the sites between the Cu atoms along the b axis as illustrated in Fig. 3.1(b). The orthorhombic state of $YBa_2Cu_3O_{7-\delta}$ is the stable phase at room temperature.

The transition from the tetragonal to the orthorhombic modification, which is a phase with lower symmetry, leads to the formation of a twinned structure of $YBa_2Cu_3O_{7-\delta}$ due to the strain release during the transition. In order to achieve

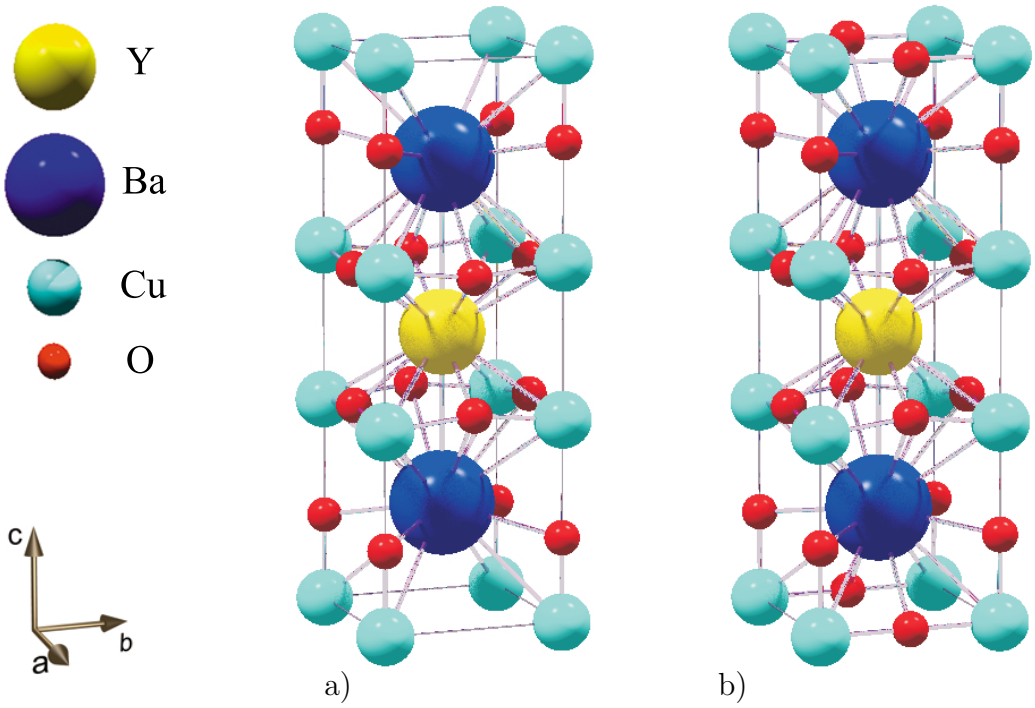

Figure 3.1: *Unit cell of* $YBa_2Cu_3O_{7-\delta}$*, a) thetragonal, b) orthorhombic.*

a good strain compatibility the orthorhombic phase must adopt those orientations for which the area of contact of its unit cell with that of the tetragonal phase is conserved at the interface. To a first approximation this requires that the diagonals of the *ab*−planes of the unit cells of the two phases be superimposed at the interface [47].

In Fig. 3.2 the epitaxial relations between the tetragonal and the orthorhombic phases are shown schematically. The dashed square is a projection of the original tetragonal structure onto the *ab*-plane. There are two possible orientations of the orthorhombic cell: S_1 and S_2 if the sides of the orthorhombic and tetragonal cells stay parallel to each other. Because the diagonal chosen for epitaxial matching with the tetragonal cell can be either [110] or $[1\bar{1}0]$, each state S_1 and S_2 can adopt two suborientations, denoted by superscripts "+" (an anticlockwise suborientation) and "−" (a clockwise suborientation). For the diagonal [110] two orientations of the orthorhombic structure are possible: S_1^- and S_2^+ (notation is

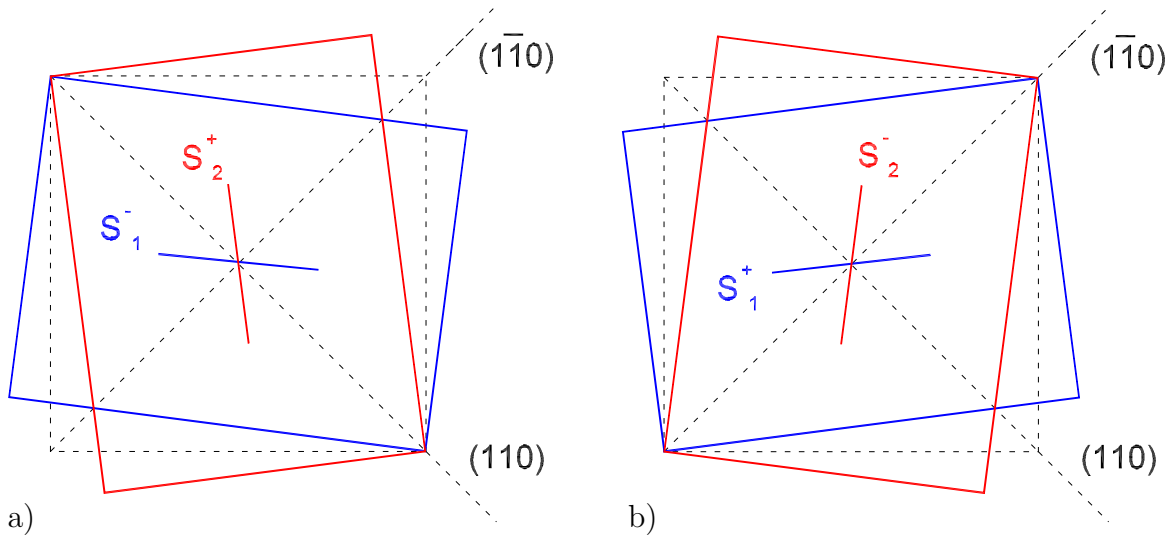

Figure 3.2: *Epitaxial relationship between the tetragonal phase (solid rectangles) and the orthorhombic phase of* $YBa_2Cu_3O_6$ *(dashed squares). The figure is drown not to scale, to emphasize an orthorhombic distortion of* $YBa_2Cu_3O_{7-\delta}$.

according to Wadhawan [48]). For the [1$\bar{1}$0] diagonal the directions are accordingly S_1^+ and S_2^-. Twin walls are called coherent if only the sub-orientation states S_1^- and S_2^+ or only S_1^+ and S_2^- are contiguous in the crystal, otherwise they are incoherent. Fig. 3.3 illustrates a projection of a crystal structure containing a (110) twin wall on the *ab*-plane.

Usually coherent and incoherent twins coexist in $YBa_2Cu_3O_{7-\delta}$ single crystals, whereas the twinning in thin films depends strongly on the structure of the underlying substrate. The most often used substrates for $YBa_2Cu_3O_{7-\delta}$ thin film deposition are $SrTiO_3$, $NdGaO_3$, MgO, and $LaAlO_3$.

$SrTiO_3$ has a cubic structure with lattice parameter $a = 0.3905$ nm and is widely used for $YBa_2Cu_3O_{7-\delta}$ thin film deposition because of the good lattice fit with the $YBa_2Cu_3O_{7-\delta}$ crystal structure.$NdGaO_3$, on the other hand, has an orthorhombic crystal structure with lattice constants a=0.5428 nm, b=0.5493 nm, c=0.7729 nm [49]. The crystal structure of $NdGaO_3$ can be also described by a pseudocubic perovskite lattice with unit vectors $\mathbf{a}_c = \frac{1}{2}(a, b, 0)$, $\mathbf{b}_c = \frac{1}{2}(-a, b, 0)$,

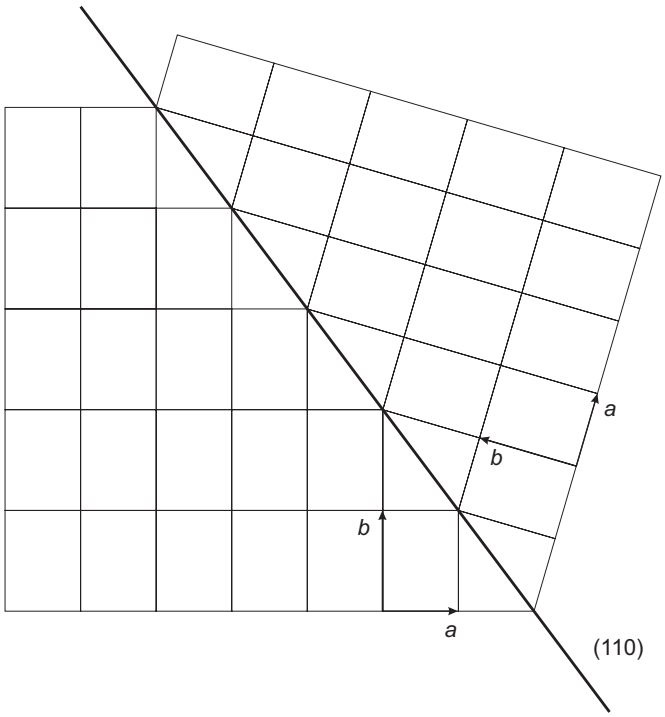

Figure 3.3: *Twinning with (110)-plane as a twin wall. Axis ratio* $b : a = 4 : 3$.

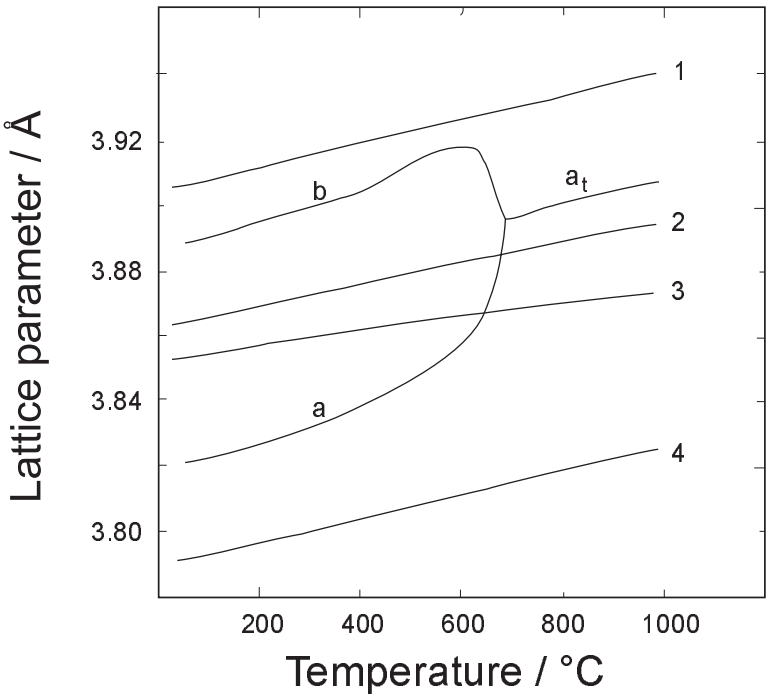

Figure 3.4: *Temperature dependences of lattice parameters for substrate materials having a perovskite-like structure and $YBa_2Cu_3O_{7-\delta}$ (after [53]) 1: $SrTiO_3$; 2: pseudocubic $NdGaO_3$ with lattice constant a_p; 3: pseudocubic $NdGaO_3$ with lattice constant c_p; 4: $LaAlO_3$; a_t: $YBa_2Cu_3O_{7-\delta}$ tetragonal; a, b: $YBa_2Cu_3O_{7-\delta}$ orthorhombic.*

and $\mathbf{c}_c = \frac{1}{2}(0, 0, c)$. The angle between the a_c and b_c axis in the (001) plane is $\gamma = \arccos[(b^2 - a^2)/(b^2 + a^2)] = 89.3°$, which deviates only slightly from a right angle by 0.7°. From Fig. 3.4 is clear that the parameter a_t of $YBa_2Cu_3O_{7-\delta}$ fits perfect the pseudocubic cell of the $NdGaO_3$ for temperatures $T > 700$°C. The other commonly used substrates have a larger lattice mismatch at the interface to a *c*-oriented $YBa_2Cu_3O_{7-\delta}$ film which often leads to the formation of incoherent twins. On $NdGaO_3$ substrates even almost twin free $YBa_2Cu_3O_{7-\delta}$ films with *c*-axis orientation can be grown [50].

The unit cell diagonal of the *ab*-plane of the orthorhombic $YBa_2Cu_3O_{7-\delta}$ is $d = \sqrt{a^2 + b^2} = 0.5449$ nm. The pseudocubic cell of $NdGaO_3$ has two slightly different

	$YBa_2Cu_3O_{7-\delta}$ tetragonal	$YBa_2Cu_3O_{7-\delta}$ orthorhombic	$SrTiO_3$ cubic	$NdGaO_3$ orthorhombic	$NdGaO_3$ pseudocubic
a, nm	0.3865	0.3821	0.3901	0.5428	0.3861
ϵ_a	–	–	2.1%	–	1.0%
b, nm	0.3865	0.3885	0.3901	0.5493	0.3861
ϵ_b	–	–	0.41%	–	-1.0%
c	1.1825	1.1676	0.3901	0.7729	0.3865

Table 3.1: *Lattice parameters a, b, c and lattice mismatch* $\epsilon_x = (x_{sub}/x_{YBCO\,tetr}) - 1$, $x = a, b$ *between different substrates and* $YBa_2Cu_3O_{7-\delta}$ *at room temperature (for tetragonal* $YBa_2Cu_3O_{7-\delta}$ *at* $818\,^\circ C$*).*

diagonals in the *ab*-plane: $d_1 = 0.5428$ nm and $d_2 = 0.5493$ nm. The mismatch ϵ defined analogously to ϵ_x in Table 3.1 for the diagonal d_1 is $\epsilon_{d1} = -0.39\%$, and for the other diagonal $\epsilon_{d_2} = 0.80\%$. Accordingly, there is a prefereable direction for the $YBa_2Cu_3O_{7-\delta}$ diagonal alignment when growing on the (001) $NdGaO_3$ substrate, which can lead to the formation of unidirected twins.

T. Steinborn et al. studied the growth of $YBa_2Cu_3O_{7-\delta}$ thin films on different substrates [51, 54]. It was found that *c*-axis oriented $YBa_2Cu_3O_{7-\delta}$ films grown onto (001) $SrTiO_3$ show the same twin structure as a bulk single crystals, i.e. both, (110) and $(1\bar{1}0)$ twin walls are present in the films. The films grown on $NdGaO_3$ substrates also showed twinning in two directions, but the slight orthorhombicity of the substrate leads to different volume fractions occupied with the two different twin directions.

3.2 Film preparation and X-ray analysis

$YBa_2Cu_3O_{7-\delta}$ films on $SrTiO_3$ and $NdGaO_3$ substrate were prepared using the standard sputter technique. This method is based on a discharge between an anode (substrate) and a cathode, representing a target of the material to be

sputtered, under a DC bias of approximately 300 V. A mixture of argon gas and oxygen with a ratio 4:1 at a pressure of approximately 3 hPa was used. The ions and electrons created and accelerated by the discharge strike the cathode and produce sputtered atoms and secondary electrons which in turn produce additional ionization [52]. After deposition the films were annealed in oxygen atmosphare at 550° C during 30 min.

The crystal quality of the prepared films was analyzed by X-ray diffractometry. The diffractograms measured in Bragg-Bretano geometry show c-axis growth, and the rocking curves of the (005) reflex of $YBa_2Cu_3O_{7-\delta}$ have full width at half maximum of about 0.2° indicating good epitaxial growth on both types of substrates. Twin orientation were explored using a four circle diffractometer with Euler cradle and graphite-monochromatized Cu $K\alpha$ radiation ($\lambda = 1.540$Å). The diameter of the irradiated area on the sample was about 1.2 mm.

To analyze the twins orientation, a series of q-scans for the different (hkl) reflections in the (hk2)-plane of the orthorhombic $YBa_2Cu_3O_{7-\delta}$ structure were performed. For a better understanding of the obtained results the reciprocal lattice of $YBa_2Cu_3O_{7-\delta}$ is considered. The reciprocal unit cell is defined by the unit vectors

$$\mathbf{a}^* = \frac{[\mathbf{b} \times \mathbf{c}]}{V},\ \mathbf{b}^* = \frac{[\mathbf{c} \times \mathbf{a}]}{V},\ \mathbf{c}^* = \frac{[\mathbf{a} \times \mathbf{b}]}{V},$$

where $\mathbf{a}$, $\mathbf{b}$, $\mathbf{c}$ are the unit cell vectors in direct space and V is the volume of the unit cell. In the case of orthogonal crystal systems in reciprocal space only the lengths of the axes change but not the directions when compared with direct space. The angles remain also unchanged. Thus the four possible twin orientations of an orthogonal crystal system showed in Fig. 3.5 are the same for both direct and reciprocal space, except the length of the axis.

Fig. 3.6 shows a scan of the (hk2) plane of a $YBa_2Cu_3O_{7-\delta}$ film deposited on a $NdGaO_3$ substrate. This is a scan with steps of the width Δh, Δk in the vicinity of an chosen point hkl in reciprocal space. This technique gives a possibility to analyze a crystal structure of thin films. Twofold splitting of reflections in

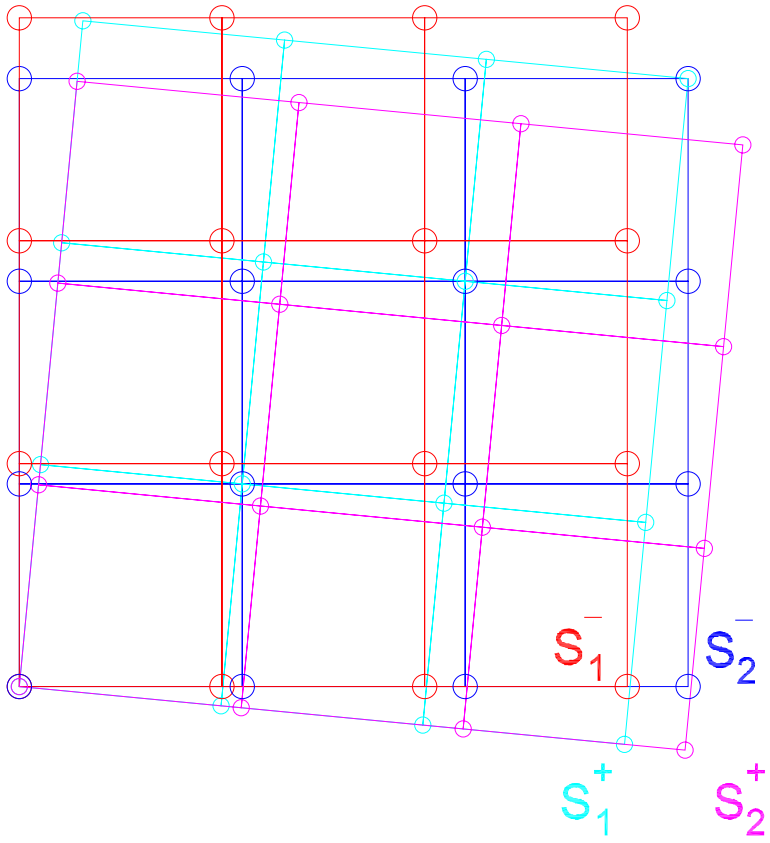

Figure 3.5: *Splitting of the reflections for the four possible twin orientations of* $YBa_2Cu_3O_{7-\delta}$. *The axis ratio is a/b=1.1. The notation is given according to Wadhawan [48] (see also [54]).* S_1^-, S_2^- *– big circles,* S_1^+, S_2^+ *– small circles.*

Fig. 3.6 indicates the existence of twins in the film. A closer look of some of these reflections is shown in Fig. 3.7. A twofold splitting of the reflections (302), (032), ($\bar{2}22$), ($\bar{3}02$), ($0\bar{3}2$), ($2\bar{2}2$) is consistent with the existence of only two twin orientations of the crystal structure, namely S_1^+ and S_2^-. From this it can be concluded that there exist twins aligned only along the (110) plane in the film. For comparison the same (hkl)-scan of a $YBa_2Cu_3O_{7-\delta}$ film grown on a (100) $SrTiO_3$ substrate is shown in Fig. 3.8. The peaks (032), (302), ($0\bar{3}2$), ($\bar{3}02$) show a fourfold splitting, whereas (222), ($\bar{2}22$), ($\bar{2}\bar{2}2$), and ($2\bar{2}2$) are three times split. This can be explained by the existence of four different crystal orientations, i.e. all the orientations S_1^+, S_2^+, S_1^-, S_2^- are present in the film (compare with Fig. 3.5).

The reported X-ray measurements prove the existence of correlated twin planes in the $YBa_2Cu_3O_{7-\delta}$ films grown on (001)-oriented $NdGaO_3$ substrate. The films grown on (100)-oriented $SrTiO_3$ substrates displays uncorrelated twins with twin walls (110) and ($1\bar{1}0$) of $YBa_2Cu_3O_{7-\delta}$.

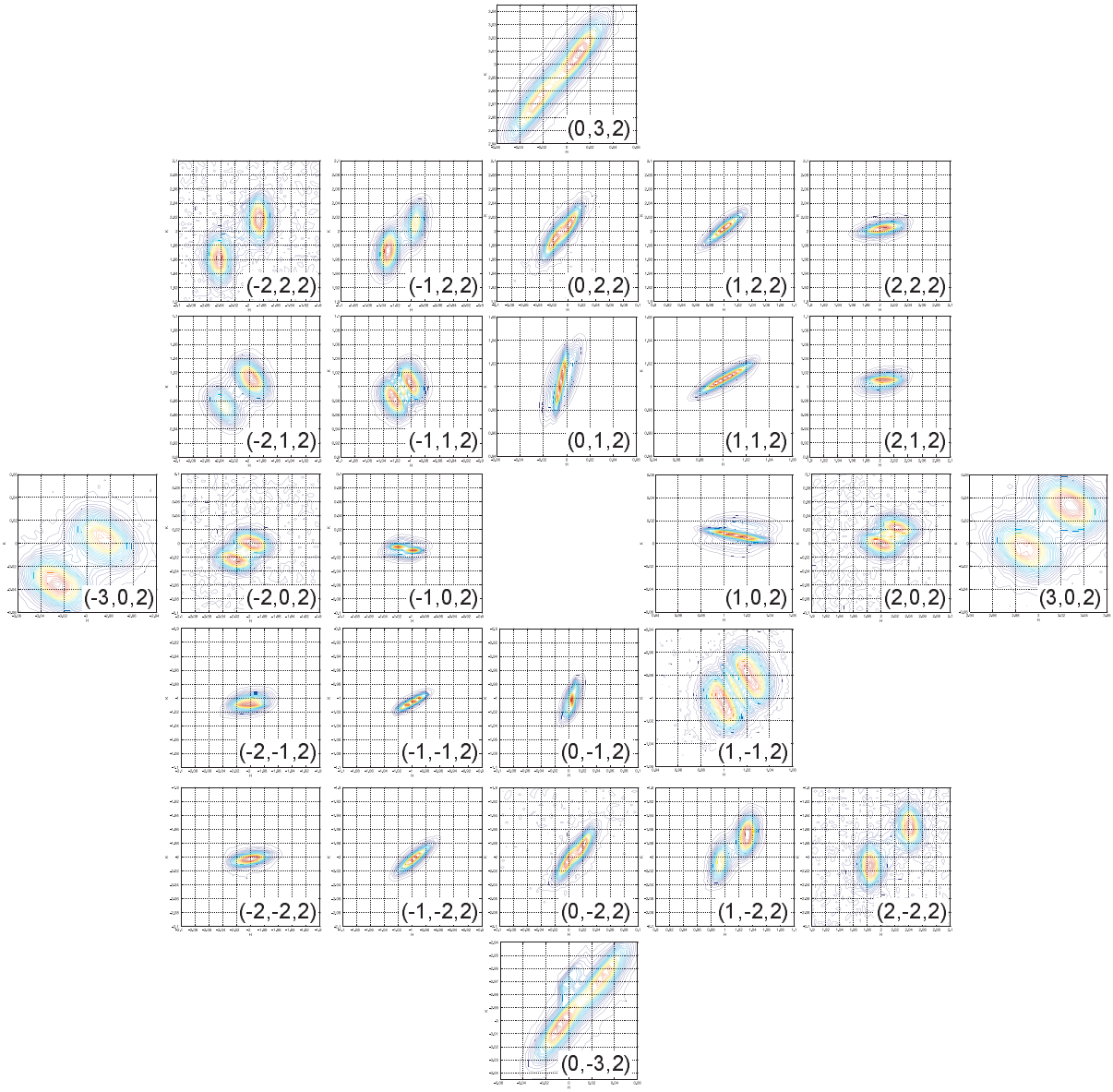

Figure 3.6: *A scan of the (hk2)-plane of* $YBa_2Cu_3O_{7-\delta}$ *film grown on* $NdGaO_3$.

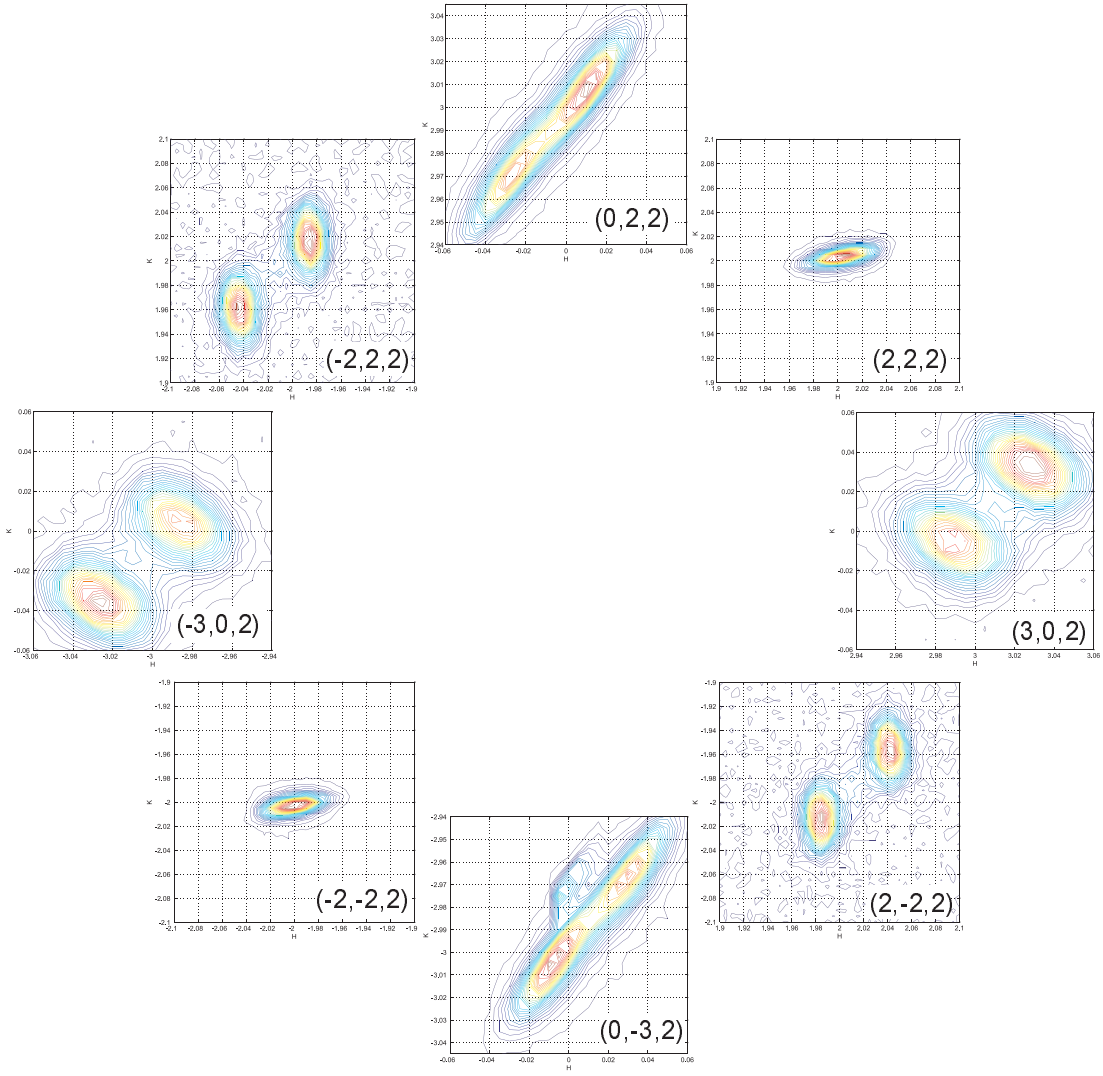

Figure 3.7: *Splitting of the reflections on the scan of the (hk2)-plane of* $YBa_2Cu_3O_{7-\delta}$ *film grown on* $NdGaO_3$.

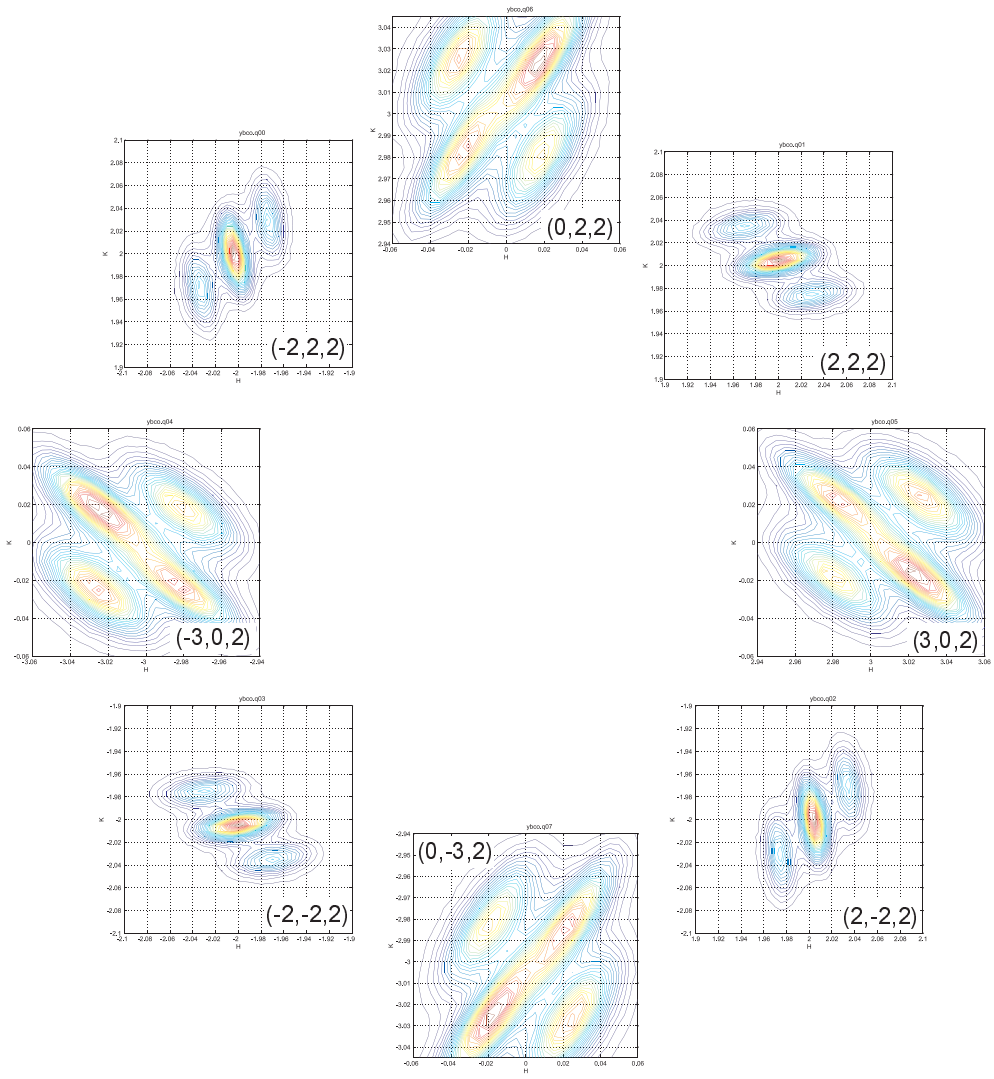

Figure 3.8: *Splitting of the reflections on the scan of the (hk2)-plane of* $YBa_2Cu_3O_{7-\delta}$ *film grown on* $SrTiO_3$.

3.3 Magnetoresistivity measurements

For all the resistivity measurements on the unidirectionally twinned $YBa_2Cu_3O_{7-\delta}$ films the standard four-probe technique was used. Well-defined geometries were required for the measurements of the longitudinal and transversal magnetoresistivities of the samples. Sputtered films were structured into suitable geometry by photolitography and ion-beam etching. A structure as was used for the sample preparation is shown in Fig. 3.9. It consists of seven micro-bridges with a width of 100 μm and a length of 800 μm. This mask configuration allows to measure the longitudinal and transversal voltages for different transport current directions with respect to the twinning planes: $\alpha = 0°$, 10°, 30°, 45°, 60°, 80°, and 90° on the one film.

The patterned samples were mounted on a suitable sample holder and contacted using a wire bonder. All the magnetoresistivity measurements were performed in external magnetic fields perpendicular to the film surface, and the even and the odd longitudinal and transversal magnetoresistivity components were

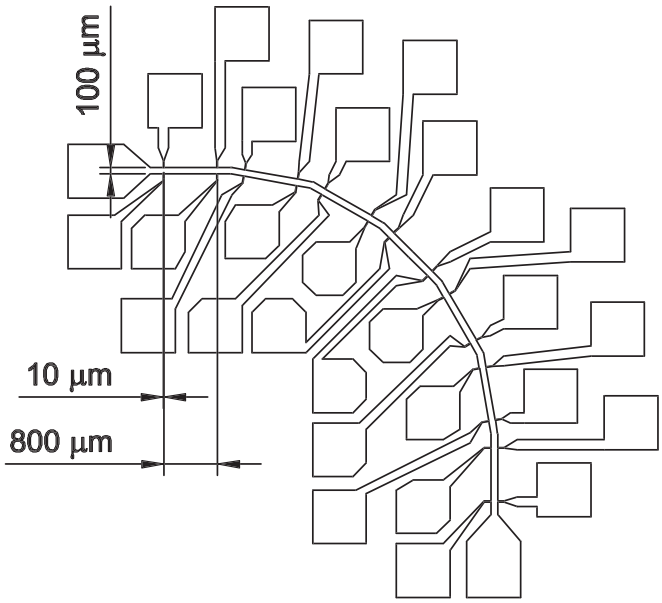

Figure 3.9: *Structure as used for the magnetoresistivity measurements.*

calculated according to the following simple relations:

$$\rho^{\pm}_{\parallel,\perp} = (\rho_{\parallel,\perp}(+\mathbf{H}) \pm \rho_{\parallel,\perp}(-\mathbf{H}))/\mathbf{2} \tag{3.1}$$

The resistively measured superconductive transitions of the samples $ak69$ and $ak81$ are shown in Fig. 3.11 and 3.12. The critical temperature in zero magnetic field is for both samples 90.5 $\pm$0.1 K, with a transition width of about 1 K. The resistivity variations induced by the twins are very small for sample $ak81$ but is noticeably larger for the other sample. However, there is no well-defined systematics in the behaviour of the curves when compared with the results obtained on the Nb-samples (see Chapt. 4).

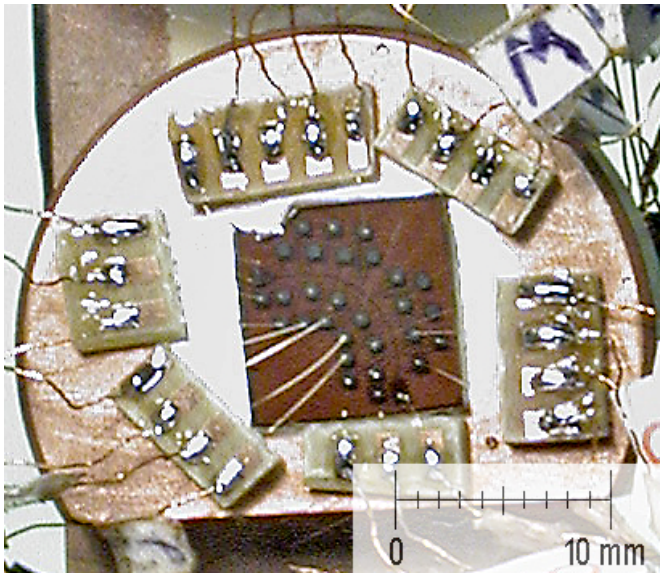

Figure 3.10: *Sample mounted on the sample holder.*

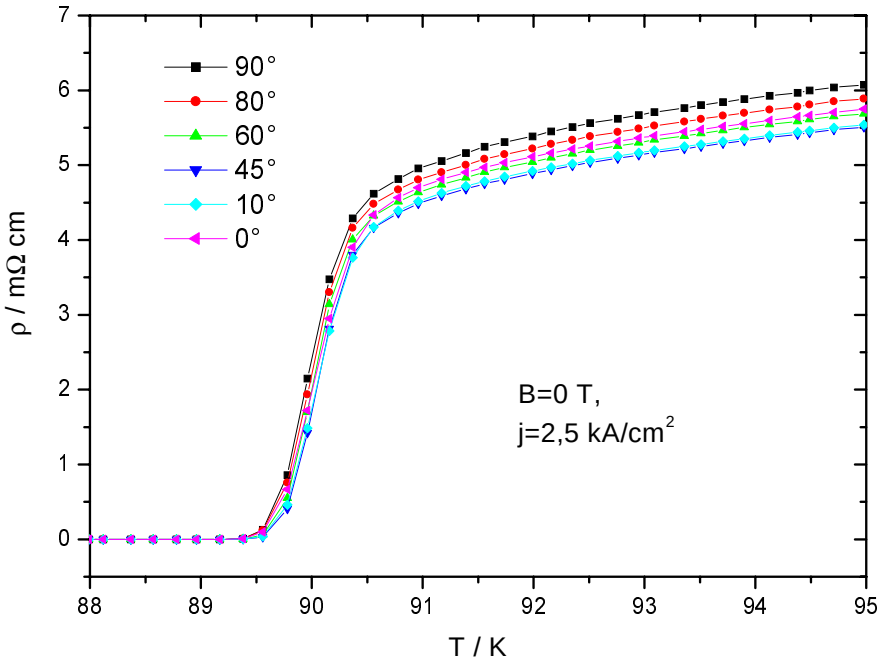

Figure 3.11: *Resistive superconductive transition of sample ak69.*

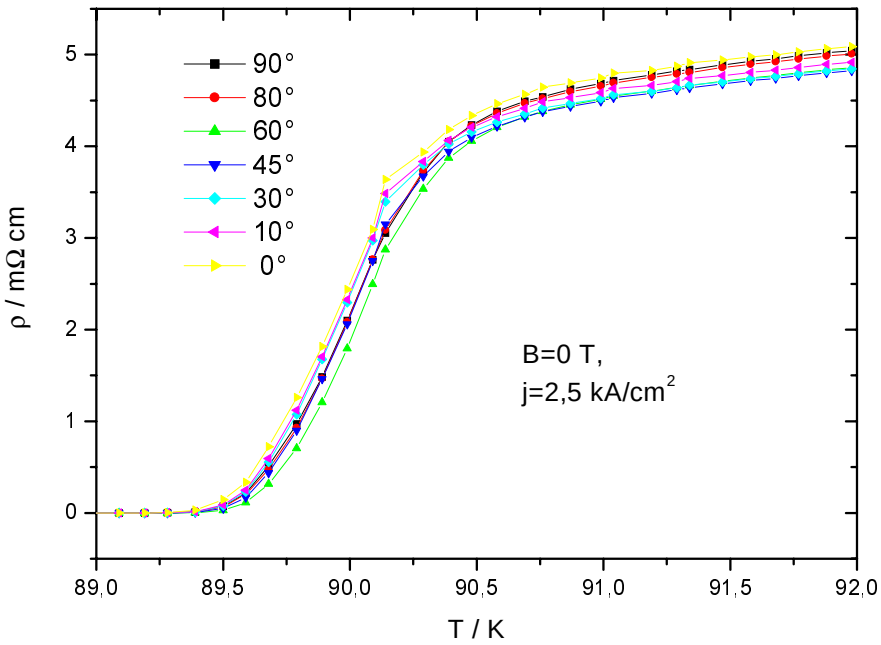

Figure 3.12: *Resistive superconductive transition for sample ak81.*

Fig. 3.13 and 3.14 show magnetic field dependence of the longitudinal even resistivity $\rho_{\parallel}^{+}(B)$ calculated from the experimental data according to relation 3.10 for the samples *ak69* and *ak81*, respectively. The curves do not show a good systematic behaviour so the anisotropy induced by the unidirected twin walls is weak in both samples.

Theory predicts guided vortex motion in this system because of the pinning anisotropy induced by the unidirected twins. One of the consequences of this is the appearance of new components in the magnetoresistivity of the samples, which would be absent in the case of pure isotropic pinning. These components are the odd longitudinal and even perpendicular (odd and even with regard to the magnetic field direction) magnetoresistivity components. Magnetic field dependencies of the odd longitudinal components $\rho_{\parallel}^{-}$, calculated according to relation 3.10, for the samples $ak69$ and $ak81$ are shown in Fig. 3.15 and Fig. 3.16. The resistivity response is not zero (which would correspond to isotropic pinning), but all the curves for both, $ak69$ and $ak81$, samples are very similar. This is in contrast to theory which predicts the odd longitudinal components to be dependent on the angle α between the transport current and the twins direction.

The magnetoresistivity measurements on the unidirectionally twinned $YBa_2Cu_3O_{7-\delta}$ films did not provide evidence for a pronounced guided motion of vortices. A clear anisotropy of the pinning force induced by the twins was not observed.

As a possible explanation of this observation the strong influence of isotropic pinning must be taken into account. Possibly, pinning caused by point-like defects dominates over the plane pinning caused by the unidirected twins. This leads to a suppression of the effects caused by the pinning anisotropy and to a marked isotropization of the vortex pinning. From X-ray analysis, as made for the film characterization, the homogeneity of the twin boundaries in the measured films cannot be proved, i.e. there can be regions in the film where twins are completely absent, which would lead again to the isotropization of the pinning force and

thus to the reduction of the effects connected with the pinning anisotropy in the samples.

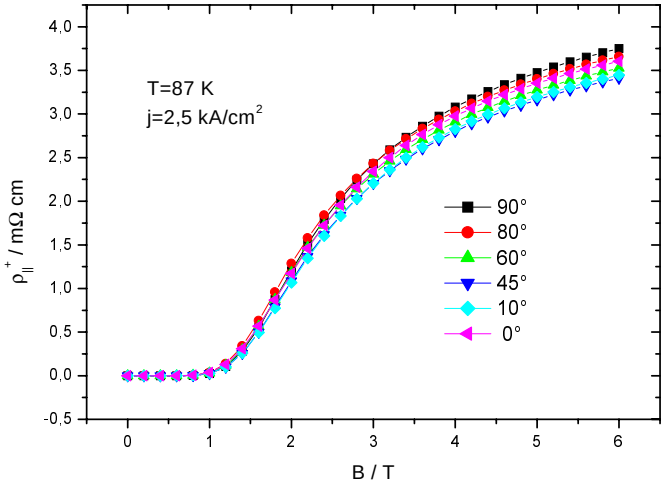

Figure 3.13: *Magnetic field dependence of the even longitudinal component of the magnetoresistivity for the different transport current orientations with respect to the twins as indicated for sample ak69.*

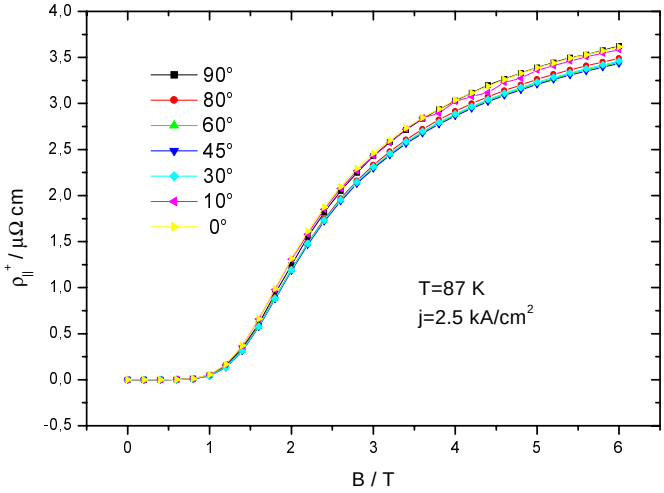

Figure 3.14: *Magnetic field dependencies of the even longitudinal components of the magnetoresistivity for the different transport current orientations with respect to the twins as indicated for the sample ak81.*

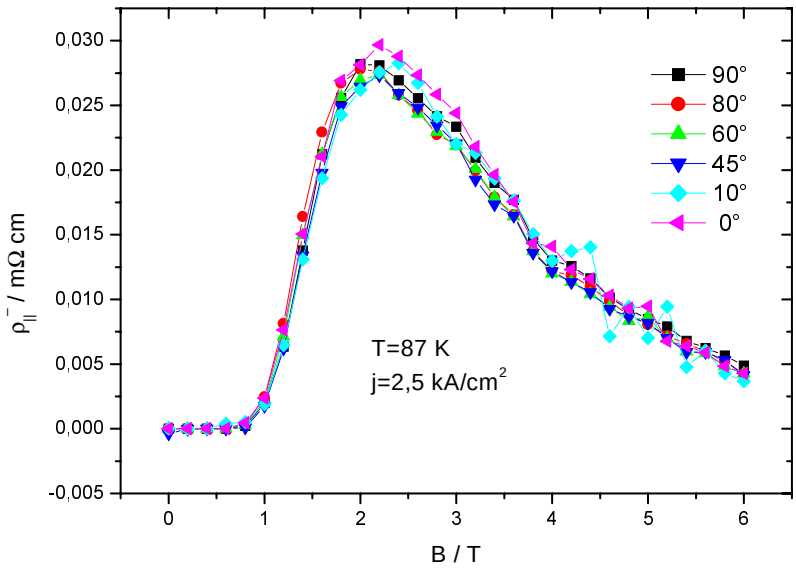

Figure 3.15: *Magnetic field dependencies of the odd longitudinal components of the magnetoresistivity for the sample ak69.*

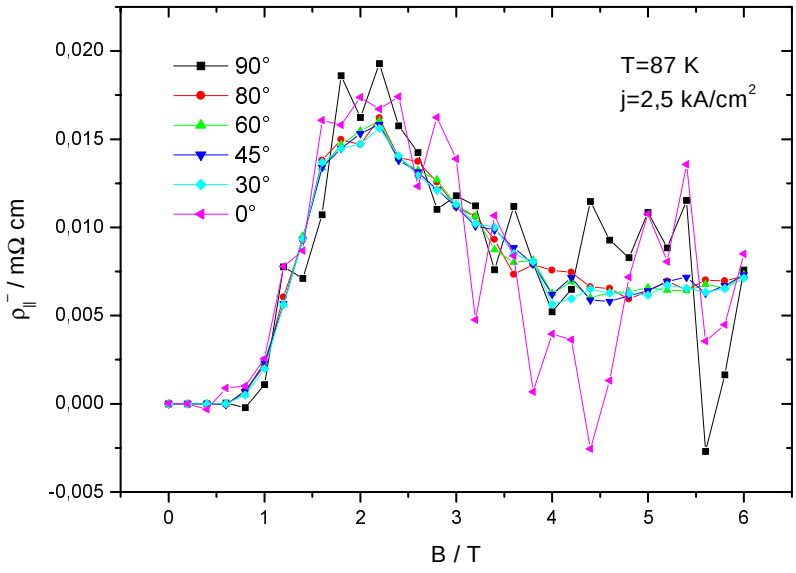

Figure 3.16: *Magnetic field dependencies of the odd longitudinal components of the magnetoresistivity for the sample ak81.*

Chapter 4

Guided vortex motion in Nb films grown on faceted substrates

4.1 Faceting of the Al_2O_3 $\{10\bar{1}0\}$ surface

It is known that the surfaces of metals, semiconductors, and ceramics change under certain conditions from flat ones into such of a faceted hill-and-valley structure [55, 56, 57, 58]. This can result from external perturbations, such as chemical adsorption, or as the result of the surface being thermodynamically unstable. The classical explanation for the driving force of this process was developed by Herring [59]. According to this approach the surfaces other than those found on the equilibrium crystal shape will decompose into a hill-and-valley structure to reduce the overall surface free energy. The type of the developed structure depends on the material and the orientation of the surface.

$(10\bar{1}0)$-cut (m-plane) α-Al_2O_3 develops a semi periodic faceted surface when annealed at high temperatures in air [60]. This is, driven by the large surface energy of the $(10\bar{1}0)$ surface, occurs into a hill-and-valley structure consisting of

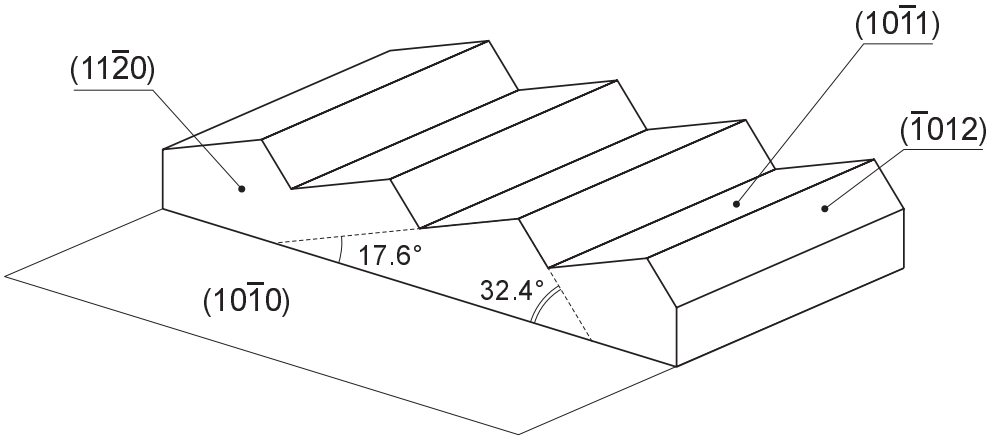

Figure 4.1: *Faceted surface of the* (10$\bar{1}$0)-Al_2O_3 *substrate.*

the (10$\bar{1}$1) and ($\bar{1}$012) planes of the Al_2O_3 substrate [61, 62]. The faceted substrate surface is schematically shown in Fig. 4.1. The surfaces (10$\bar{1}$1) and ($\bar{1}$012) form the angles of 17.6° and 32.4° with the (10$\bar{1}$0) plane of Al_2O_3, respectively [63]. It was shown that the facets form with an average periodicity of 350 to 420 nm with aspect ratios (height-to-period length) of about 1:8 [64]. Al_2O_3 is known to be an excellent substrate for the body centered cubic metals [65]. In the experiments reported in this thesis such a faceted surface serves as a template for coherent epitaxial overgrowth of Nb layer. It is known that pure Nb is a type II superconductor [66]. The Nb films grown on this substrates using molecular beam epitaxy technique replicate the faceted substrate surface, and the facet ridges in the such films act as pinning planes [64].

4.2 Sample preparation

Nb-films with different thickness were grown on the faceted α-Al_2O_3 substrates using molecular beam epitaxy techniques[1] [64]. The films grow epitaxially and

[1]Author thanks J. Oster for the help in the film deposition. Details about the deposition procedure and substrate treatment can be found elsewhere [67].

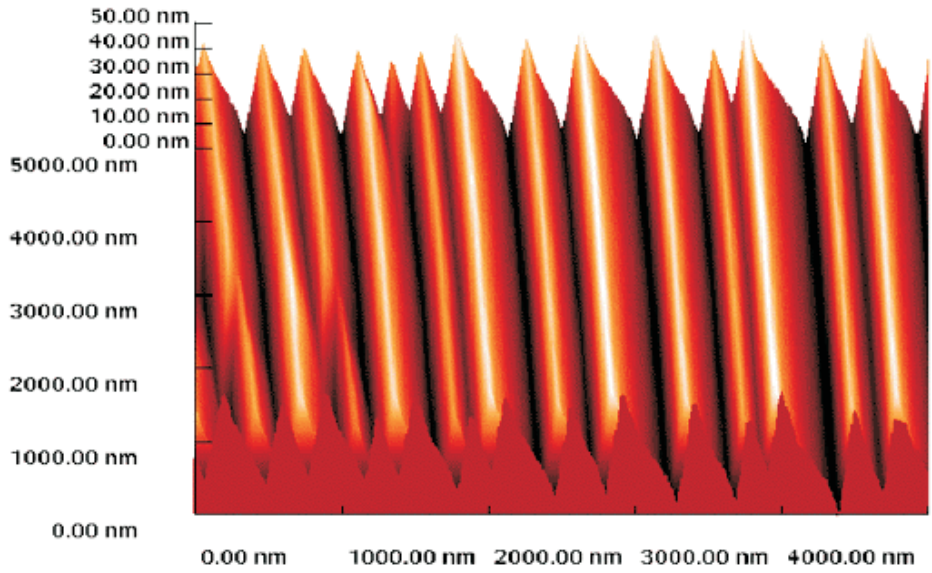

Figure 4.2: *STM image of Nb-film deposited on the faceted Al_2O_3 substrate surface*

replicate the faceted substrate surface as shown in Fig. 4.2. For all resistivity measurements the standard four-probe technique was used. Well defined geometries were required for the measurements of the longitudinal and transversal magnetoresistivities of the samples. For the experiments two different types of micro-structures were used. The first structure used is shown in Fig. 4.3(a). It consists of one micro-bridge with a width of 50 μm and a length of 380 μm. This structure allows to measure the longitudinal and transversal voltages for one transport current direction on the same sample. To remedy this restriction to only one current direction another structure has been developed. It consists of five equal micro-bridges oriented at the different angles α, as shown in the Fig. 4.3(b). The micro-bridges have a width of 25 μm and a length of 510 μm. This structure allows to measure the longitudinal and transversal voltages for the different transport current directions with respect to the facet ridges at the angles $\alpha = 0°$, 30°, 45°, 60°, and 90° on the same sample.

The films were patterned by photolithography and ion-beam etching using

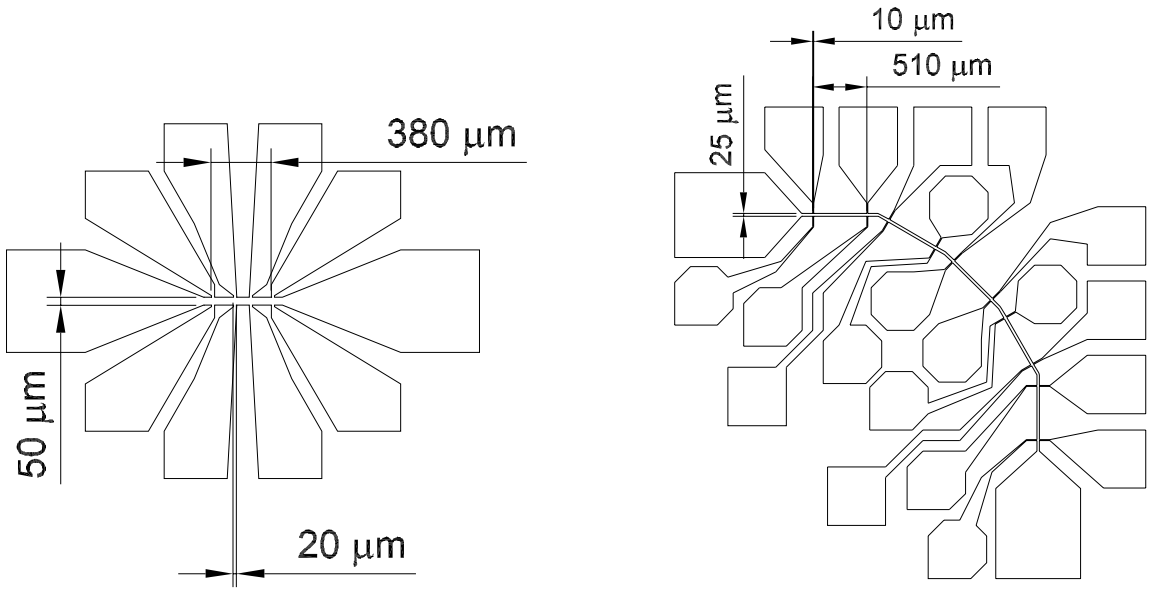

a) b)

Figure 4.3: *Hall structures as used for the magnetoresistivity measurements: (a) Simple geometry for one current direction. The structure (b) allows to send a transport current at the angles* 0°, 30°, 45°, 60°, 90° *with respect to a pre-defined direction.*

the masks with structures as shown in Fig. 4.3. The patterned samples were mounted on a suitable sample holder and contacted using a wire bonder. All the magnetoresistivity measurements were performed in an external magnetic field $+\mathbf{H}$ and $-\mathbf{H}$ directed perpendicular to the film surface, and the even and odd magnetoresistivity components were calculated according to the following simple relation:

$$\rho^{\pm} = (\rho(+\mathbf{H}) \pm \rho(-\mathbf{H}))/\mathbf{2} \tag{4.1}$$

4.3 Magnetoresistivity data of the first sample set

For the first experiment three Nb films with a thickness of 390 Å were grown during one deposition process on faceted α-Al_2O_3 substrates. As substrates for the film deposition three pieces cut from the same faceted α-Al_2O_3 wafer were used. The micro-bridges were patterned having different orientations to the facet ridges: three samples were prepared by photolithography and ion etching using the mask shown in Fig. 4.3(a) allowing measurements with the transport current directed at the angles $\alpha = 0°$, 45° and 90° with regard to the facet ridges.

Fig. 4.4 shows the superconductive transitions for all three samples, i.e. the $\rho(T)$ dependences in zero magnetic field. The transition width is about 0.05 K for all samples, but the sample with $\alpha = 45°$ shows a shift of the transition and reduction of the critical temperature by about 0.05 K. The normal resistivity of the film with $\alpha = 0°$ orientation, i.e. when the transport current is directed parallel to the facets, is larger than for $\alpha = 90°$, whereas one would expect the larger value for the $\alpha = 90°$ orientation because of the faceted film geometry.[1] The shift of the superconductive transition and the unexpected behaviour of the resisitivity of the films for the different current orientations can be explained by

[1]Detailed explanation of this is given on page 67.

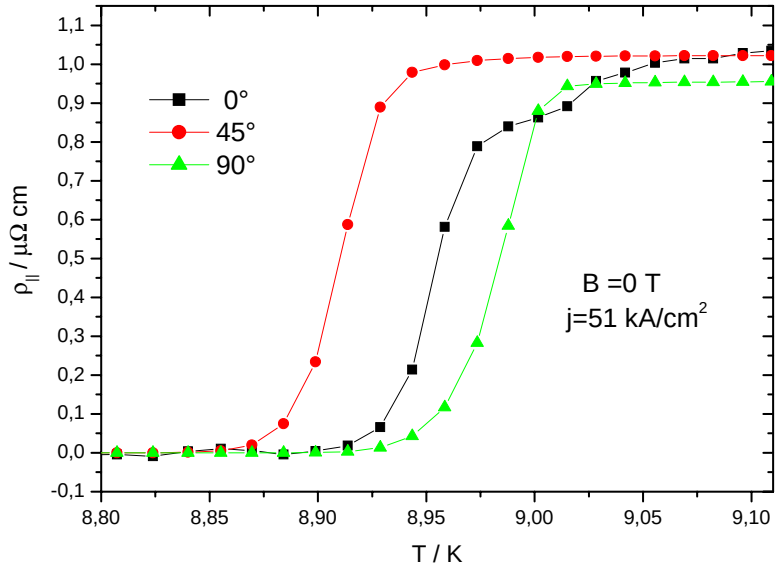

Figure 4.4: *Superconductive transition in zero magnetic field of the three samples with different transport current orientation with respect to the facets, as indicated, in zero magnetic field.*

inhomogeneities created during the film preparation process. Though all films were deposited on the different pieces of the same substrate and in the same deposition process, one cannot exclude a possible non-homogenious temperature distribution in the sample holder and thus slightly different preparation conditions for the three films.

The dependences of the even longitudinal resistivity $\rho_{\parallel}^{+}$ on the temperature and the magnetic field are shown in Fig. 4.5. In the temperature dependence shown in Fig 4.5(a), the curve for the $\alpha = 45°$ sample is shifted to lower temperatures by about 0.05 K, which corresponds to the shift of this curve in zero field (see Fig. 4.4). Also the magnetic field dependence of this component shows a shift of the transition toward smaller fields as can be expected (see Fig. 4.5(b)). The curves for $\alpha = 0°$, $90°$ show almost the same superconductive transition except of the different values of the resistivity in the normal state.

In Fig. 4.6 the temperature and magnetic field dependences of the odd longi-

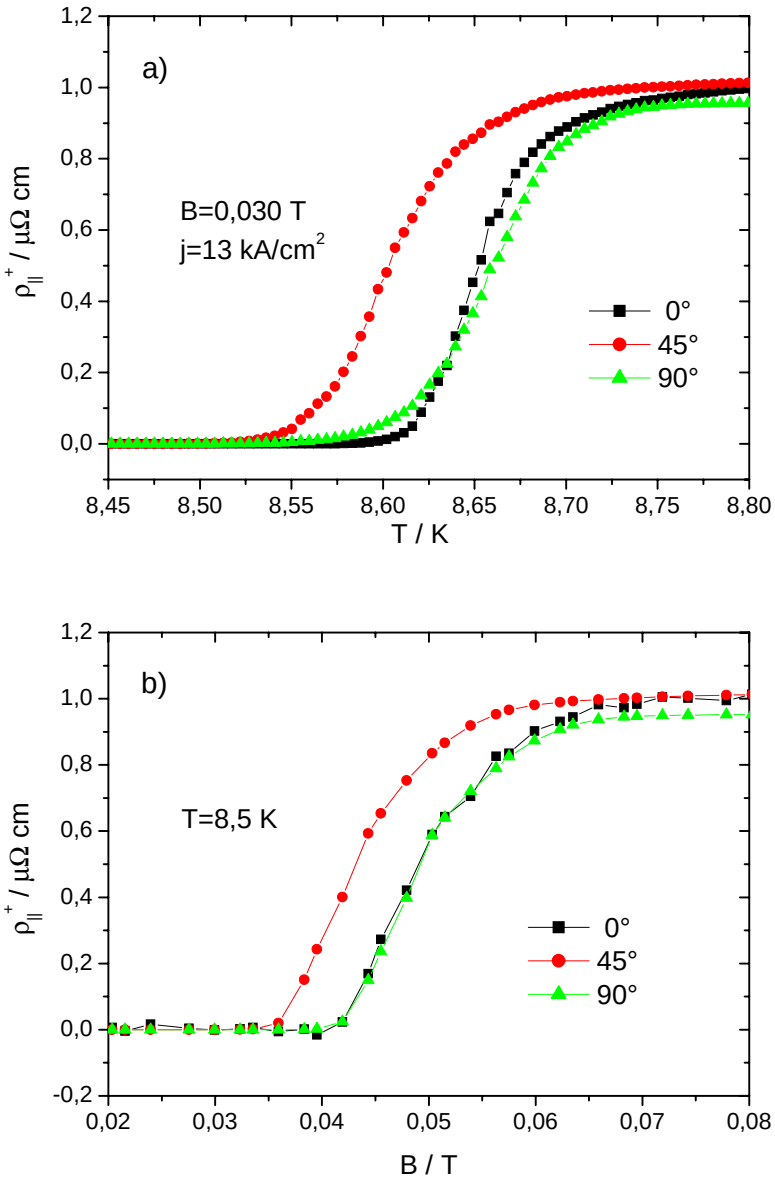

Figure 4.5: *Temperature (a) and magnetic field (b) dependences of the even longitudinal magnetoresistivity component* $\rho_{\|}^{+}$ *for the different transport current orientations with respect to the facet ridges, as indicated.*

tudinal resisitivity components $\rho_{\parallel}^{-}$ are shown. The curves for $\alpha = 45°$ are shifted into the lower temperature and field regions by approximately the same values as in Fig. 4.5, respectively. As was shown in Chapt. 2, the appearance of this component is a characteristic feature of the guided vortex motion, and is caused by a pinning anisotropy. In an isotropic superconductor this component must be zero. The first experimental observation of this component was made by A. A. Prodan, V. V. Chabanenko et. al in an unidirectionally twinned $YBa_2Cu_3O_{7-\delta}$ single crystal [22], [23]. They measured an odd longitudinal magnetoresistivity of the sample for the transport current directed at an angle of 0° and 45° with respect to the twins as a function of the magnetic field and found, qualitatively, the same behaviour as shown in Fig 4.6(b) for the 45° orientation. The amplitude of the peak was about 3% from the resistivity of the sample in the normal state, whereas an amplitude about 20% of the normal state resistivity was observed in the reported measurements. The response for 0°-oriented current was almost zero in [22], but in Fig. 4.6(b) one can see almost the same behaviour for all three current orientations.

The temperature and magnetic field dependences of the even transversal components of the magnetoresistivity (even Hall components) $\rho_{\perp}^{+}$ are shown in Fig. 4.7. From the theoretical viewpoint the appearance of this component is caused by the presence of a pinning anisotropy in the superconductor. For the temperature dependences shown in Fig. 4.7(a) the theoretical model described in this thesis predicts $\rho_{\perp}^{+}$ to be maximal for the $\alpha = 45°$ transport current orientation, see Eq. 2.40, and zero for $\alpha = 0°$, 90°, if one neglects the Hall constant. The observed response is indeed maximal for the $\alpha = 45°$ orientation and is relatively small for $\alpha = 0$ (see Fig 4.7). In the magnetic field dependences of the even transversal components $\rho_{\perp}^{+}$ (Fig. 4.7(b)) a sign change of the curve for the $\alpha = 0°$ transport current orientation is observed, whereas the two other curves have almost the same shape of the temperature and magnetic field dependences.

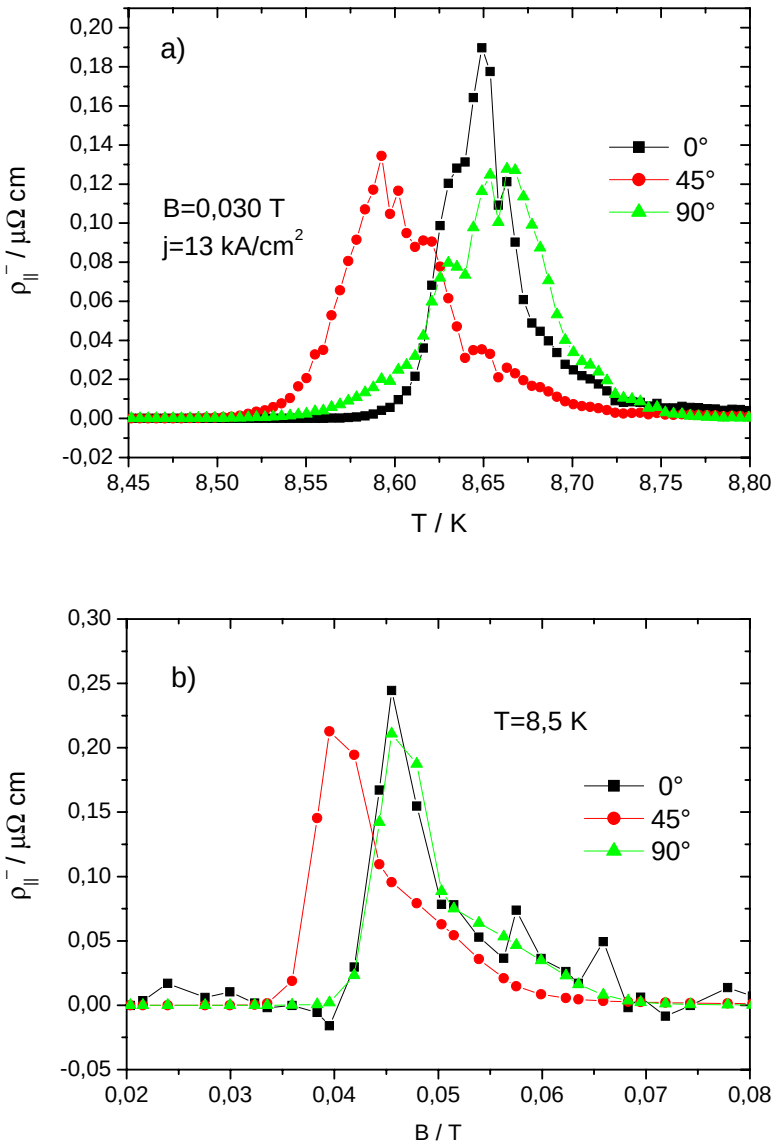

Figure 4.6: *Temperature (a) and magnetic field (b) dependences of the odd longitudinal magnetoresistivity component $\rho_{\parallel}^{-}$ for the different transport current orientations with respect to the facet ridges, as indicated.*

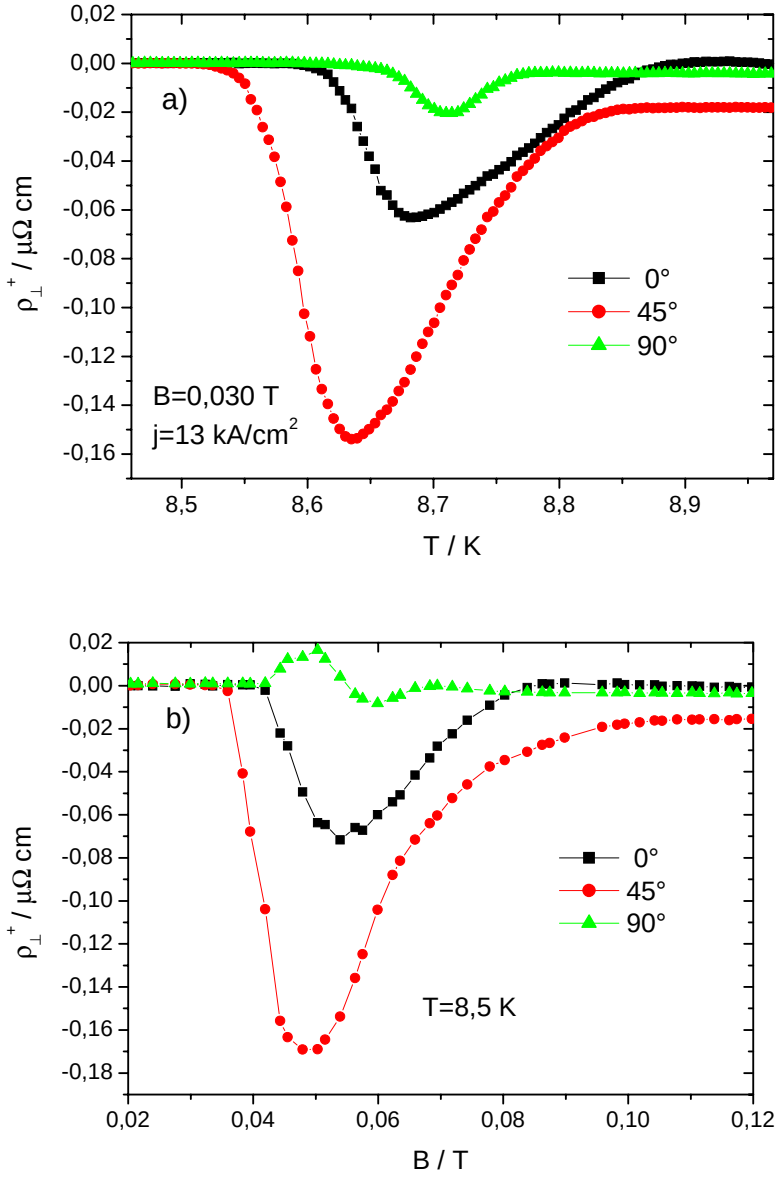

Figure 4.7: *Temperature (a) and magnetic field (b) dependences of the even transversal magnetoresistivity component $\rho_{\perp}^{+}$ for the different transport current orientations with respect to the facet ridges, as indicated.*

Dependences of the odd transversal component of the magnetoresistivity (odd Hall components) $\rho_{\perp}^{-}$ on the temperature and magnetic field are shown in Fig. 4.8. This is a conventional Hall resistivity, because this component is odd with respect to the magnetic field direction reversal. Qualitatively the temperature dependences are very similar to the magnetic field dependences; the maximal response shows the sample with $\alpha = 45°$ orientation. An anomalous Hall effect is observed, the Hall resistivity changes its sign with increasing temperature or magnetic field. Such an anomalous behaviour of the Hall resistivity has been observed widely in ceramics, single crystals as well as in epitaxial thin films of high temperature superconductors [68, 69, 70, 71, 72, 73] and in some conventional superconductors [74, 75, 76, 77]. An interesting question is, how the pinning anisotropy affects the Hall behaviour, i.e., whether an anomalous Hall effect is an intrinsic property of the material or whether it can also be caused by the presence of a pinning anisotropy. The theoretical model described in Chapt. 2 allows for such a change of the Hall resistivity sign, even if the Hall coefficient ϵ is constant, only due to the pinning anisotropy in the sample. However, it was found that flat Nb films show a sign change of the Hall coefficient ϵ [68, 77]. Thus, in order to use the theoretical model proposed in Chapt. 2 for the description of the behaviour of the Hall components, one must know the behaviour of the Hall coefficient ϵ in a flat Nb film.

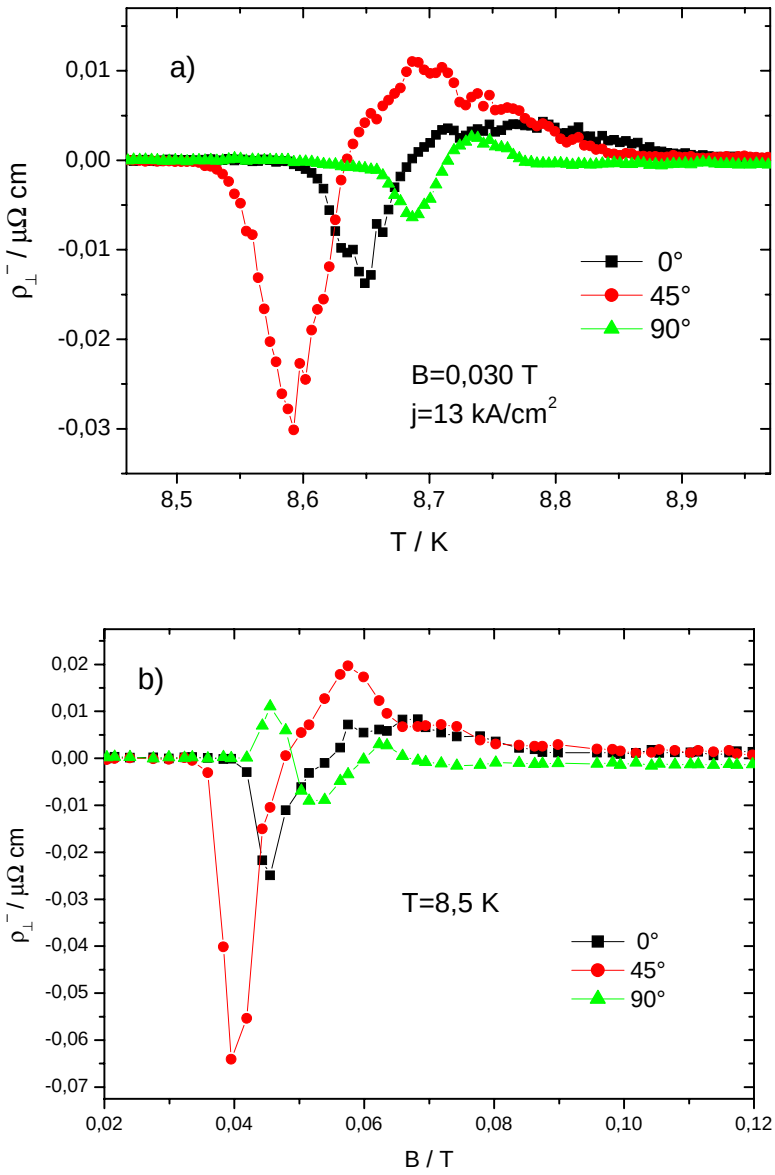

Figure 4.8: *Temperature (a) and magnetic field (b) dependence of the odd transversal magnetoresistivity component $\rho_{\perp}^{-}$ for the different transport current orientations with respect to the facet ridges, as indicated.*

4.4 Magnetoresistivity data of the second sample set

For the second type of experiment a Nb films with a thickness of 250 Å were grown on a faceted α-Al_2O_3 substrates. For the magnetoresistive measurements the structure shown in Fig. 4.3(b) was patterned using photolithography which allowed to measure the longitudinal and transversal magnetoresistivities for the different transport current orientations with respect to the facets on one film in contrast to the experiment described before. Two samples were prepared for the magnetoresistive measurements in this way but, unfortunately, it was not possible to obtain all desired data with the first sample. Contacting a such patterned sample on a sample holder is a quite complicated procedure and it did not work well with the first sample, not all contacts could be successfully put. For this sample only the measurements of the longitudinal resisitivities as a function of temperature in fields 0 and 15 mT were made. All results reported below were obtained from the second sample. All observed effects for the longitudinal resistivity components are in a good agreement with the data collected from the first film.

The superconductive transition of this sample for the different current orientations is shown in Fig. 4.9. The critical temperature for this sample in zero magnetic field is $T_c = 8.46$ K, the width of the superconductive transition is about 0.04 K. Because the film surface is not flat but faceted (see Figs. 4.1, 4.2), different normal state resistances for the micro-bridges oriented at different angles to the facets can be expected. Indeed, for $\alpha = 0°$ transport current flows parallel to the facet ridges so the effective width of the bridge is larger as compared with a bridge patterned on a flat film. For $\alpha = 90°$ orientation current flows perpendicular to the facets so the effective length of the bridge is larger in this case. From this it is clear that the normal state resistivity must be larger for $\alpha = 90°$ which agrees with experimental data shown in Fig. 4.9. However,

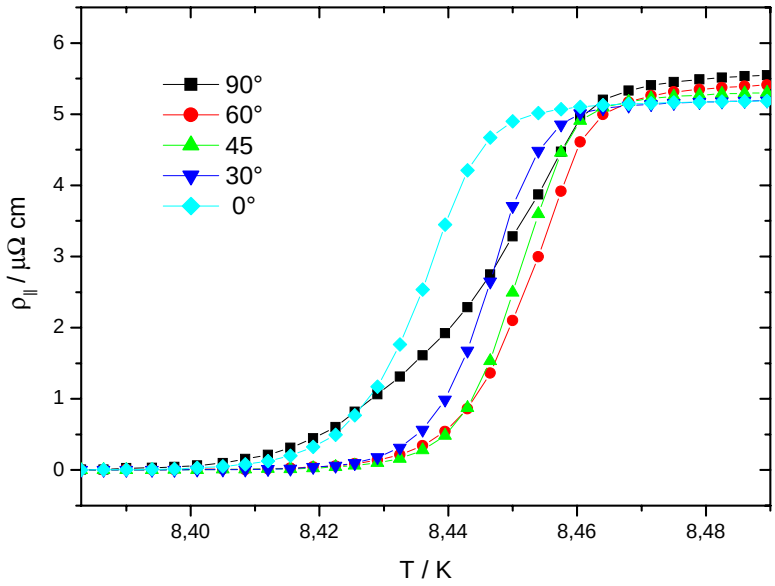

Figure 4.9: *Superconductive transition in zero magnetic field for the different transport current orientations with respect to the facet ridges, as indicated.*

such a simple calculation gives a resisitance difference about 20% for this two orientations for this film whereas the measured difference is about 7%. The most probable explanation for this is that the each facet rigde does not extend throuth the whole bridge as it was assumed for the calculation above. There exist defects in facet structure where the convex and concave facet ridges change place and the facets are not perfect periodic [64]. It is evident fom this argumentation that such defects will make a resisitance difference lower as calculated using the easy ideas about the film geometry.

The temperature dependence of the even component of the longitudinal resistivity $\rho_{\|}^{+}$ in magnetic field of $\mu_0 H = 15$ mT is shown in Fig. 4.10. The spacing between vortices at this field is approximately 400 nm, assuming an equilibrium hexagonal flux-line lattice structure, which corresponds to the averaged facet periods in the films. The curves show very good systematic behaviour. The dependence of the normal state resistivity on the angle α can be given with the

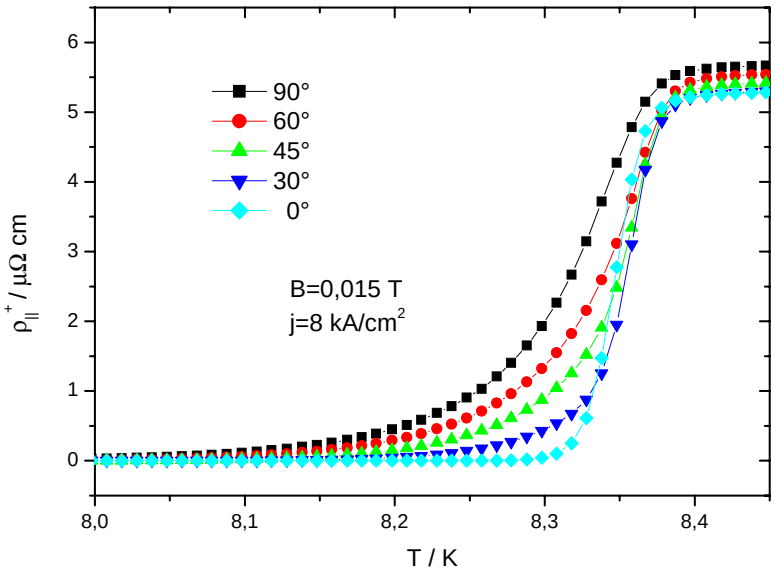

Figure 4.10: *Temperature dependence of the even longitudinal magnetoresistivity component $\rho_{\parallel}^{+}$ for the different transport current orientations with respect to the facet ridges as indicated.*

following relations which can be derived within the described theoretical model:

$$\rho_{\parallel N}(\alpha) = \rho_N(1 - \Delta \cos 2\alpha), \tag{4.2}$$

$$\rho_{\perp N}(\alpha) = -\Delta\rho_N \sin 2\alpha, \tag{4.3}$$

where $\rho_N = \rho_{\parallel N}(45°)$ is the longitudinal magnetoresistivity in the normal state for the $\alpha = 45°$ transport current orientation with regard to the facet ridges; $\Delta = -\frac{\rho_{\perp N}(45°)}{\rho_{\parallel N}(45°)} = \gamma - 1$, γ is the anisotropy parameter defined in chapter 2; $\rho_{\perp}(45°)$ is the transversal magnetoresistivity for the transport current directed at an angle $\alpha = 45°$ with respect to the facet ridges. This two equations (4.2 and 4.3) reflect the tensorial behaviour of the resistivity components. The measured values of the longitudinal resistivities differ from the calculated ones according to Eq. 4.2, by about 0.4% for all measured angles except $\alpha = 0°$, for which this difference is 2.5%. From Figs. 4.9 and 4.10 one can see that the normal state curves almost coincide for $\alpha = 0°$ and 30°, which could be due to a small angle

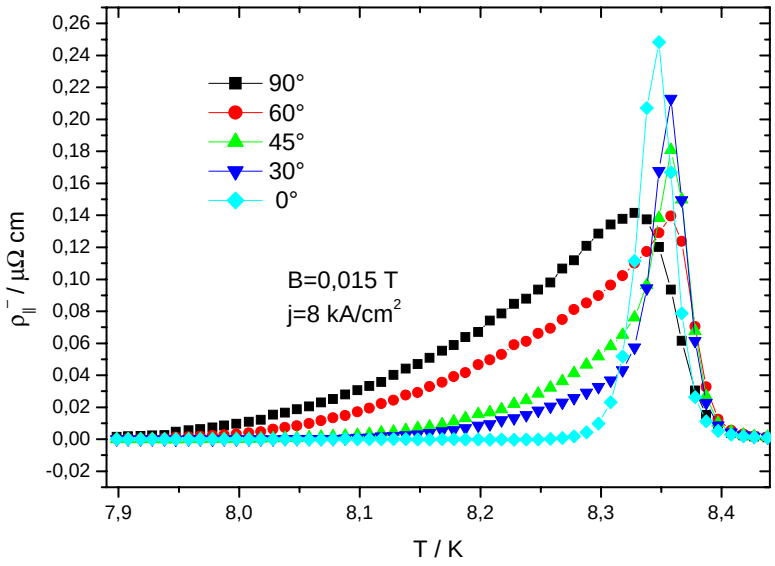

Figure 4.11: *Temperature dependence of the odd longitudinal magnetoresistivity component $\rho_{\parallel}^{-}$ for the different transport current orientations with respect to the facet ridges, as indicated.*

misalignmet of the measuring structure with regard to the exact direction of the facet ridge lines.

In Fig. 4.11 the temperature dependence of the longitudinal odd component $\rho_{\parallel}^{-}$ for the different angles α is shown. The peak magnitude is maximal for $\alpha = 0°$. The same measurements in magnetic fields $\mu_0 H = 0.003$, 0.007, 0.030, 0.060, 0.090 T show that with increasing magnetic field all peaks become broader and the peaks for $\alpha = 0°$, 30°, 45° reduce their amplitude. The appearance of this component is a characteristic feature of the guided vortex motion [35].

The dependence of the even transversal magnetoresisitivity component $\rho_{\perp}^{+}$ on the temperature shown in Fig. 4.12, demonstrates a maximal magnitude for $\alpha = 45°$ and almost zero response for $\alpha = 0°$, 90°. The behaviour of all these curves does not qualitatively change while changing the magnetic field. The appearance of this component in the superconductive state is caused by the guided vortex motion. It is again possible to describe the anisotropy of this magnetoresistivity

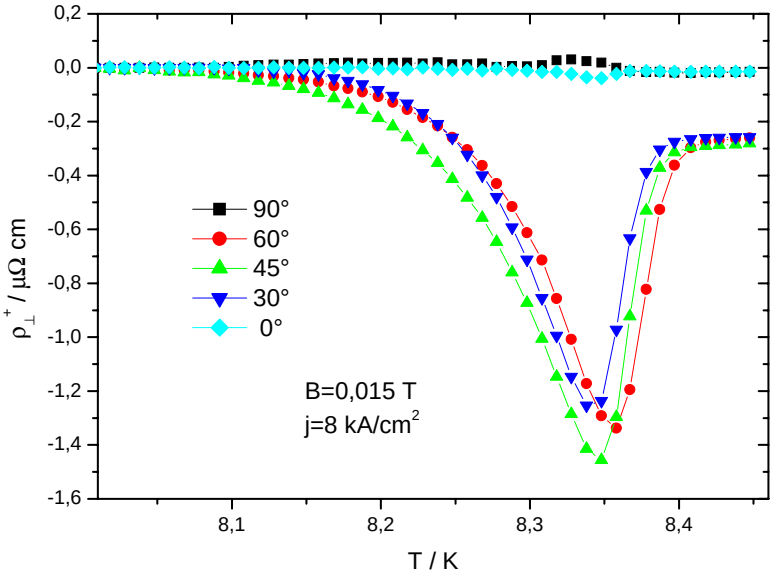

Figure 4.12: *Temperature dependence of the even transversal magnetoresistivity component $\rho_{\perp}^{+}$ for the different transport current orientations with respect to the facet ridges, as indicated.*

in the normal state using relation 4.3. In particular, according to this relation the transversal resistivities for the currents oriented at the angles α and $(90° - \alpha)$ must coincide and indeed, the curves for $\alpha = 30°$ and $\alpha = 60°$ in Fig. 4.12 are the same in the normal state (T>8.4 K) within the experimental resolution. The measured normal resisitivities are also in good agreement with the resisitivities as calculated using relation 4.3.

The dependence of the odd transversal magnetoresistivity $\rho_{\perp}^{-}$ on temperature, see Fig. 4.13, shows the so-called anomalous Hall behaviour: $\rho_{\perp}^{-}$ changes its sign from negative to positive with increasing temperature. With increasing magnetic field the amplitude of the negative peak increases whereas the height of the positive peak decreases.

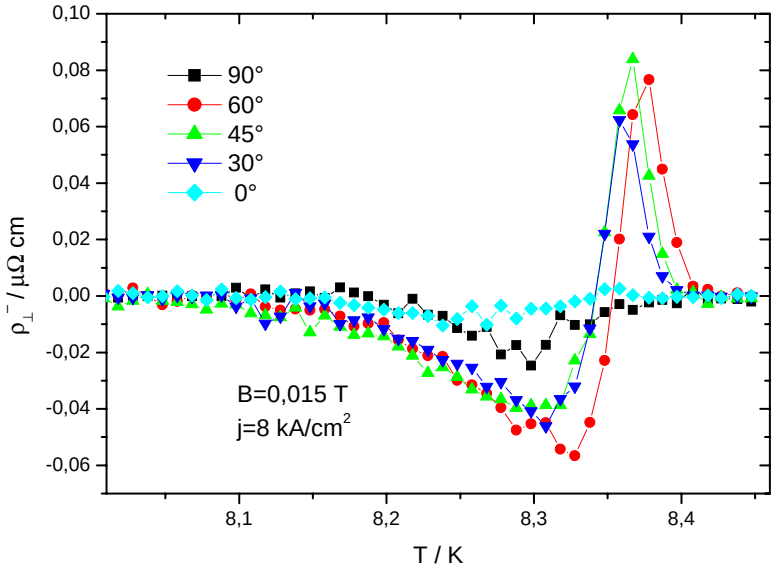

Figure 4.13: *Temperature dependence of the odd transversal magnetoresistivity component $\rho_{\perp}^{-}$ for the different transport current orientations with respect to the facet ridges, as indicated.*

4.5 Discussion of the experimental data

4.5.1 Guiding in Nb films

An important characteristic of guided vortex motion along the the pinning planes is the angle β between the average vortex velocity vector and pinning planes. This quantity can be easily calculated from the experimental data (see also Eq. 2.44):

$$\cot\beta = -\frac{\rho_{\perp}^{+}}{\rho_{\parallel}^{+}}. \tag{4.4}$$

The guided angle β was calculated for both sample sets. The dependence of the guiding angle β on the temperature is shown in Figs. 4.14. In the first experiment, with three different Nb films, the angle β is always larger than the angle between the facet ridges and the transport current. Consequently, there is no pronounced guided motion of vortices. However, in the second experiment an evidence for perfect guiding is found. The guiding angle β is almost equal to

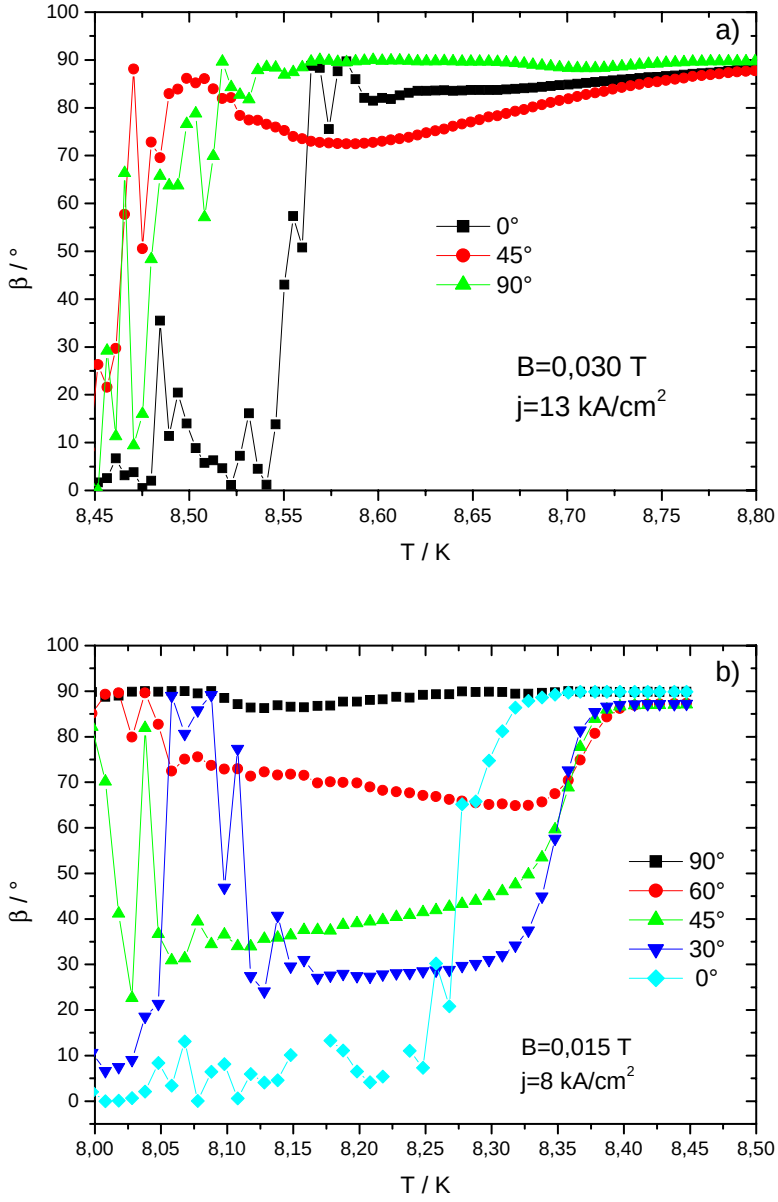

Figure 4.14: *The dependence of the guiding angle β on temperature: a) for three films with different current orientations, as indicated; b) for one film with different current orientations, as indicated.*

the angle α as seen from Fig. 4.14(b). At temperatures near T_c isotropization of the pinning is observed. In this region pinning planes do not affect the vortex motion any more and the vortex velocity becomes parallel to the Lorentz force, i.e. perpendicular to the transport current direction. The guiding angle β becomes equal to 90° in this case.

It can be concluded, that the Nb films used in the second type of experiment show much better guided vortex motion, which means that the anisotropic pinning prevails over the isotropic pinning much more than in the first experiment with three Nb films. In general, the Nb films offer a good possibility to study vortex dynamics in the presence of anisotropic pinning, since the effects caused by it are not masked by point-like pinning as is the case in the explored $YBa_2Cu_3O_{7-\delta}$ films (see Chapter 3).

4.5.2 Arrhenius analysis of the even longitudinal resistivity component

To estimate the activation energy for the vortex motion produced by the pinning barriers, an Arrhenius analysis of the temperature dependence of the longitudinal magnetoresistivity was performed for the different magnetic fields $\mu_0 H = 0.007$, 0.015, 0.030 T for the second sample set. The vortex motion is supposed to be thermally activated and thus the resistivity of the sample can be described by the Arrhenius law.

$$\rho = \rho_0 \exp \frac{-U_{\text{eff}}}{k_B T} \tag{4.5}$$

where k_B is the Boltzmann constant, ρ_0 is a constant, and U_{eff} is an effective activation energy. If one plots $\ln \rho$ vs. the inverse temperature T^{-1}, the slope of the curve gives directly the activation energy U_{eff} in units of T. The result of this analysis is shown in Figs. 4.15, 4.16, 4.17. The thus obtained activation energies for the different transport current orientations calculated from the linear parts of the plot for $\mu_0 H = 0.015$ T (Fig. 4.16) are given in Table 4.5.2. It should be

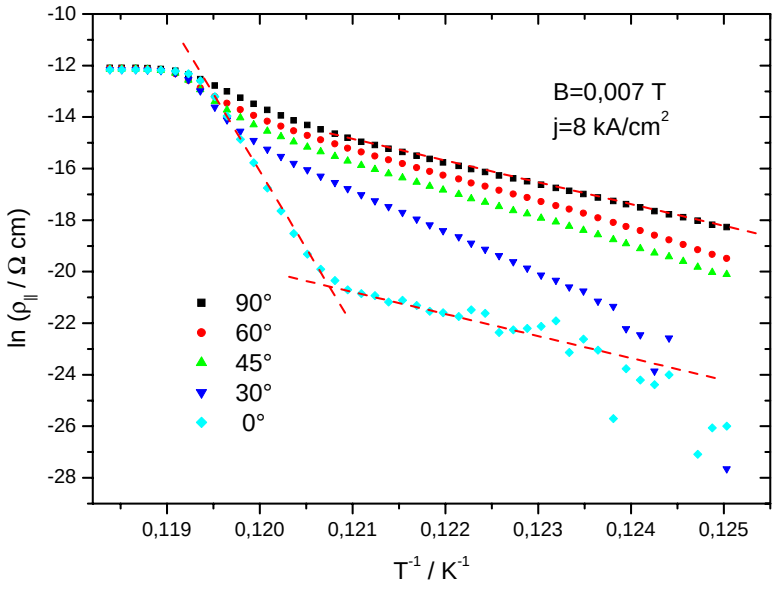

Figure 4.15: *Arrhenius plot of the even longitudinal magnetoresistivity in a magnetic field of* $\mu_0 H = 0.007$ *T for the different transport current orientations with respect to the facet ridges, as indicated.*

mentioned for comparison that typical values for the activation energy in high temperature superconductors are about 200 – 3000 K [78, 79].

From the represented Arrhenius plots one can see, that in the superconductive state the pinning anisotropy plays a more important role than the anisotropy of the film in the normal state. The curves practically coincide in the left part of the Arrenius plots which corresponds to the normal state, whereas in the superconductive state their behaviour is strongly dependent on the transport current orientation with regard to the facet ridges.

Within the theory, as described earlier, the even longitudinal magnetoresistivity component can be given by the following relation[1]

$$\rho_{\parallel} = \nu_i \rho_{\parallel a}, \tag{4.6}$$

[1]The superscript "+" is left out here and in all the following formulas for the even longitudinal component $\rho_{\parallel}^{+}$ to simplify the notation.

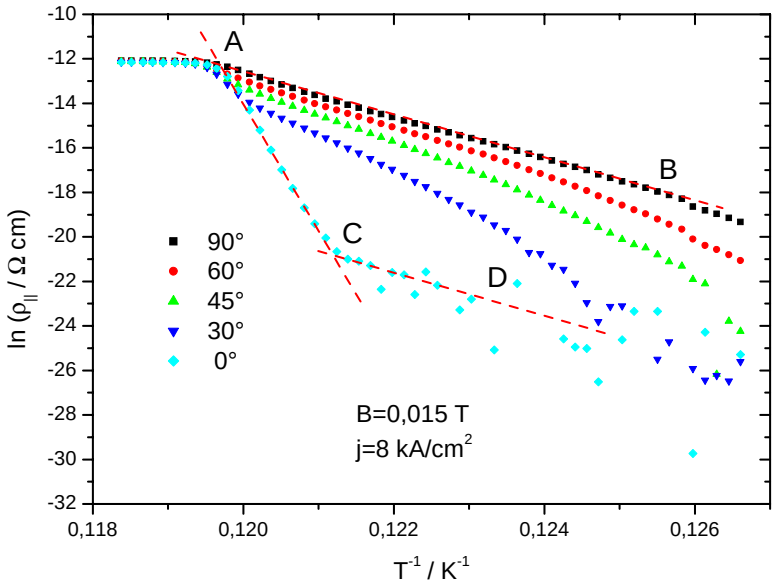

Figure 4.16: *Arrhenius plot of the even longitudinal magnetoresistivity in a magnetic field of* $\mu_0 H = 0.015$ *T for the different transport current orientations with respect to the facet ridges, as indicated.*

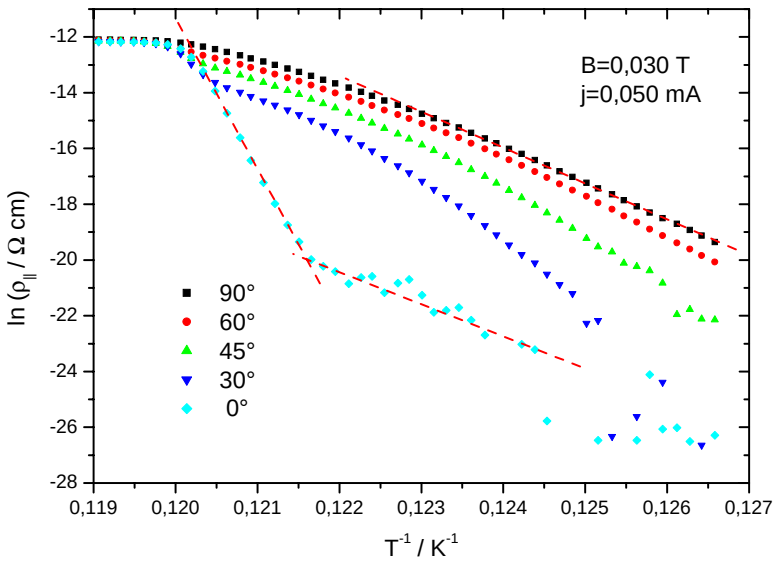

Figure 4.17: *Arrhenius plot of the even longitudinal magnetoresistivity in a magnetic field of* $\mu_0 H = 0.030$ *T for the different transport current orientations with respect to the facet ridges, as indicated.*

Current orientation α	Activation energy U_{eff}, K	Temperature range T, K
90°	949	8.08 – 8.32
60°	1032	8.08 – 8.32
45°	1237	8.08 – 8.32
30°	1655	8.12 – 8.32
0°	5599	8.26 – 8.32

Table 4.1: *Activation energies calculated from the linear parts of the Arrhenius plots of the even longitudinal magnetoresistivity in a magnetic field of* $\mu_0 H = 0.015$ *T (Fig. 4.16) for the different transport current orientations with respect to the facet ridges.*

where $\rho_{\|a} = \rho_f(\sin^2\alpha + \nu_a \cos^2\alpha)$, ρ_f is the flux flow resistivity, ν_i, ν_a are the probability functions for a vortex to overcome the isotropic and anisotropic pinning barrier, respectively. Taking logarithm of this expression one obtains for $\alpha \neq 90°$

$$\ln\rho_{\|} = \ln\nu_i + \ln(\tan^2\alpha + \nu_a) + \ln(\rho_f \cos^2\alpha). \tag{4.7}$$

The last term in this expression is almost independent of temperature. So, to understand the dependence of $\ln\rho_{\|}^{+}$ on temperature only the temperature dependences of the first two terms in Eq. 4.7 need to be taken into account.

It was shown in Chapt. 2 that the probability function ν is proportional to $\exp(-U_0/k_BT)$ in the weak current limit $Fb \ll U$, where the length b characterizes the dimension of the potential well. To analyze the behaviour of $\ln\rho_{\|}$ vs. $1/T$ one can use the following model function for the representation of ν_i and ν_a:

$$\nu(T,F) = \exp(-\frac{\theta\, U_{\text{eff}}}{k_BT}), \tag{4.8}$$

where $\theta = 1 - T/T_c$, T_c is a critical temperature, the effective potential $U_{\text{eff}} = U_0 - Fb$, U_0 is the depth of the pinning potential well, F is the external force acting

on the vortex, b is a length characterizing the pinning potential. In general, both probability functions ν_i and ν_a can be represented by relation 4.8 with different parameters U_{0i}, U_{0a}, b_i, b_a, and variables F_i, F_a, where the subscripts i and a denote the quantity related to isotropic and anisotropic pinning, respectively.

Let us consider the curves for the $\alpha = 0°$, $\alpha = 90°$ transport current orientation in Arrhenius represintation for the magnetic field $\mu_0 H = 0.015\,\mathrm{T}$ as shown in Fig. 4.16. The Arrhenius plot for $\alpha = 90°$ can be well fitted by a straight line AB with a slope of 949 K. The curve for $\alpha = 0°$ has two linear parts: AC with a slope of 5599 K and CD which is parallel to AB (compare also with Figs. 4.15, 4.17). As seen from Eq. 4.6 the longitudinal resisitivity for $\alpha = 90°$ is $\rho_\parallel(90°) = \rho_f \nu_i$, and

$$\ln \rho_\parallel(90°) = \ln \rho_f + \ln \nu_i$$

. So the slope of Arrhenius plot is defined only by the probability function ν_i.

For the $\alpha = 0°$ transport current orientation from Eq. 4.7 follows

$$\ln \rho_\parallel(0°) \approx \ln \nu_i + \ln \nu_a$$

and thus a slope of Arrhenius plot is defined by both probability functions, ν_i and ν_a. However, in a real experiment one usually has a small misalignment of the measuring structure with respect to the facet ridges, and thus the angle α differs by a small amount $\delta\alpha$, caused by this misalignment, from the nominal value. So, to describe the case $\alpha = 0$ one has to use Eq. 4.7. Let us take a closer look on its second term $\ln(\tan^2 \alpha + \nu_a)$. With decreasing temperature (increasing 1/T in Arrhenius presentation) the probability function $\nu_a \to 0$ (see Chap. 2, [35]); so there exists a temperature region where even for small α, $\tan^2 \alpha > \nu_a$, and one can neglect ν_a in this term when considering the temperature dependence. This means that at low enough temperatures the temperature dependence of $\ln \rho_\parallel$ will be defined only by the probability function ν_i,

$$\ln \rho_\parallel(0°) \approx \ln \nu_i \quad \text{at low temperatures.}$$

One can see that the slope of the Arrhenius plot at low enough temperatures will be the same for the $\alpha = 0°$ and $\alpha = 90°$ orientations if a small deviation of the transport current orientation is present in the measurements. The described effect is easily visible in the plots 4.15, 4.16, 4.17.

As was shown in theory ([46, 45], see also Chapt. 2), the forces F_a and F_i which are the arguments of the probability functions ν_a and ν_i, respectively, in the case of a small Hall effect can be given by the expressions

$$\begin{aligned} F_a &= F\cos\alpha, \\ F_i &= F\cos\alpha\sqrt{\tan^2\alpha + \nu_a^2(T,\ F_a,\ \alpha)}, \end{aligned} \tag{4.9}$$

where $F = F_L \cdot l$ is the Lorentz force acting on the vortex, F_L is the Lorentz force acting on a unit length of the vortex (see Eq. 2.1), l is the vortex length. From this follows that the behaviour of the probability function ν_a, and thus also $\rho_{\parallel,\,a}$, is anisotropic and dependent only on the variables T, F, and α. The behaviour of ν_i, on the other hand, is more complicated and depends additionally on the nonlinear $\nu_a(T, F)$ function besides the already mentioned parameters.

Using these ideas about the probability functions behaviour, one can concern the dependence of $\ln\rho_\parallel$ on the temperature. The ν-functions are probability functions and always fulfill the condition $0 \le \nu_a \le 1$. Taking into account that $\tan^2\alpha$ competes with ν_a in $\rho_{\parallel a}$ (Eq. 4.6) and with ν_a^2 in the $F_i(\alpha)$ dependence (Eq. 4.9), one can distinguish three different limiting cases using the form for the probability functions ν_a and ν_i proposed in Eq. 4.8, and simplify Eq. 4.7 in these cases to

$$\ln\rho_\parallel \approx \begin{cases} -(\theta/k_BT)\{(U_{0i}+U_{0a}) - [b_i\nu_a(F\cos\alpha) - b_a]F\cos\alpha\} + \ln(\rho_N\cos^2\alpha), \\ \qquad\qquad\qquad\qquad\qquad\qquad\qquad\qquad \tan^2\alpha \ll \nu_a^2 \\ -(\theta/k_BT)\{(U_{0i}+U_{0a}) - (b_i\sin\alpha + b_a\cos\alpha)F\}, \qquad \nu_a^2 \ll \tan^2\alpha \ll \nu_a \\ \\ -(\theta/k_BT)(U_{0i} - Fb_i\sin\alpha) + \cot^2\alpha\cdot\nu_a(F\cos\alpha) + \ln(\rho_N\sin^2\alpha), \\ \qquad\qquad\qquad\qquad\qquad\qquad\qquad\qquad \nu_a \ll \tan^2\alpha < \infty \end{cases} \tag{4.10}$$

The first limiting case is $\nu_a \ll \tan^2\alpha < \infty$. Because of $\nu_a \leq 1$ always, this relation is realized for large enough angles α in whole temperature range. This condition is also fulfilled for smaller angles at low temperatures and currents where the probability function $\nu_a \to 0$. It follows that

$$\ln \rho_{\parallel}(T) \approx (-\theta/k_B T)(U_{0i} - F b_i \sin\alpha) + \ln(\rho_N \sin^2\alpha), \tag{4.11}$$

if one neglects the second term in the corresponding case in Eq. 4.10. Consequently, the Arrhenius plot will show a linear behaviour for large enough angles over the whole temperature range. Indeed, the Arrhenius plot for $\alpha = 90°$ and $60°$ can be very well fitted with a straight line over the whole temperature range for a magnetic field of $\mu_0 H = 0.015$ T (Fig. 4.16) and is also linear in the low temperature region (i.e. the right part of the Arrhenius plot) for magnetic fields of $\mu_0 H = 0.007$ and 0.030 T (Figs. 4.15, 4.17).

The next limiting case is $\nu_a^2 \ll \tan^2\alpha \ll \nu_a$. This condition is more complicated: it corresponds to moderate temperatures and low angles. Though $\nu_a \ll 1$ and thus $\nu_a \gg \nu_a^2$ at low enough temperatures, in addition the angle α must be small enough and the probability function ν_a must be large enough to satisfy the condition $\nu_a^2 \ll \tan^2\alpha \ll \nu_a$. As can bee seen from Eq. 4.10, the Arrhenius plot of $\ln\rho_{\parallel}$ is also linear in this case but the slope differs from the value of $(U_{0a} - F b_a \cos\alpha)$ as was obtained in the previous case.

In the last case the condition $\tan^2\alpha \ll \nu_a^2$ holds. This case can be realized at small angles and high temperatures ($\nu_a \to 1$ for $T \to T_c$). From Eq. 4.10 follows that $\ln\rho_{\parallel}(T) \approx -(\theta/k_B T)\{(U_{0i}+U_{0a}) - [b_i \nu_a (F\cos\alpha) - b_a] F\cos\alpha\} + \ln(\rho_N \cos^2\alpha)$. This dependence contains the term $(\theta/k_B T)[b_i \nu_a (F\cos\alpha) - b_a] F\cos\alpha$ which will cause a nonlinearity of the Arrhenius plot in the temperature and angle region corresponding to its validity range. The nonlinearity is caused by the nonlinear dependence of the probability function ν_a on the temperature. This nonlinear dependence of $\ln\rho_{\parallel}$ is observed in the Arrhenius plot of the longitudinal magnetoresistivity near T_c for small values of the angle α as seen from Fig. 4.15, 4.16, 4.17.

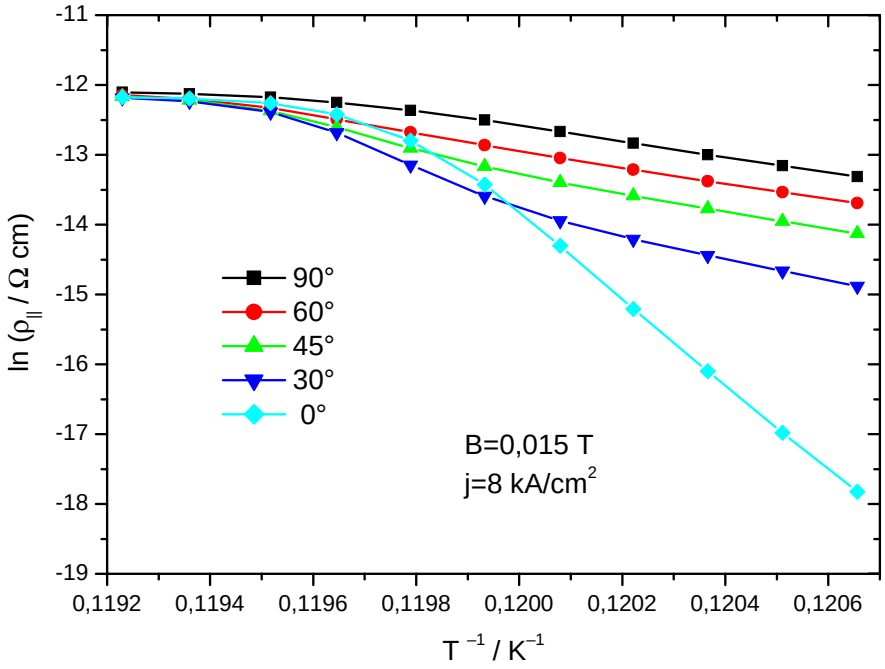

Figure 4.18: *Arrhenius plot of the even longitudinal magnetoresistivity for the temperature range of* $8.39\ K > T > 8.29\ K$. *The dependences for* $\alpha = 90°$, $60°$ *are linear for* $1/T > 0.1197$ *(*$T < 8.36\ K$*) whereas for* $\alpha = 0°$, $30°$ *the linear part exists for* $1/T > 0.1200$ *(*$T < 8.33\ K$*).*

For clarity, the Arrhenius plot of the longitudinal magnetoresistivity in a magnetic field of $\mu_0 H = 0.015$ T for the temperature range of 8.39 K > T > 8.29 K is shown in Fig. 4.18.

For the following analysis the data from the Arrhenius plot in a magnetic field of $\mu_0 H = 0.015\,\mathrm{T}$ will be considered. Using Eq. 4.11 for two different transport current orientations for large enough α and low temperatures (the condition $\tan^2\alpha \gg \nu_a$ must be satisfied) one can estimate the value of the term Fb_i and the depth of the pinning potential well U_{0i}. It is easy to see, that for two different angles α_1 and α_2

$$\begin{aligned} Fb_i &= (U_{\mathrm{eff}}(\alpha_1) - U_{\mathrm{eff}}(\alpha_2))/(\sin\alpha_2 - \sin\alpha_1), \\ U_{0i} &= (U_{\mathrm{eff}}(\alpha_1)\sin\alpha_2 + U_{\mathrm{eff}}(\alpha_2)\sin\alpha_1)/(\sin\alpha_2 - \sin\alpha_1), \end{aligned} \tag{4.12}$$

where $U_{\mathrm{eff}} = U_{0i} - Fb\sin\alpha$ is the activation energy measured from the Arrhenius plot. If one takes the angles $\alpha_1 = 90°$ and $\alpha_2 = 60°$ and the corresponding U_{eff} from Table 4.5.2, the following estimation is obtained:

$$\begin{aligned} Fb_i &= 619\ \mathrm{K}, \\ U_{0i} &= 1568\ \mathrm{K}. \end{aligned} \tag{4.13}$$

Note that for this estimation the term depending on the ν_a function is neglected in Eq. 4.10 .

If the transport current flows perpendicular to the magnetic field, the Lorenz force F acting on the vortex can be estimated using the formula $F = l(j \cdot \Phi_0)$, where l is the vortex length, j is the density of the transport current, and $\Phi_0 = 2,07 \cdot 10^{-15}\,\mathrm{T\ m^2}$ is the magnetic flux quantum. Taking $l = 250$ Å which corresponds to the thickness of the used Nb film, and $j = 8\,\mathrm{kA/cm^2}$, one obtains $F = 0.3\,\mathrm{K/nm} = 4,14 \cdot 10^{-15}\mathrm{N}$. Taking into account the estimation 4.13, the following value for the period of the isotropic potential is obtained: $b_i \approx 2000\,\mathrm{nm}$.

To estimate the parameters of the anisotropic pinning potential it is supposed that the period b_a of this potential corresponds to the period of the facets ridges, which is about 400 nm [64]. Thus the value of Fb_a can be estimated

as $Fb_a \approx 120\,K$, which is much smaller than the measured activation energies U_{eff} (see Table 4.5.2). For the estimation of the depth of the potential well U_{0a} the Arrhenius plot for the $\alpha = 0°$ transport current orientation is considered. The relation $\tan^2\alpha \ll \nu_a^2$ can be satisfied at temperatures near T_c and one can use the corresponding expression for $\ln\rho_\parallel$ from Eq. 4.10. Because of the arguments stated above the term $[b_i\nu_a(F\cos\alpha) - b_a]F\cos\alpha$ can be neglected, and $\ln\rho_\parallel \approx -(\theta/k_BT)(U_{0a} + U_{0i})$, and thus $U_{\text{eff}} \approx (U_{0a} + U_{0i})$ for this geometry. The thus obtained estimation gives the value of the depth of the potential well for the anisotropic pinning $U_{0a} = 4031\,K$.

From the estimations above the temperature dependence of the longitudinal magnetoresistivity can now be calculated and its Arrhenius plot was generated, using as probability functions ν_a and ν_i the function obtained for the washboard model potential (Eq. 2.26) with $q = 1$ and the corresponding parameters U_0, b for the isotropic and anisotropic pinning potential as estimated. These ν_a and ν_i functions were additionally normalized so that $\nu_{a,i}(T_c) = 1$ for the calculations.[1] The best fit of the experimental data was obtained for $b_i/b_a = 15$ and an assumed misalignment of α of about $-3°$ (see Fig. 4.19). The program used for the calculations of the temperature dependence of the longitudinal resistivity is given in the Appendix.

One can see that the experimental data are in good agreement with the theoretical model described in Chapt. 2. The measured temperature dependences of the longitudinal magnetoresistivity can be fitted using the probability functions ν_a and ν_i in the form proposed in [35]. The observed anisotropy of the normal state does not significantly affect the superconducting properties of the films because of the large pinning anisotropy present which suppresses all effects caused by the normal state anisotropy in the superconductive state.

[1] This turned out to be necessary because the studied system has a large activation energy and in the proposed theoretical model the critical temperature is defined via the pinning potential: $k_BT_c = U_0$; a definition that cannot be realized at all in the experiment.

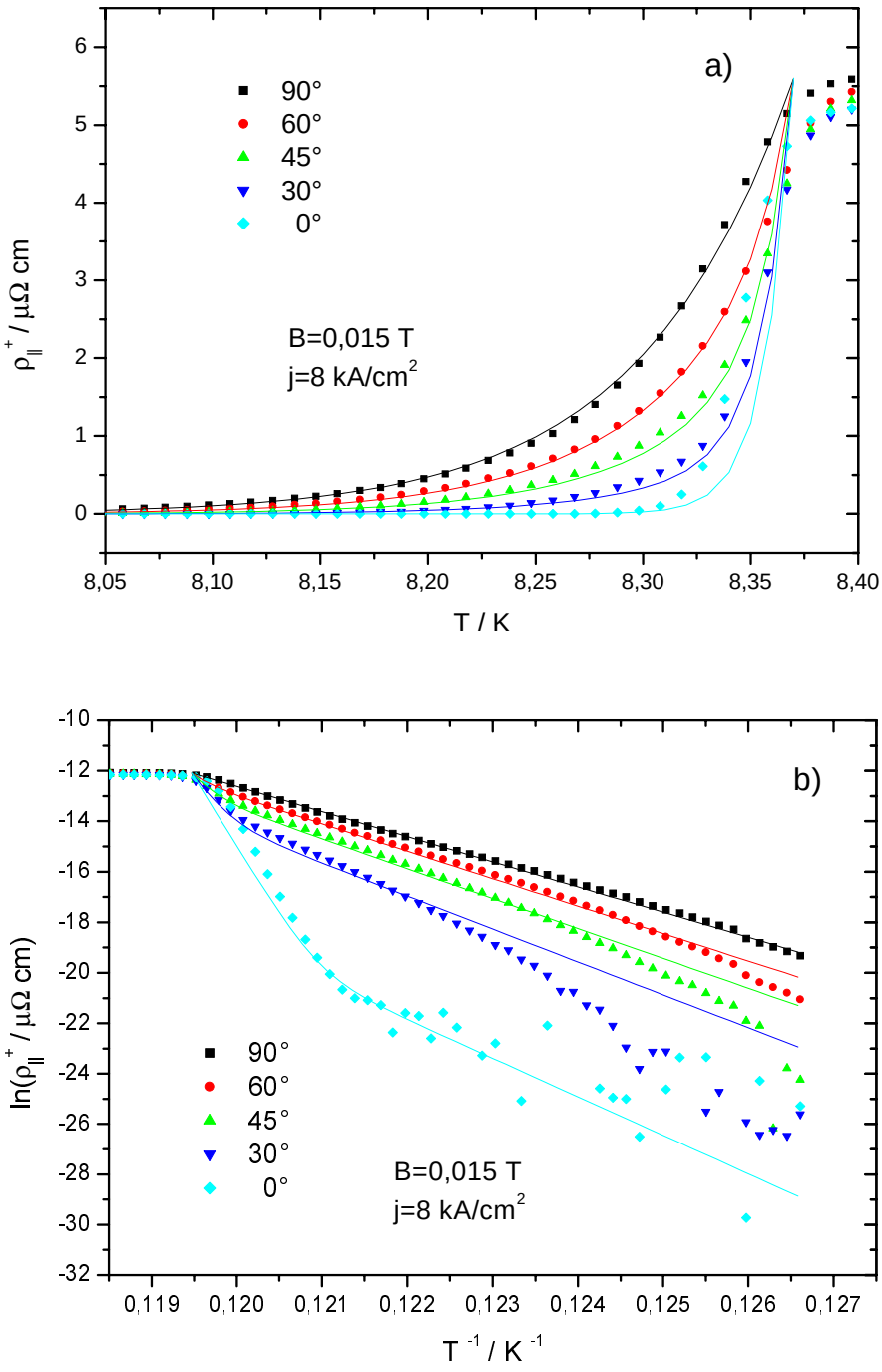

Figure 4.19: *Calculated (line) and measured (data points) dependences of the even longitudinal magnetoresistivity on the temperature (a) and its Arrhenius plot (b). The parameters for the calculated dependences are as following:* $U_{0a} = 4031$ K, $U_{0i} = 1568$ K, $b_i/b_a = 15$, $\delta\alpha = -3°$.

4.5.3 Nature of the pinning in faceted Nb films

As was shown in the previous section, Nb films deposited on faceted substrates show a pronounced anisotropy of the pinning force, which leads to guided vortex motion in such films. The described theoretical model used for the interpretation of the experimental data makes the assumption for the anisotropic pinning potential to have a washboard form (see Eq. 2.25 and Fig. 2.3) for the numerical calculations. An interesting question is the origin of the anisotropic pinning potential in the Nb films deposited on the faceted Al_2O_3 substrates.

The film used in the experiments had thicknesses of 39 nm and 25 nm, respectively. The value for the London penetration depth in Nb films is $\lambda_L \approx 39$ nm [80]. Because the penetration depth defines the dimension of the vortex and thus the lateral extent of the screening superconductive current around the vortex core, and it has a value about of the thickness of the films, the screening currents must flow parallel to the film surface. This means that the magnetic field of each vortex core is perpendicular to the film surface. Since the surface of the employed Nb films is faceted, the magnetic field must enter the film perpendicularly to the facet planes. In this way one obtains a nonhomogeneous magnetic field distribution in the film as one schematically shown in Fig. 4.20. The local magnetic field density is periodically modulated. The density of the vortices is defined by the local magnetic field, so the equilibrium density of the vortices will also be periodically modulated, which leads to periodic modulations of the mean vortex energy.

From Fig. 4.20 it is clear that there is a maximum of the field density distribution on each surface of the facets. So over one facet period length one has two wells and thus the period of the magnetic field density distribution can be assumed to be equal to $T/2$, where T is the facet period. At this point it must be stressed that the described picture gives only a very rough qualitative idea about the possible origin of the pinning in such films.

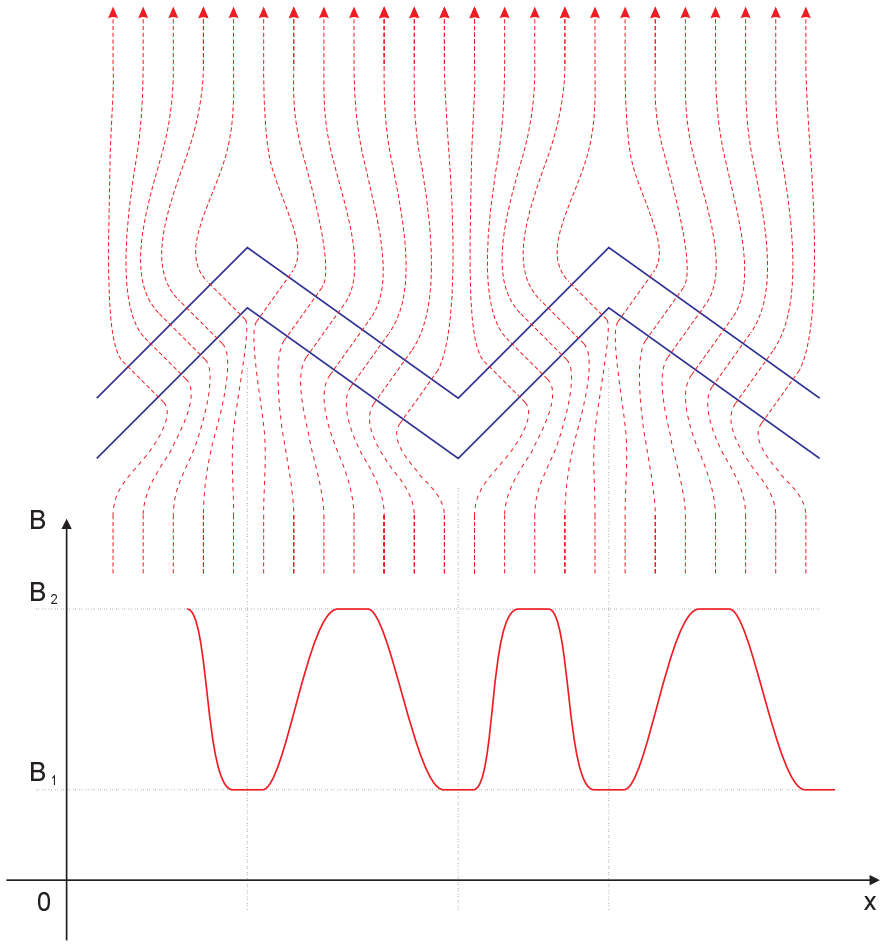

Figure 4.20: *Distribution of the magnetic field density. Dashed lines represent the magnetic field lines. For simplicity, only two levels of the magnetic field density B are supposed: B_1, corresponding to the facet hill or facet valley, and B_2 corresponding to the facet slope.*

From the numerical calculations within the theory described in this thesis, the best fit of the experimental data is obtained for a ratio between the isotropic and anisotropic pinning potential periods $b_i/b_a = 15$ nm. The estimated value for the period of the isotropic pinning potential is given on page 82 and is about $b_i = 2000$ nm, and the period of the faceted structure is about $b_a = 400$ nm [64], which gives the ratio of $b_i/b_a = 5$. Supposing that the period of the magnetic field distribution is, as was argued before, $T/2 = 200$ nm, one gets $b_i/b_a = 10$, which is reasonably close to the ratio obtained by the numerical fit of the experimental data.

The problem of calculating the pinning potential in such a faceted film is rather complicated. But already from the simple arguments given above it is clear that a faceted surface of a superconductive film can generate a pinning potential merely due to the geometry of its surface.

Chapter 5

Conclusions

In the present thesis the vortex dynamics in two different material classes of superconductors with anisotropic unidirected pinning sites was experimentally investigated by way of magnetoresistivity measurements. The reported experiments were carried out on unidirectionally twinned $YBa_2Cu_3O_{7-\delta}$ films and Nb films deposited on faceted Al_2O_3 substrate surfaces. A suitable Hall structure was designed to measure the longitudinal and transversal components of the sample magnetoresisitivity for different transport current orientations with respect to the unidirected pinning sites on the same film. For the interpretation of the experimentally obtained results a theoretical model based on the Fokker-Planck equation was used.

It was proved by means of X-ray diffraction measurements that $YBa_2Cu_3O_{7-\delta}$ films prepared on (001) $NdGaO_3$ substrates exhibit only one twin orientation in contrast to $YBa_2Cu_3O_{7-\delta}$ films grown on (100) $SrTiO_3$ substrates. The magnetoresistivity measurements of the $YBa_2Cu_3O_{7-\delta}$ films with unidirected twin boundaries showed a guided vortex motion along the twin planes. The appearance of two new magnetoresistivity components, which is a characteristic feature of a guided motion, could be demonstrated: an odd longitudinal component with respect to the magnetic field sign reversal and an even transversal component. However, due to the small coherence length in $YBa_2Cu_3O_{7-\delta}$ and the

larger amount of point-like defects as compared to high-quality $YBa_2Cu_3O_{7-\delta}$ single crystals, the strength of the isotropic pinning was comparable with the strength of the pinning produced by twins in these films. This smeared out all effects caused by the pinning anisotropy in the $YBa_2Cu_3O_{7-\delta}$ films. For example, the behaviour of the odd longitudinal component was found to be independent of the transport current direction with respect to the twin planes.

The magnetoresistivity measurements of Nb films deposited on faceted Al_2O_3 substrates showed that a perfect guided vortex motion along the facets can be observed in such films. The appearance of an odd longitudinal and even transversal component of the magnetoresistivity in these samples could be demonstrated. The temperature and magnetic field dependences of the all relevant magnetoresistivity components were measured for these films. The angles between the mean vortex velocity vector and the transport current direction calculated from the experimental data for the different transport current orientations with respect to the facet ridges showed that the vortices move indeed along the facet ridges. Because the coherence length in Nb is much larger than in $YBa_2Cu_3O_{7-\delta}$, point like defects did not play such a crucial role in this experiment, in contrast to the experiment with $YBa_2Cu_3O_{7-\delta}$ films. Due to this fact all the effects caused by the pinning anisotropy and the guided vortex motion were clearly visible, which gave the possibility to compare the obtained results with the reported theoretical approach.

The theory used for the explanation of the experimental data has shown very good agreement with the experiment. The temperature dependence of the even longitudinal magnetoresistivity component of the samples could be very well fitted within considered theoretical approach, using for the isotropic and anisotropic pinning potential, a simple one dimensional potential with a symmetric triangular potential wells. The isotropic and anisotropic potentials, used to fit the experimental results, had a triangle form with $q = 1$, the anisotropy parameter characterizing the electronic viscosity anisotropy was taken $\gamma = 1$ and the periods

and the depths of the potential wells were estimated from the experimental data.

An anomalous Hall effect, i.e. a sign change of the odd transversal magnetoresistivity component, has been found in the temperature and magnetic field dependences of the Hall resisitivity of the samples. The reported theoretical approach allows for such a sign change; it is further known that even flat Nb films display anomalous behaviour of the Hall coefficient ϵ. Consequently, in order to describe the observed dependencies of the Hall resistivity using the considered theoretical approach, one has to know the dependence of the Hall coefficient on temperature and magnetic field for a flat Nb film.

It can be concluded that Nb films deposited on the faceted α-Al_2O_3 $(10\bar{1}0)$ surface can serve as a model system for experimentally studying guided vortex motion and the effects caused by it. Relevant parameters, such as the film thickness and facet period (to some extent), can be varied when the films are prepared.

The described theoretical approach showed to be in good agreement with the experimental data. Nevertheless, for the explanation of the experiment it was necessary to consider point-like pinning in conjunction with the dominating anisotropic pinning also in the theoretical model. However, to describe theoretically the Hall components dependences, one has to know the behaviour of the Hall coefficient in an analogous Nb film deposited on the flat substrate.

Appendix A

The following program developed with the Mathematica 4 software was used to fit the experimentally measured dependence of the even longitudinal magnetoresistivity components on temperature (see chapter 4).

```
<<Graphics‘Colors‘

        (* defining the constants: *)

Ua=4031;                (* depth of the anisotr. potential *)
Ui=1568;                (* depth of the isotr. potential *)
t1=7.9;
t2=8.37;                (* temperature interval t1-t2 *)
ta1:=t1/Ua;
ta2:=t2/Ua;
ti1:=t1/Ui;
ti2:=t2/Ui;             (* dimensionless temperatures *)
d=-5;                   (* misalignment of the structure *)
rN=0.0000056;           (* normal-state resistivity *)


        (* dimensionless temperatures, forces *)

ta[T_] = T/Ua;
ti[T_] = T/Ui;

faAlpha[fax_, Alphax_] := fax * Cos[((Alphax + d)/180)\[Pi]];
fiAlpha[fix_, Alphax_, fax_, tax_] :=
    fix*(Sin[((Alphax + d)/180)\[Pi]]^2 +
```

```
    (Cos[((Alphax + d)/180)\[Pi]]^2) Nua[tax, fax, Alphax])^(1/2);

Nu0[f_] := 1 - 1/f^2;
Nu[t_, f_] := Nu0[f]/(1 - (f/(Tanh[f/t]*(f^2*(f^2 - 1))))*
    2*t*(1 - Cosh[1/t]/Cosh[f/t]));

        (* definition of the Nu-anisotr. function *)
Nua[tax_, fax_, Alphax_] := Nu[tax, faAlpha[fax, Alphax]];
        (* normalization *)
Nuap[tax_, fax_, Alphax_] := Nua[tax, fax, Alphax]/
    Nua[ta2, fax, Alphax];

        (* definition of the Nu-isotr. function*)
Nui[tix_, fix_, tax_, fax_, Alphax_] :=
    Nu[tix, fiAlpha[fix, Alphax, fax, tax]];
        (* normalization *)
Nuip[tix_, fix_, tax_, fax_, Alphax_] :=
    Nui[tix, fix, tax, fax, Alphax]/Nui[ti2, fix, tax, fax, Alphax];

        (* definition of the longit. even resist. component *)
r[tix_, fix_, tax_, fax_, Alphax_] :=
    rN * Nuip[tix, fix, tax, fax, Alphax]*
    (Sin[((Alphax + d)/180)\[Pi]]^2 +
    Cos[((Alphax + d)/180)\[Pi]]^2 * Nuap[tax, fax, Alphax]);

         (* relation between dimensionless forces *)
fir[fax_] := (Ua/Ui)*k*fax;


        (* this plots the dependencies ln(r(t)) *)
faa = 0.01;
k = 14;
d = -3;
t1=7.9;
t2=8.37;
ParametricPlot[{{1/x, Log[r[x/Ui, fir[faa], x/Ua, faa, 0]]},
        {1/x, Log[r[x/Ui, fir[faa], x/Ua, faa, 30]]},
        {1/x, Log[r[x/Ui, fir[faa], x/Ua, faa, 45]]},
        {1/x, Log[r[x/Ui, fir[faa], x/Ua, faa, 60]]},
        {1/x, Log[r[x/Ui, fir[faa], x/Ua, faa, 90]]}},
        {x, t1, t2},
    PlotStyle -> {Cyan, Blue, Green, Red, Black},
    GridLines -> Automatic,
```

```
    Frame -> True, PlotRange -> All];

(*
   The following creates a file with the data :
   <1/t> <delimiter> <ln(r90)> <delimiter> <ln(r60)>...<ln(r0)>

   x1, x2 are the limits of T.
*)

        (* output options *)
dir = "d:/work/mathematica/output";
SetDirectory[dir]

x1 = 7.9;
x2 = 8.37;
step = 0.01;
fileName = "ln79b837new";
delim = " ";
outFile = OpenWrite[fileName];
For[x = x1, x <= x2,
  x = x + step, {
    WriteString[outFile, N[1/x], delim,
      Log[r[x/Ui, fir[faa], x/Ua, faa, 90]], delim,
      Log[r[x/Ui, fir[faa], x/Ua, faa, 60]], delim,
      Log[r[x/Ui, fir[faa], x/Ua, faa, 45]], delim,
      Log[r[x/Ui, fir[faa], x/Ua, faa, 30]], delim,
      Log[r[x/Ui, fir[faa], x/Ua, faa, 0]], "\n"]}]
Close[outFile];
```

Bibliography

[1] H. Kamerlingh Onnes, *Leiden Comm.* **120b, 122b, 124c** 1911.

[2] W. Meissner, R. Ochsenfeld, *Naturwissenschaften* **21** (1933) 787.

[3] F. and H. London, *Proc. Roy. Soc.* (London) **A149** (1935) 71.

[4] V.L. Ginzburg and L.D. Landau, *Zh. Experim. i Teor. Fiz.* **20** (1950) 1064.

[5] A. A. Abrikosov, *Zh. Eksperim. i Teor. Fiz.* **32** (1957) 1442 [*Sov. Phys.–JETP* **5** (1957) 1174].

[6] J. Bardeen, M.J. Stephen, *Phys. Rev.* **140** (1965) A1197.

[7] K. S. Harshavardhan, M. Rajeswari, D. M. Hwang, C. Y. Chen, T. Sands, T. Venkatesan, J. E. Tkaczuk, K. W. Lay, A. Safari, *Appl. Phys. Lett.* **60** (1992) 1902.

[8] E. Mezzetti, R. Gerbaldo, G. Ghingo, L. Gozzelino, B. Minetti, C. Camerlingo, A. Monaco, G. Cuttone, A. Rovelli, *Phys. Rev.* **B60** (1999) 7623.

[9] K. E. Bagnall, I. V. Grigorieva, J. W. Steeds, G. Balakrishnan, D. McK Paul, *Supercond. Sci. Technol.* **8** (1995) 605.

[10] Ch. Gerber, D. Anselmetti, J. G. Bendorz, J. Mannhart, D. G. Schlomm, *Nature* **350** (1991) 279.

[11] A. Diáz, L. Mechin, P. Berghuis, J. E. Evetts, *Phys. Rev. Lett.* **80** (1998) 3855.

[12] C. Villard, G. Koren, D. Cohen, E. Polturak, B. Thrane, D. Chateignier, *Phys. Rev. Lett.* **77** (1996) 3913.

[13] S. Fleshler, W. K. Kwok, U. Welp, V. M. Vinocur, M. K. Smith, J. Downey, G. W. Crabtree, *Phys. Rev.* **B47** (1993) 14448.

[14] W. K. Kwok, U. Welp, G. W. Crabtree,K. G. Vandervoort, R. Hulscher, J. Z. Liu, *Phys. Rev. Lett.* **64** (1990) 966.

[15] G. Blatter, M.V. Feigelman, V.B. Geshkenbein, A.I. Larkin, V.M. Vinokur, *Rev. Mod. Phys.* **66** (1994) 1125.

[16] P.W. Anderson, *Phys. Rev. Lett.* **9** (1962) 309.

[17] P.W. Anderson, Y.B. Kim, *Rev. Mod. Phys.* **36** (1964) 39.

[18] P. H. Kes, J. Aarts, J. van den Berg, C. J. van der Beek, J. A. Mydosh, *Supercond. Sci. Technol.* **1** (1989) 242.

[19] G. Bendorz, K.A. Müller, *Z. Phys.* **B64** (1986) 189.

[20] C. Kittel, *Introduction to Solid State Physics* 7th ed., Jonh Wiley & Sons, Inc., New York, Chichester, Brisbane, Toronto, Singapore.

[21] A. K. Niessen and C. H. Weijsenfeld, *J. Appl. Phys.* **40** (1969) 384.

[22] A. A. Prodan, V. A. Shklovskij, V. V. Chabanenko, A. V. Bondarenko,M. A. Obolenskii, H. Szymczak, S. Piechota, *Phys. C* **302** (1998) 271.

[23] V. V. Chabanenko, A. A. Prodan, V. A. Shklovskij, A. V. Bondarenko, M. A. Obolenskii, H. Szymczak, S. Piechota, *Phys. C* **314** (1999), 133.

[24] V. A. Shklovskij, *Fiz. Nizk. Temp.* **23** (1997) 1134.

[25] V. A. Shklovskij, *Fiz. Nizk. Temp.* **25** (1999) 153.

[26] H. Pastoriza, S. Candia, G. Nieva, *Phys. Rev. Lett.* **83** (1999) 1026.

[27] G. D'Anna, V. Berseth, L. Forro, A. Erb, E. Walker, *Phys. Rev.* **B61** (2000) 4215.

[28] V. Berseth, *Ph.D. Thesis*, Lausanne, EPFL, 1999.

[29] E. B. Sonin, A. L. Kholkin, *Fiz. Tverd. Tela* (Leningrad) **34** (1992) 1147 [*Sov. Phys. Solid State* **34** (1992) 610].

[30] E. B. Sonin, *Phys. Rev.* **B48** (1993) 10487.

[31] Y. Mawatari, *Phys. Rev.* **B56** (1997) 3433.

[32] Y. Mawatari, *Phys. Rev.* **B59** (1999) 12033.

[33] G. W. Gardiner, *Handbook of Stochastic Methods* 2nd ed. Springer, Berlin, Heidelberg, New York.

[34] H. Risken, *The Fokker-Planck Equation* 2nd ed. Springer, Berlin, Heielberg New York.

[35] V. A. Shklovskij, A. A. Soroka, A. K. Soroka, *Jornal of Exp. and Theor. Phys.* **89** (1999) 1138.

[36] V. A. Shklovskij, A. A. Soroka, *J. Low Temp. Phys.* **130** (2003) 407.

[37] V. A. Shklovskij, *Phys. Rev.* **B65** (2002) 1.

[38] V. A. Shklovskij, *Phys. Rev.* **B248** (2000) 825.

[39] G. W. Crabtree, G. K. Leaf, H. G. Kaper et al., *Phys. C* **263** (1996) 401.

[40] J. Groth, C. Reichhardt, C. J. Olson et al., *Phys. Rev. Lett.* **77** (1996) 3625.

[41] B. U. Zhu, J. Dong, D. Y. Xing, Z. D. Wang, *Phys. Rev.* **B52** (1998) 5075.

[42] M. Tinkham, *Introduction to Superconductivity* 2nd ed. McGraw-Hill International Press, New York, 1996.

[43] B. Shen, J. Dong, *Phys. Rev.* **B44** (1991) 10206.

[44] O. V. Usatenko, V. A. Shklovskoj, *J. Phys.* **A27** (1994) 5043.

[45] V. A. Shklovskij, *to be published.*

[46] V. A. Shklovskij, *J. Low Temp. Phys.* **131** (2003) 899.

[47] C. Boulesteix, *Phys. Status Solidi (a)* **86** (1984) 11.

[48] V.K. Wadhawan, *Phys. Rev.* **B38** (1988) 8936.

[49] M. Sausara, S. Miyazawa and M. Mukaida, *J. Appl. Phys.* **68** (1990) 3643.

[50] T. Scherer, P. Marienhoff, R. Herwig, M. Neuhaus, W. Jutzi, *Phys. C* **197** (1992) 79.

[51] T. Steinborn, G. Miehe, J. Wiesner, E. Brecht, H. Fuess, G. Wirth, B. Schulte, M. Speckmann, H. Adrian, M. Maul, K. Petersen, W. Blau and M. McConnel, *Phys. C* **220**, 219.

[52] *Methods of Experimental Physics* **V11** Solid State Physiks Academic Press New York and London, 1974.

[53] H. J. Scheel, M. Berkovski, B. Chabot, *Phys. C* **185** (1991) 2095-6.

[54] T. Steinborn, *Ph.D. Thesis*, TH Darmstadt 1994.

[55] W. W. Mullins, *Phil. Mag.* **6** (1961) 1313.

[56] E. D. Williams, N. C. Bartelt, *Science* **251** (1991) 393.

[57] R. J. Phaneuf, E. D. Williams, *Phys. Rev. Lett.* **58** (1987) 2563.

[58] O. Kurnosikov, L. Pham Van, J. Cousty, *Surf. Interface Anal.* **29** (2000) 608.

[59] C. Herring, *Phys. Rev.* **82** (1951) 87.

[60] S. Ramamurthy, B. C. Herbert, C. B. Carter, *Philos. Mag. Lett.* **72** (1995) 269.

[61] J.R. Heffelfinger, C.B. Carter, *Serf. Science* **343** (1995) L1161-L1166.

[62] J.R. Heffelfinger, C.B. Carter, *Serf. Science* **389** (1997) 188-200.

[63] L. Wiehl, J. Oster, M. Huth, *accepted for J. Appl. Cryst.*

[64] M. Huth, K. A. Ritley, J. Oster, H. Dosch, H. Adrian, *Adv. Funct. Mater.* **12** (2002) 333.

[65] S. M. Durbin, J. E. Cunningham, C. P. Flynn, *J. Phys. F: Met.Phys.* **12** (1982) L75.

[66] D. K. Finnemore, T. F. Stromberg, C. A. Swenson, *Phys. Rev.* **149** (1966) 231.

[67] J. Oster, *Ph.D. Thesis* Johannes Gutenberg University Mainz 2004.

[68] S. J. Hagen, C. J. Lobb, R. L. Greene, M. G. Forrester, J. H. Kang, *Phys. Rev.* **B41** (1990) 11630.

[69] S. J. Hagen, C. J. Lobb, R. L. Greene, M. Eddy, *Phys. Rev.* **B43** (1991) 6246.

[70] S. J. Hagen, A. W. Smith, M. Rajeswari, J. L. Peng, Z. Y. Li, R. L. Greene, S. N. Mao, X. X. Xi, S. Bhattacharya, Qi Li, C. J. Lobb, *Phys. Rev.* **B47** (1993) 1064.

[71] A. Casaca, G. Bonfait, C. Dubourdieu, F. Weiss, J. P. Sénateur, *Phys. Rev.* **B59** (1999-II) 1538.

[72] T. R. Chien, T. W. Jing, N. P. Ong, Z. Z. Wang, *Phys. Rev. Lett.* **66** (1991) 3075.

[73] J. P. Rice, N. Rigakis, D. M. Ginsberg, J. M. Mochel, *Phys. Rev.* **B46** (1992) 11050.

[74] J. Luo, T. P. Orlando, J. M. Graybeal,W. R. White, M. R. Beasley, *Bull. Am. Phys. Soc.* **37** (1992) 698.

[75] C. H. Weijsenfeld, *Phys. Lett.* **28A** (1968) 362.

[76] A. W. Smith, T. W. Clinton, C. C. Tsuei, C. J. Lobb, *Phys. Rev.* **B49** (1994) 12927.

[77] H. Van Beelen, J. P. Van Braam Houckgeest, M. H. Thomas, C. Stolk, R. De Bruyn Ouboter, *Physica* **36** (1967) 241.

[78] T. T. M. Palstra, B. Batlogg, L. F. Schneemeyer, J. V. Waszczak, *Phys. Rev. Lett.* **61** (1988) 1662.

[79] C. Ren, F. Y. Lin, Z. M. Li, S. A. Aruna, L. Qui, X. X. Yao, S. L. Yan, M. S. Si, *Supercond. Sci. Technol.* **12** (1999) 400.

[80] B. W. Maxfield, W. L. McLean, *Phys. Rev.* **139** (1965) A1515.

[81] V. A. Shklovskij, *Phys. C* **388** (2003) 655.

[82] N. Grewe and F. Steglich, *Heavy Fermions*, in *Handbook on the Physics and Chemistry of Rare Earths*, Vol. 14, chapter 97, Elsevier Science Publishers, Amsterdam (1991).

[83] S. Ramamurthy, B.C. Herbert, C.B. Carter, *Philos. Mag. Lett.* **72** (1995) 269.

[84] G. Roth, B. Renker, G. Heger, M. Hervieu, B. Domenges and B. Raveau, *J. Phys. B Condens. Matt.* **69** (1987) 53.

[85] S. Fleshler, W.-K. Kwok, U Welp et al., *Phys. Rev.* **B47** (1993) 14448.

[86] T. R. Chien, T. W. Jing, N. P. Ong, Z. Z. Wang, *Phys. Rev. Lett.* **66** (1991) 3075.

[87] G. D'Anna, V. Berseth, L. Forro, A. Erb, E. Walker, *Phys. Rev. Lett.* **81** (1998) 2530.

[88] V. M. Vinokur, V. B. Geshkenbein, M. V. Feigel'man, G. Blatter, *Phys. Rev. Lett.* **71** (1993) 1242.

V. A. Shklovskij, A. A. Soroka, O. K. Soroka "Guiding of vortices and the Hall effect in super-conductors with unidirected twins." *Proceedings of MSM-99 Conference* (1999) Iran.

V. A. Shklovskij, A. A. Soroka, O. K. Soroka "Nonlinear dynamics of vortices pinned to unidirectional twins." *Jornal of Exp. and Theor. Phys.* **89** (1999) 1138.

O. K. Soroka, M. Huth, V. A. Shklovskij, J. Oster, H. Adrian "Guided vortex motion in Nb films on faceted substrate surfaces" Physica C **388-389** (2003) 733.

O. K. Soroka, M. Huth "Guided vortex motion in faceted niobium films." *Low Temp. Phys.* **28** (2002) 842.

Eidesstattliche Erklärung

Hiermit erklre ich an Eides statt, daß ich die vorliegende Arbeit selbstständig und nur unter Verwendung der angegebenen Hilfsmittel angefertigt habe.

Bisher habe ich noch keinen Promotionsversuch unternommen.

Mainz, im November 2004